DESIGN, SYNTHESIS, AND CHARACTERIZATION OF POROUS DENDRITIC POLYMERS FOR GAS SENSOR APPLICATIONS

A Thesis Submitted to
the Graduate School of
İzmir Institute of Technology
in Partial Fulfillment of the Requirements for the Degree of

DOCTOR OF PHILOSOPHY

in Chemistry

by
Hüseyin Zeybek

December 2024
İZMİR

We approve the thesis of Hüseyin ZEYBEK

Examining committee members:

_____
Assist. Prof. Dr. Onur BÜYÜKÇAKIR
Department of Chemistry, İzmir Institute of Technology

_____
Prof. Dr. Gülşah ŞANLI MOHAMED
Department of Chemistry, İzmir Institute of Technology

_____
Prof. Dr. Yaşar AKDOĞAN
Department of Materials Science and Engineering, İzmir Institute of Technology

_____
Assoc. Prof. Dr. Muhammed ÜÇÜNCÜ
Department of Pharmacy, İzmir Katip Çelebi University

_____
Prof. Dr. Armağan KINAL
Department of Chemistry, Ege University

20 December 2024

_____
Assist. Prof. Dr. Onur BÜYÜKÇAKIR
Supervisor, Department of Chemistry,
İzmir Institute of Technology

_____
Prof. Dr. Gülşan ŞANLI MOHAMED
Head of the Department of Chemistry

_____
Prof. Dr. Mehtap EANES
Dean of the Graduate School

ACKNOWLEDGMENTS

During my PhD studies, many people have contributed to this study. I sincerely thank those who provided invaluable help, support, and guidance throughout my graduate studies at İzmir Institute of Technology.

I would like to sincerely thank my supervisor, Assist. Prof. Dr. Onur BÜYÜKÇAKIR, for providing me with stimulating and engaging assignments, valuable insights and talks, and patiently addressing my questions. I express my profound gratitude to Prof. Dr. Hasan ŞAHİN for their assistance and support in providing me with theoretical studies.

To my labmates, Gizem ŞİMŞEK, Ferit BEGAR, Yaren Naz ERÖZEN, Utku Cem ÇANAKÇI, Yasmin GEÇALP, Mustafa ERDOĞMUŞ, Sercan CANTÜRK, Betül AKKUŞ, Ali Cem DEMİROK; thank you for the good lab atmosphere and spirit. I want to thank them for their support, help, friendship, and patience for three years. They were like brothers and sisters to me, and I am grateful for everything they have done for me.

Also, special thanks to Prof. Dr. Yaşar AKDOĞAN, Prof. Dr. Gülşah ŞANLI MOHAMMED, Prof. Dr. Armağan KINAL and Doç. Dr. Muhammed ÜÇÜNCÜ for participating as a committee member and reviewing my work as well as all the technical stuff of TAM for instrumental analysis.

I would like to thank to The Scientific and Technological Research Council of Türkiye - TÜBİTAK (120C132) and TÜBİTAK 2211-A for their support for the thesis studies. I also want to thank to the YÖK 100/2000 and İZTECH for their support.

Finally, I would like to express my heartfelt gratitude to my family and friends who supported me throughout my thesis work and listened to my successes and complaints. To mom Filiz ZEYBEK and dad Mehmet Kemal ZEYBEK, for their sacrifices and encouragement in my academic journey. I am indebted to my brother Tevfik Can ZEYBEK, for his unconditional love and support.

ABSTRACT

DESIGN, SYNTHESIS, AND CHARACTERIZATION OF POROUS DENDRITIC POLYMERS FOR GAS SENSOR APPLICATIONS

Polyphenylene dendrimers (PPDs) are macromolecules distinguished by their highly branched 3D globular structures. PPDs are generally constructed around a central multi-functional core molecule with branches having phenyl moieties and end groups. PPDs consist of rigid, shape-persistent phenyl rings offering physicochemically stable and robust structures. Although these characteristic features make PPDs promising compounds to be used in many applications such as light harvesting, organic electronics, and catalysts, their gas and energy storage usage is limited due to their non-porous structure in the solid state. This thesis aims to take a novel modular approach to incorporate functional PPDs into porous dendritic polymers (PDendPs), which is accomplished by polymerizing "shape-persistent dendrimers" with organic linkers. Using shape-persistent PPDs as monomers offers a local order in PDendPs, improving the predictability and controllability of their surface area and porosity. In this regard, this approach allows precise molecular control over structure and functionality in PDendPs.

This thesis proposed polymerizing three generations of PPDs using a ditopic linker to prepare three different PDendPs. Therefore, three generations of PPDs having bromo atoms at the periphery were synthesized, and these PPDs were polymerized using 1,4-bis(4,4,5,5-tetramethyl-1,3,2-dioxaborolan-2-yl)benzene as linker via Suzuki coupling reactions. PDendPs and PPDs have been characterized using various analytical techniques, including NMR, FT-IR, BET, TGA, XRD, SEM, and EDX. All synthesized polymers were exposed to ethanol vapor in order to investigate PDendPs' potential as a sensing material for chemiresistor sensor applications. Computational simulations were exploited to reinforce outcomes in wet-lab media.

Keywords: polyphenylene dendrimers, porous dendritic polymers, chemiresistors

ÖZET

GAZ SENSÖR UYGULAMALARI İÇİN GÖZENEKLİ DENDRİTİK POLİMERLERİN TASARIMI, SENTEZİ VE KARAKTERİZASYONU

Polifenilen dendrimerler (PPD'ler), yüksek oranda dallanmış 3D küresel yapıları ile ayırt edilen makromoleküllerdir. PPD'ler genellikle merkezi çok fonksiyonlu bir çekirdek molekül etrafında fenil halkaları ve uç gruplara sahip dallarla inşa edilir. PPD'ler fizikokimyasal olarak kararlı ve sağlam yapılar sunan rijit, şekil değiştirmeyen fenil halkalarından oluşur. Bu karakteristik özellikleri PPD'leri ışık hasadı, organik elektronik, katalizörler gibi birçok uygulamada kullanılmak üzere umut verici bileşikler haline getirse de, katı haldeki gözeneksiz yapıları nedeniyle gaz ve enerji depolamada kullanımları sınırlıdır. Bu tez, fonksiyonel PPD'leri gözenekli dendritik polimerlere (PDendP'ler) dahil etmek için yeni bir modüler yaklaşım benimsemeyi amaçlamaktadır; bu yaklaşım, "kalıcı-şekilli dendrimerleri" organik bağlayıcılarla polimerize ederek gerçekleştirilmektedir. Şekli bakımından kalıcı PPD'lerin monomer olarak kullanılması, PDendP'lerde yüzey alanlarının ve gözenekliliklerinin öngörülebilirliğini ve kontrol edilebilirliğini artıran yerel bir düzen sunar. Bu bağlamda, bu yaklaşım PDendP'lerde yapı ve işlevsellik üzerinde hassas moleküler kontrol sağlar.

Bu tez, üç farklı PDendP hazırlamak için ditopik bir bağlayıcı kullanarak üç nesil PPD'nin polimerleştirilmesini önermiştir. Bu nedenle, yüzeyde bromo atomlarına sahip üç nesil PPD sentezlenmiş ve bu PPD'ler Suzuki eşleşme reaksiyonları yoluyla bağlayıcı olarak 1,4-bis(4,4,5,5-tetrametil-1,3,2-dioksaborolan-2-il)benzen kullanılarak polimerleştirilmiştir. PDendP'ler ve PPD'ler NMR, FT-IR, BET, TGA, XRD, SEM ve EDX dahil olmak üzere çeşitli analitik teknikler kullanılarak karakterize edilmiştir. Sentezlenen tüm polimerler, PDendP'lerin kemorezistör sensör uygulamaları için bir algılama malzemesi olarak potansiyelini araştırmak amacıyla etanol buharına maruz bırakılmıştır. Islak laboratuvar ortamındaki sonuçları güçlendirmek için hesaplamalı simülasyonlardan yararlanılmıştır.

Anahtar Kelimeler: polifenilen dendrimerler, gözenekli dendritik polimerler, kimyasal direnç sensörleri

TABLE OF CONTENTS

APPENDICES

LIST OF FIGURES

Figure **Page**

Figure **Page**

Figure **Page**

Figure **Page**

Figure **Page**

LIST OF TABLES

Table **Page**

LIST OF ABBREVIATIONS

PPD	Polyphenylene dendrimer
PDendP	Polyphenylene dendritic polymer
PAMAM	Polyamidoamine
PPI	Poly(propylene imine)
NMR	Nuclear Magnetic Resonance
XRD	X-ray Diffraction Analysis
FTIR	Fourier- Transform Infrared Spectroscopy
AFM	Atomic Force Microscopy
DMF	N,N'-Dimethylformamide
SEM	Scanning Electron Microscopy
EDX	Energy Dispersive X-ray
TGA	Thermogravimetric Analysis
TEM	Transmission electron microscopy
HSA	Human Serum Albumin
EtOH	Ethanol
MeOH	Methanol
THF	Tetrahydrofuran
BET	Brunauer-Emmett-Teller
TLC	Thin Layer Chromatography
$CDCl_3$	Deuterated chloroform
PAHs	Polyaromatic Hydrocarbons
CDH	Cyclodehydrogenation
GNRs	Graphene Nanoribbons
EET	Excitation Energy Transfer
NMI	Naphthalene Dicarboximide
PMI	Perylene Dicarboximide
TDI	Terrylene Tetracarboxdiimide
DCM	Dichloromethane
DMSO	Dimethyl sulfoxide
MeCN	Acetonitrile
RT	Room Temperature
TBAF	Tetrabutyl Ammonium Fluoride
TBAH	Tetrabutyl Ammonium Hydroxide
TIPS	Triisopropyl sillyl
TEA	Triethylamine
PTSA	p-Toluenesulfonic acid

DMAP	4-Dimethylaminopyridine
TBTA	Tris(benzyltriazolylmethyl)amine
Ad5	Adenovirus 5
CAR	Coxsackie-adenovirus Receptor
A$\boldsymbol{\beta}$	Amyloid-beta
APDs	Amphiphilic Polyphenylene Dendrons
MOFs	Metal-organic Frameworks
CMP	Conjugated Microporous Polymers
COF	Covalent Organic Frameworks
CTF	Covalent Triazine Frameworks
HCP	Hyper-crosslinked Polymers
PAF	Porous Aromatic Frameworks
POP	Porous Organic Polymer
Py-PP	Poly Tetraphenyl Pyrene
CNTs	Carbon Nanotubes
VOC	Volatile Organic Compound
RGO	Reduced Graphene Oxide
GQDs	Graphene Quantum Dots
PPy	Polypyrrole
PANI	Polyaniline
IoT	Internet of Things
NAP-XPS	Near Ambient Pressure X-ray Photoelectron Spectroscopy
MWCNT	Multi-Walled Carbon Nanotubes
PEDOT-PSS	Poly (3,4-ethylene dioxythiophene) and Polystyrene Sulfonate
MR	Methyl Red
AC	Activated Charcoal
MFC	Mass Flow Controller
VASP	Vienna ab initio Simulation Package
PGNRs	Porous Graphene Nanoribbons

CHAPTER 1

INTRODUCTION

1.1.An Overview

Polyphenylene dendrimers (PPDs) are densely branched, monodisperse macromolecules with a shape-consistent backbone typically composed of derived benzene rings.[1-8] Due to the rigid phenyl backbones, these dendrimers are exceedingly stable and robust, which enables site-specific functionalization.[9] In general, PPDs are divided into three components: core, scaffold, and surface, with functionalities that can be synthetically tailored at each phase, as shown in Figure 1.1.[9] PPDs are highly sophisticated macromolecules that have been integrated into organic electronics, utilized as poorly regulating anions and cations, and even mimicked biologically important proteins like human serum albumin (HSA), along with many other feasible application areas.[10-11]

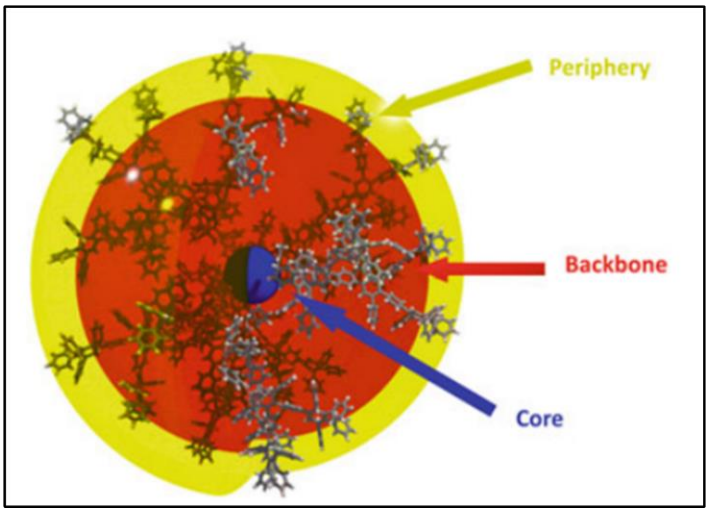

Figure 1.1. Schematic illustration of three main units of polyphenylene dendrimers (PPDs).[12]

This thesis aims to polymerize first, second, and third-generation PPDs (G1: A3 building block, G2: A6 building block, G3: A12 building block) with 1,4-bis(4,4,5,5-tetramethyl-1,3,2-dioxaborolan-2-yl)benzene (B2) building block as linkingae unit using Suzuki-Miyaura coupling reactions. The S_{BET} surface area results of the corresponding polymers, namely P1DendP, P2DendP, and P3DendP, were 266 m^2 g^{-1}, 779 m^2 g^{-1}, and 179 m^2 g^{-1}, respectively. The synthesized polymers (PDendPs) were tested as chemiresistor and were subjected to ethanol vapor as a volatile organic compound. Computational simulations were carried out to understand the mechanism of sensing.

1.2.Structure and Synthesis of PPDs

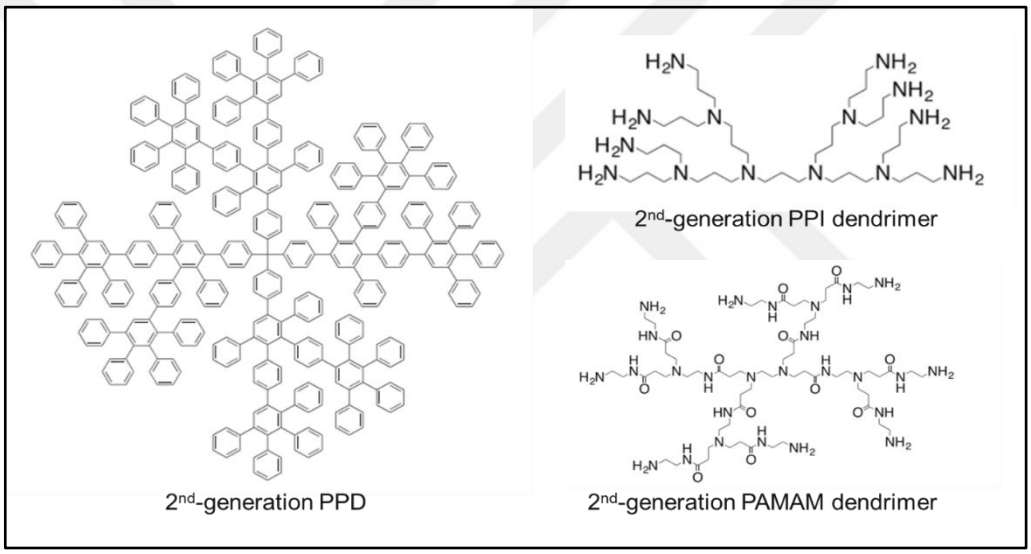

Figure 1.2. Molecular structures for a rigid second-generation PPD, and flexible second-generation PPI and PAMAM dendrimer.[9]

The rigid and shape-persistent character of PPDs is among the essential features that distinguish the PPDs from other conventional dendrimers.[9] PPD has a phenylene-based rigid backbone, whereas PAMAM and PPI have repeating chains in their flexible backbones, as shown in Figure 1.2.[9] Compared with other dendrimers, PPDs can perform structural changes resulting in a structural balance of where chemical activities are situated, this disparity in backbone rigidity illustrates why PPDs are shape-persistent and hence can be produced with nanosite accuracy.[9] Limiting the conformational flexibility makes PPDs suitable for modification from the core to the scaffold and surface in a site-

specific manner; as a result, it is possible to predict not just their exact structures but also the macromolecules' desired properties.[10,13-14] As a result of the lack of the ability to bend the dendron arms backward, the surface groups always seem to be on the exterior of the dendrimers –not engulfed within the structure's interior.[9] Patchy dendrimers with distinct inner cavities and pores are appropriately categorized as surface-dense PPDs.[15-16] The surface-bound phenylene groups become densely arranged with increasing generations, resulting in a shape-persistent and globular morphology, which has been examined using AFM, TEM, computer simulations, and solid-state NMR spectroscopy.[9]

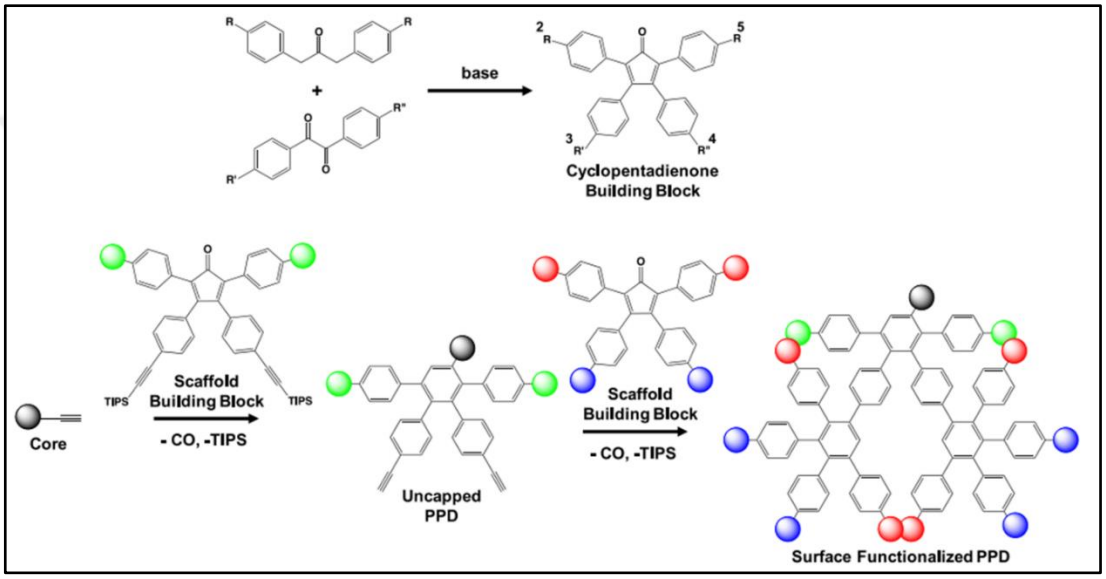

Figure 1.3. Simple representation for the synthesis of PPDs.[9]

PPDs are comprised of a core, whose design determines the number of arms and morphology of the dendrimer, and building blocks, which govern the chemical derivatization of the scaffold and surface, along with dendrimer generation.[16-19] There are two approaches to synthesizing PPDs: convergent and divergent.[9] As convergent approaches typically employ the metal-catalyzed coupling reactions between the aromatic core bearing halide and boronate-functionalized dendrons, these routes are not generally reproducible.[9] Therefore, the most commonly used method to synthesize PPDs is a divergent growth mechanism in which to form the dendrimer from the inside out, a [4+2] Diels-Alder cycloaddition process takes place between a core bearing ethynyl moieties and building components containing cyclopentadienone units as seen in Figure 1.3.[16, 20-22] This is essential in terms of creating monodisperse macromolecules and concerning the

reaction's lone prerequisite: a stable diene and dienophile at high temperatures (i.e.,~ 135–170 °C).[9] The synthetic adaptability allows for the site-specific inclusion of a wide range of chemical functions at the core, scaffold, and surface of PPDs.[9] The Diels-Alder reaction is also quantitative, with permanent transformations, implying that the molecule is stable.[23-25]

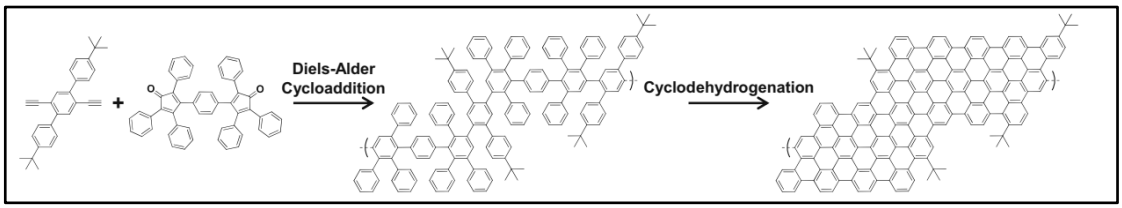

Figure 1.4. Polyphenylenes can be converted into graphene nanoribbons precursors.[9]

Furthermore, PPDs in the 3-D globular form can be transformed into 2-D nanographene derivatives.[9] This unique method lays the foundation for the molecularly demanded graphenes with outstanding electrical and mechanical capabilities.[7,15] The usage of polyphenylene dendrimers, which were produced employing successive Diels-Alder cycloaddition polymerization methodologies, is one of the earliest known synthetic methodologies to fabricate unfolded precise nanographenes through bottom-up approach.[26] Following the dendritic ribbon synthesis, a cyclodehydrogenation process was applied to it along with $FeCl_3$ as the oxidizing agent, leading to a 2-D graphene nanoribbon, which was analyzed as graphene analogs depicted in Figure 1.4.[11,13,23,26-27]

1.3.Applications of PPDs

Polyphenylene dendrimers' functionality in synthesis, coupled with their inherent monodisperse, shape-persistent, and stable structures, allows hitherto unique usage areas.[9] The bulk characteristics of distinct PPDs are regulated by complicated syntheses of their core, scaffold, and surface with a linkage of their changes.[9] Hypothetically, an emerging era of cutting-edge dendrimer syntheses has paved the way for innovative applications such as organic electronic devices, synthetic nanographene with desired functionalities, biomimicking biological molecules, therapeutics, drug nanocarriers, and more.[9]

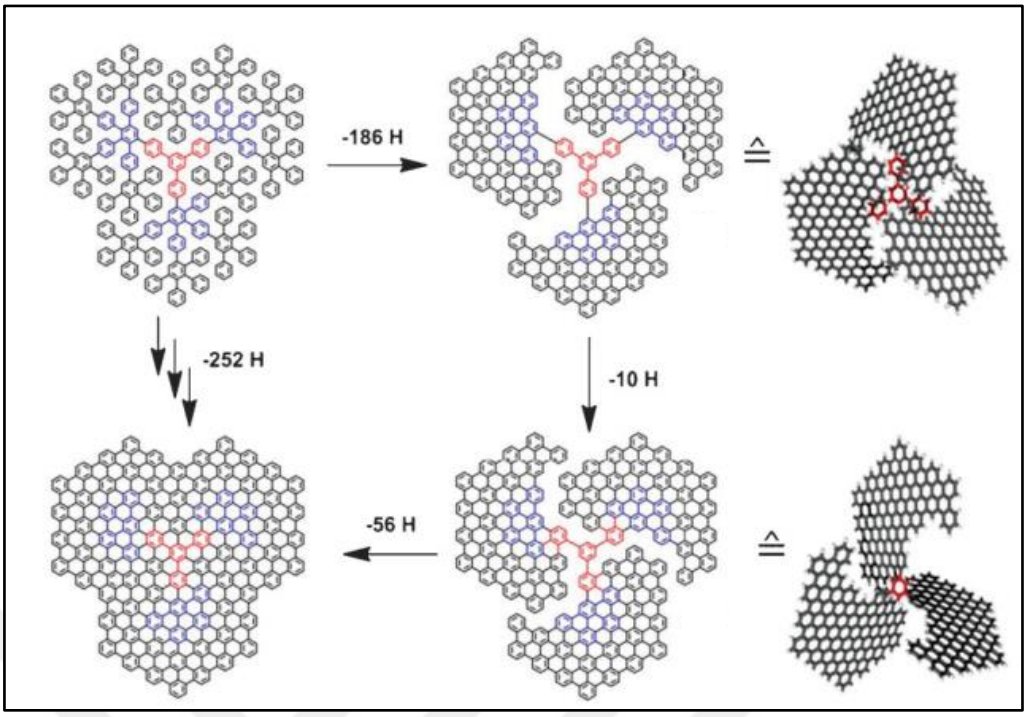

Figure 1.5. Synthesis of molecular propellers through a PPD precursor.[28]

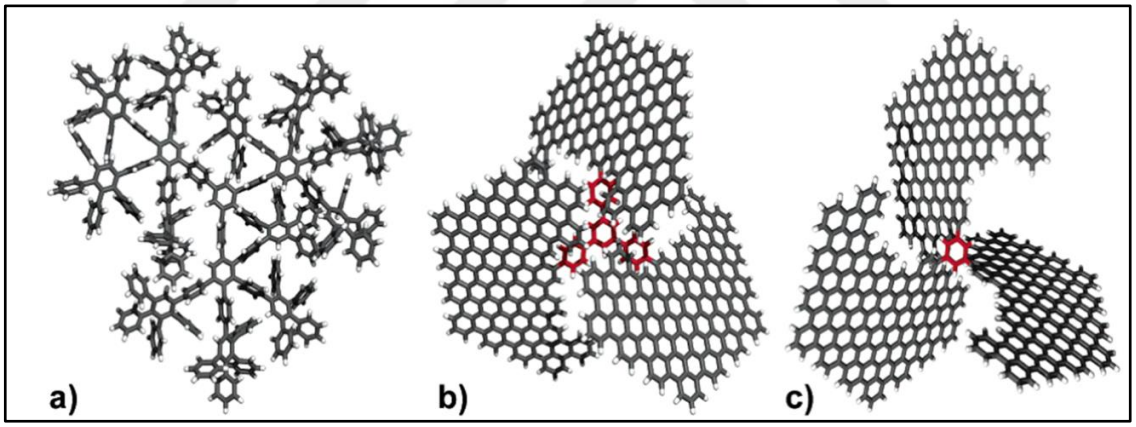

Figure 1.6. Computer assisted simulations for 3-D molecular structures of (a) PPD, (b) propeller holding triphenylbenzene core unit, and (c) benzene core molecule.[28]

Simpson et al. offered a synthetic strategy for polyaromatic hydrocarbons (PAHs), which are precursors of molecularly defined graphite model compounds. Their strategy uses the oxidative cyclodehydrogenation (CDH) process to planarize three-dimensional, dendritic oligophenylenes that could be rendered in their 2D projection without overlapping phenyl rings. Figure 1.5 shows the computer-based visualization of

the 3D structure of a dendrimer and propeller-shaped PAHs. These PAHs were characterized by UV/vis, fluorescence, Raman spectroscopy, and MALDI-TOF mass spectrometry, thereby establishing the efficiency of the cyclodehydrogenation reaction. Its determination is crucial for estimating CDH process efficacy in polymer synthesis. Furthermore, adding alkyl chain substituents on the periphery may convert macromolecular structures into more soluble and processable ones. Finally, these novel 3D nanopropeller molecules are important for investigations in hydrogen storage and their unique electronic structures (Figure 1.6).[28]

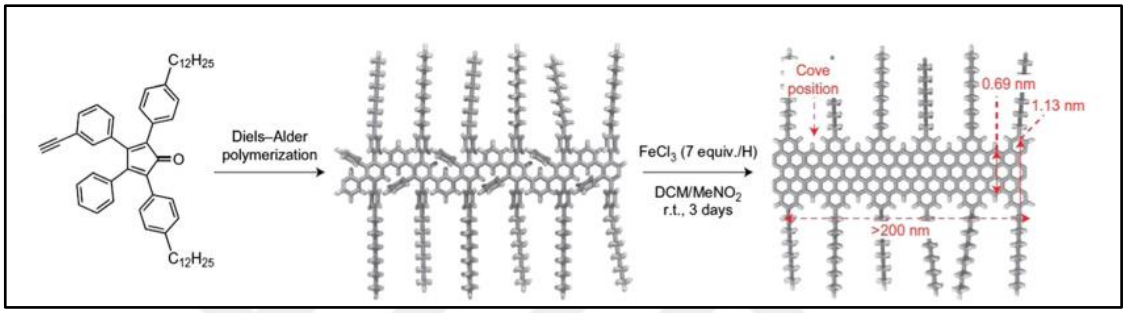

Figure 1.7. Processable graphene nanoribbons from polyphenylene precursors.[29]

The recent progress in the synthesis of graphene nanoribbons (GNRs) via PPDs as precursors includes the addition of solubilizing chain moieties, thereby allowing solution process and handling on the edge structure. This invention simplifies processing and transforms the linear PPD into one of the biggest GNRs synthesized along with thicknesses ~ 1.0 nm and lengths as long as 600 nm. The innovative bottom-up solution-synthesis method Narita and co-workers provided herein, which utilizes Diels-Alder cycloaddition polymerization, is compatible with a wide range of AB-type monomers and consequently offers a potential tailor-made synthesis of lengthy liquid phase adaptable and exactly known GNRs that have diverse dimensions (Figure 1.7). The synthesized polymers showed improved charge transport mobility values and electrical characteristics compared to semiconducting polymers, with a band gap of around 1.88 eV. Because graphene lacks a natural band gap, it requires geometrical constriction to generate one, which is highly critical for future nanoelectronics applications that involve switching on and off gadgets.[29]

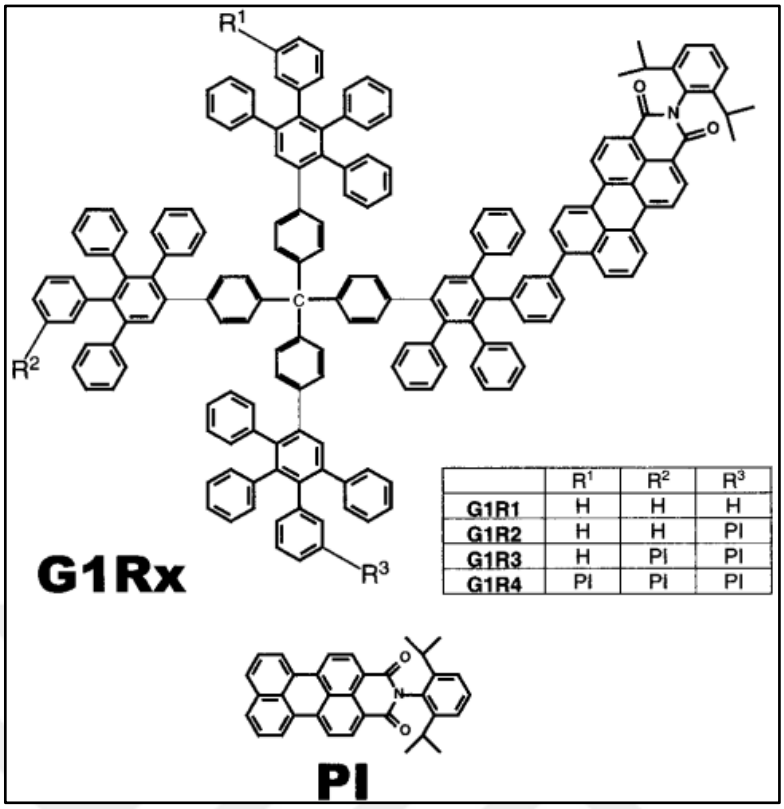

	R1	R2	R3
G1R1	H	H	H
G1R2	H	H	PI
G1R3	H	PI	PI
G1R4	PI	PI	PI

Figure 1.8. Structures of the dendrimers employed in this research.[30]

Maus et al. synthesized four first-generation PPDs bearing tetraphenylmethane core and decorated with varying numbers of peryleneimide chromophores on the surfaces in order to determine their photophysical properties and the excitation energy transfer (EET) method using steady-state and time-resolved fluorescence spectroscopy (Figure 1.8) The model dendrimer holding a single PI chromophore exhibited a 4.2 ns decay time. However, in multichromophoric dendrimers, an extra lengthy decay time of 7.4 ns was discovered as an "excimer-like" phenomenon, and its impact rises with the increasing number of chromophores. The analysis for the time-resolved polarization revealed a nanosecond-long relaxation factor caused by the rotary motion of the whole dendritic macromolecule. On the contrary, molecules with many chromophores have a faster anisotropic decay time of 100-200 ps, indicating Förster type EET of the chromophores. These findings for dendrimers are extremely promising for their usage in areas like optoelectronics, OLED devices, and fundamental photosynthetic light-harvesting antenna devices.[30]

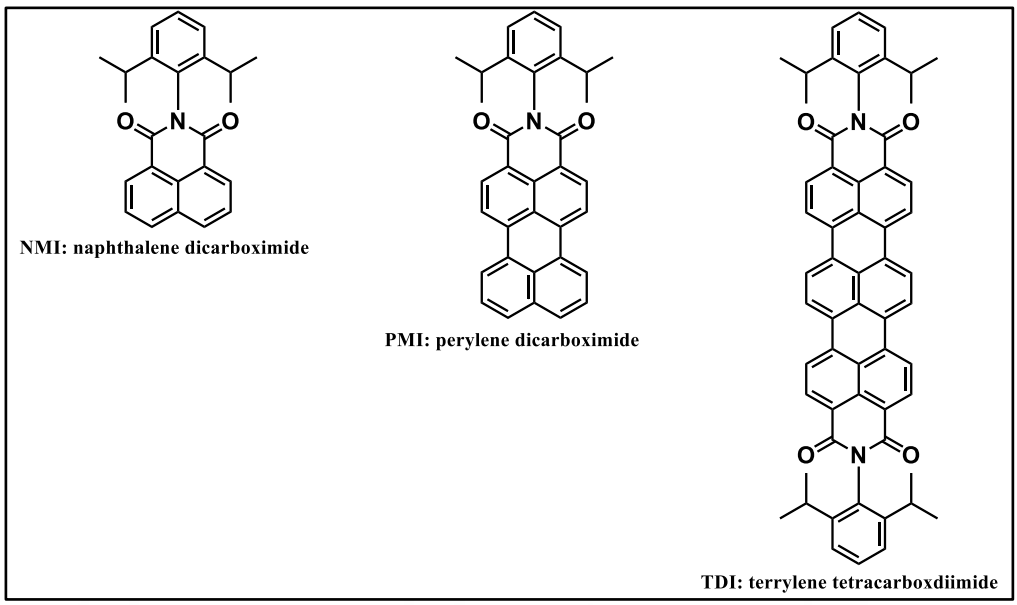

Figure 1.9. The chemical structures of three unsubstituted ryleneimide dyads, naphthalene dicarboximide (NMI), perylene dicarboximide (PMI), and terrylene tetracarboxdiimide (TDI), are being described.[31]

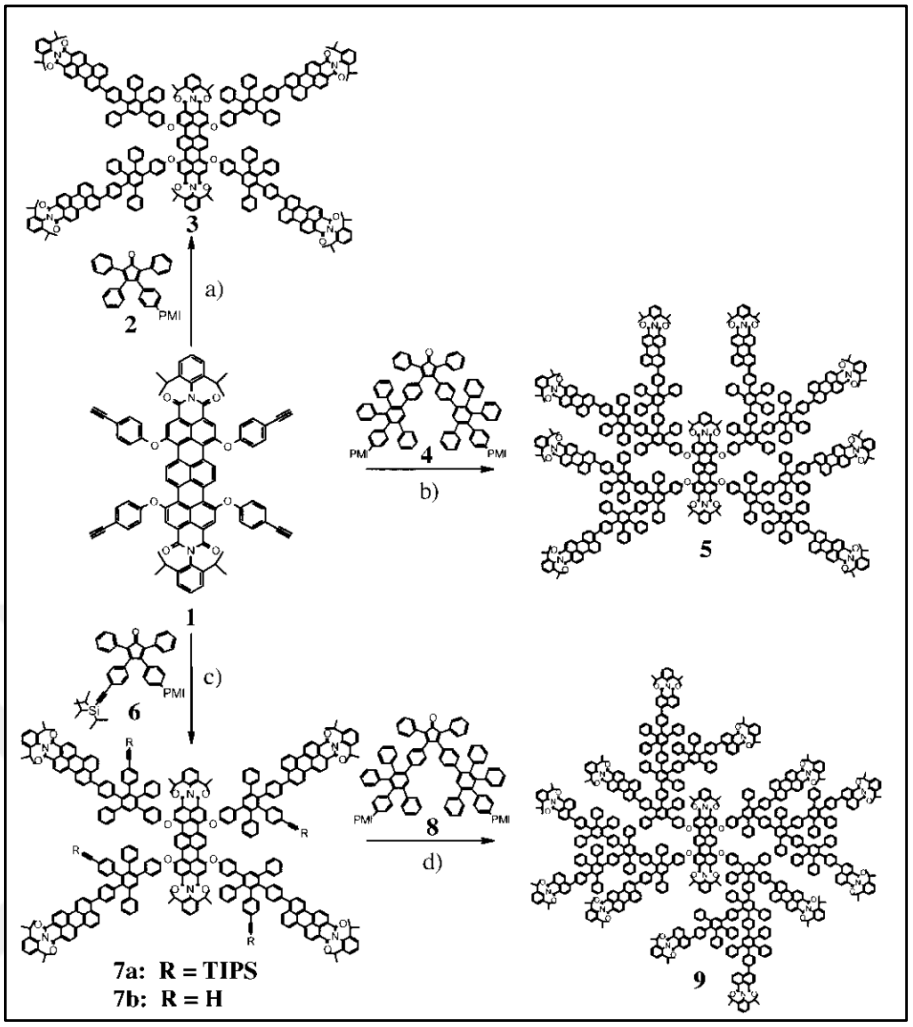

Figure 1.10. Synthesis of light harvester system employing three dyads. a) Diels-Alder reaction conditions; b) Diels-Alder reaction conditions; c) Diels-Alder reaction conditions; 2) deprotection process; d) Diels-Alder reaction conditions. TIPS=triisopropylsilyl.[31]

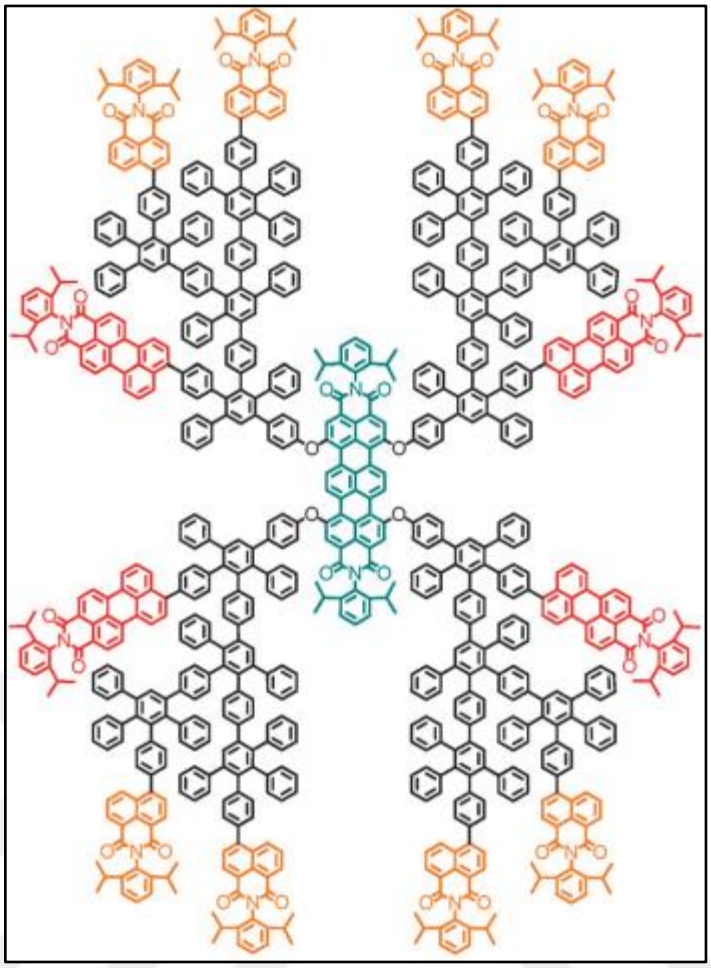

Figure 1.11. Light harvesting triad of three different chromophores.[31]

Weil et al. synthesized rigid-shaped fluorescent polyphenylene dyads using a variety of diads and even triads to visualize the notion of controlled energy transmission between precisely arranged chromophores in macromolecules. The dendritic triad macromolecule composed of the dyes naphthalenedicarboximide (NMI), perylenedicarboximide (PMI), and terrylenetetracarboxdiimide (TDI) exhibited a progressive vectorial flow of energy from NMI at the surface through PMI to TDI in the core (Figure 1.9 and Figure 1.10). Placing chromophores at specific locations creates an effective light-harvesting system that absorbs across the visible wavelengths. These innovative functionally clearly defined polyphenylene multichromophores, which contain two or three distinct chromophores in the dendrimer's core, scaffold, and surface and have exceptional photochemical stability, show significant potential for optoelectronic device design (Figure 1.11).[31]

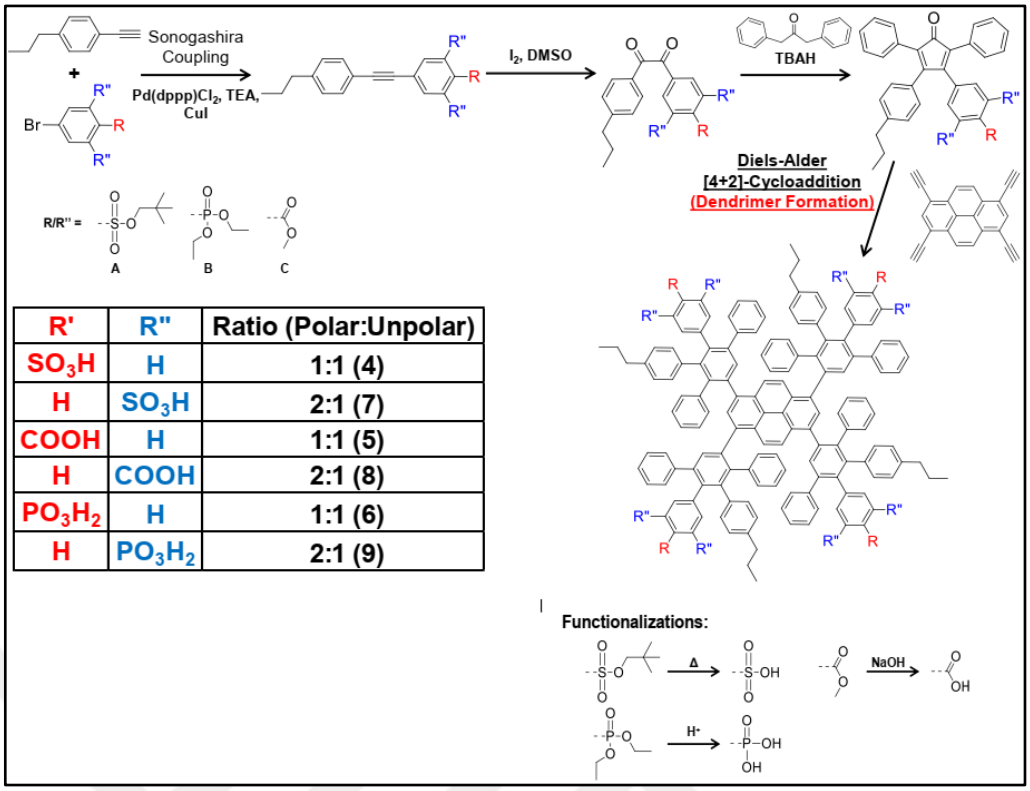

R'	R''	Ratio (Polar:Unpolar)
SO_3H	H	1:1 (4)
H	SO_3H	2:1 (7)
COOH	H	1:1 (5)
H	COOH	2:1 (8)
PO_3H_2	H	1:1 (6)
H	PO_3H_2	2:1 (9)

Figure 1.12. Synthetic procedure for PPDs with patchy surfaces.[32]

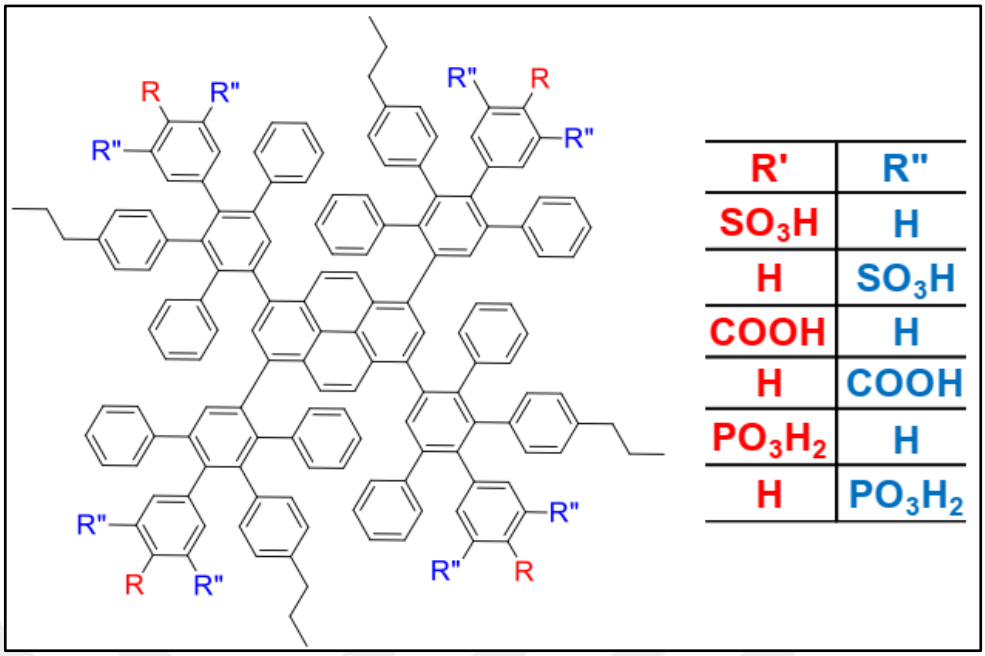

R'	R"
SO_3H	H
H	SO_3H
COOH	H
H	COOH
PO_3H_2	H
H	PO_3H_2

Figure 1.13. PPDs with patchy surfaces.[32]

Hammer et al. synthesized monodisperse and shape-persistent PPDs with features bearing patchy surfaces on the macromolecules modified with polar and non-polar moieties to provide unique lipophilic regions for binding (Figure 1.12 and Figure 1.13). Although these compounds have demonstrated the ability to combine physiologically important molecules, exhibit significant penetration into cells in multiple cell lines, and cause minimal to no toxic effects, little is known about the underlying mechanisms. This study presented if dendrimers' responses to the biological medium are more influenced by their chemical functions, comparative constituent amounts, or "patched" surface structure. Changing the polar group from sulfonic to carboxylic to phosphonic acids resulted in equivalent cellular absorption and low toxicity when combined with propyl groups in 1:1 molar proportions. Shifting the lipophilic equilibrium to a greater polarity and charge-negative balance through raising the molecular proportion of polar to nonpolar moieties resulted in substantial declines within dendrimer cell penetration efficacies. This phenomenon was probably a result of repellent interactions among the PPDs and the membrane's surface. The current research found that the ideal lipophilic shell over improved absorption by cells through minimal toxic effects comes from an intricate equilibrium between the polar and nonpolar parts of the dendrimers' exterior rather than unique chemical elements upon the periphery.[32]

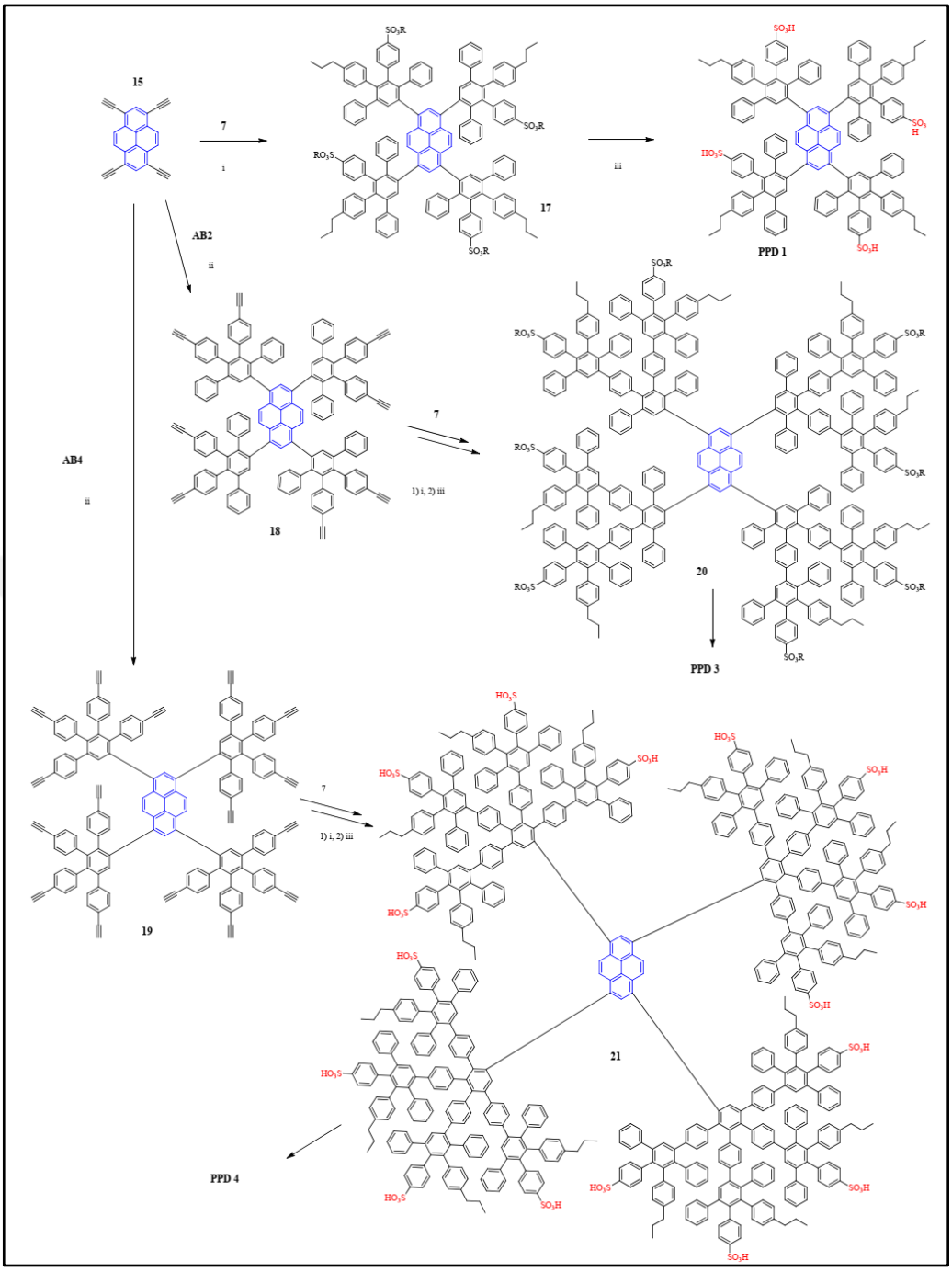

Figure 1.14. Synthetic illustration for the amphiphilic PPD precursors. i) Diels-Alder reaction conditions with molecule 7: CP building block, ii) Diels-Alder reaction conditions with CP building block, iii) acid-catalyzed deprotection process for sulfonic acid protecting group: neopentyl ester (R), iv) deprotection process for acetylene protecting group: TIPS= triisopropylsilyl.[33]

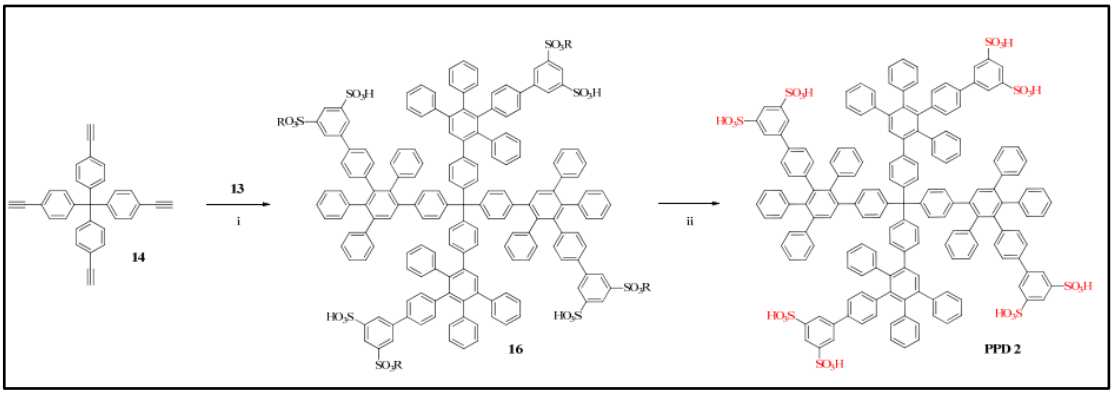

Figure 1.15. Synthesis scheme of PPD2. i) Diels-Alder reaction conditions with molecule 13: CP building block, ii) acid-catalyzed deprotection process for sulfonic acid protecting group: neopentyl ester (R).[33]

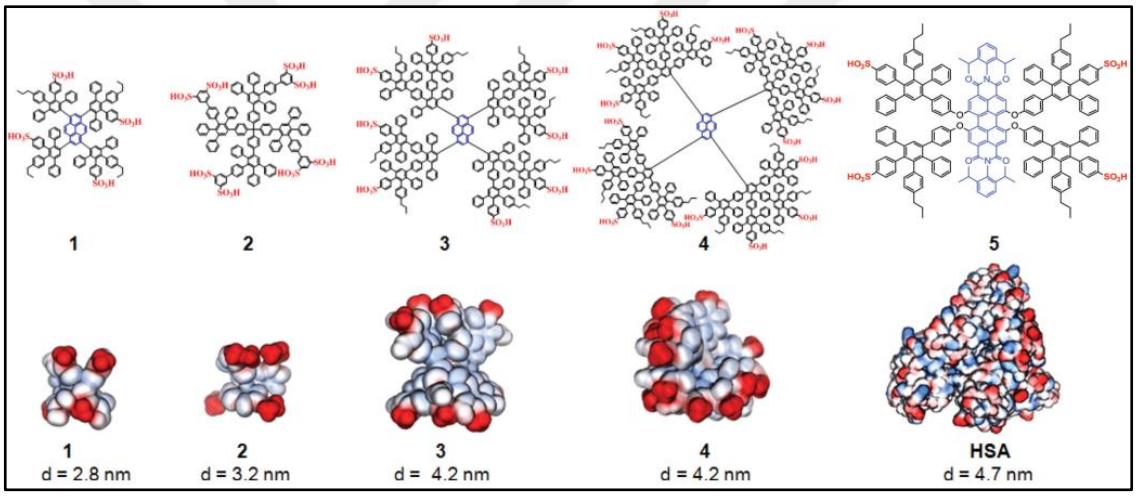

Figure 1.16. PPDs with potential for drug delivery and protein mimicry.[33]

Stangenberg et al. reported the concept and production of a polyphenylene dendrimer (PPD 3) with separate receptors to hydrophilic molecule guests and distinct surface motifs (Figure 1.14, Figure 1.15). Its semi-stability and the exact placement of lipophilic and hydrophobic moieties at the surface results in a sophisticated design with hydrophilic interaction sites that may retain particular quantities of medically essential guest compounds like lipids or medication like doxorubicin (Figure 1.16). Its diameter, design, and surface characteristics enable this macromolecule to permeate through brain endothelial cells, a crucial part of the highly impermeable blood-brain barrier. Furthermore, in vivo investigations with embryos from zebrafish have shown little to no

adverse effects. The unique features of the PPD structure enable the precise arrangement of functional regions in a particular milieu and provide a general framework for developing drug delivery systems that firmly mimic various protein properties.[33]

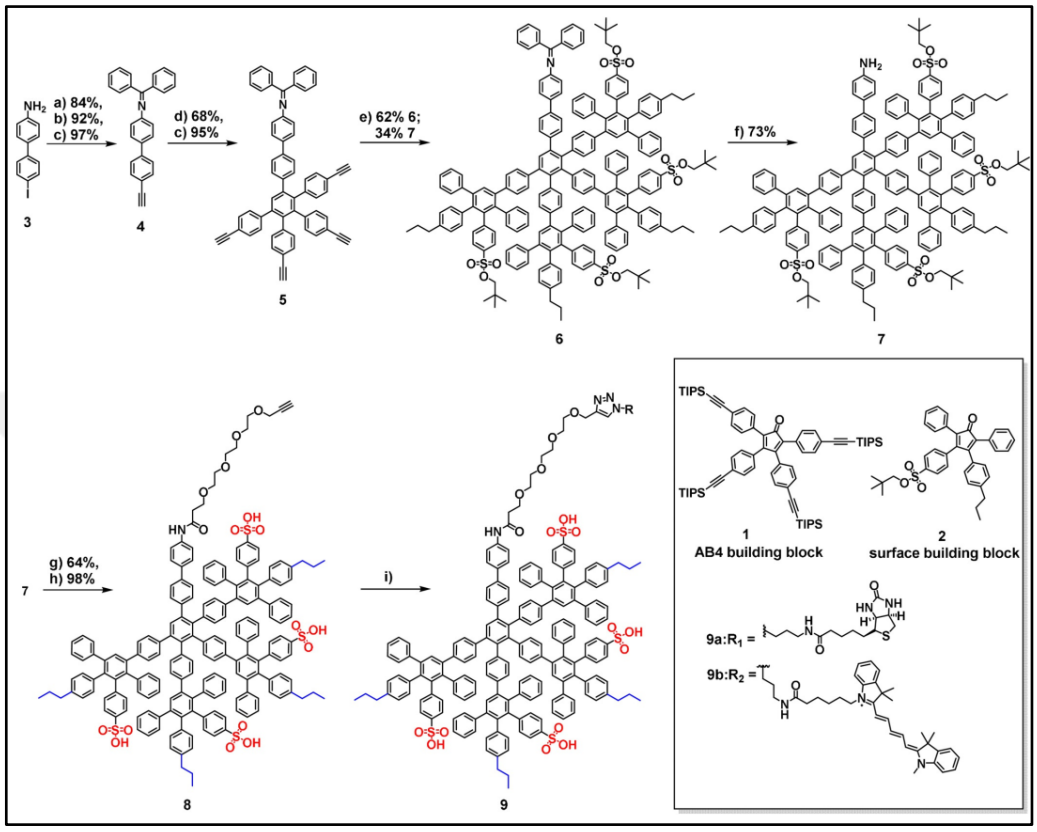

Figure 1.17. Synthesis for one of the dendritic site of PPD with amphiphilic surface groups at exterior. a) Condensation reaction conditions for imine formation; b) Sonogashira coupling reaction conditions; c) deprotection process for acetylene protecting group: TIPS=triisopropylsilyl; d) Diels-Alder reaction conditions with molecule 1: CP building block; c) deprotection process; e) Diels-Alder reaction conditions with molecule 2: CP building block; f) acid-catalyzed deprotection process for primary amine protecting group: benzophenone; g) Condensation reaction conditions for amide formation; h) deprotection process for sulfonic acid protecting group: neopentyl ester; i) Click reaction conditions.[34]

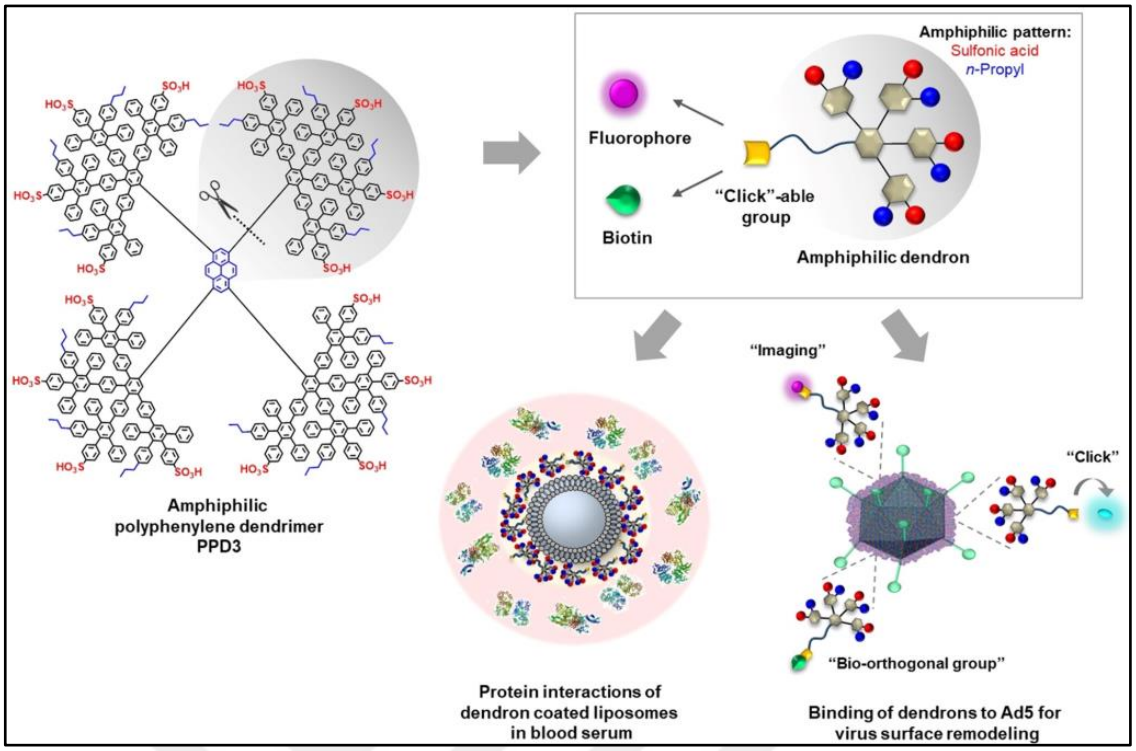

Figure 1.18. The molecular model of an amphiphilic polyphenylene dendron from amphiphilic PPD and its interaction with adenovirus 5 (Ad5).[34]

Amphiphilic moieties on the surface serve a critical function in several biological mechanisms. Wagner et al. described the synthesis of amphiphilic polyphenylene dendrimer dendrons with changing hydrophobic and hydrophilic groups on the exterior and the ethynyl group in the core, which are open-for-click reactions (Figure 1.17). The amphiphilic groups on the surface function just like biorecognition components, binding to the outermost layer of adenovirus 5 (Ad5), a popular vector in the field of gene therapy (Figure 1.18). In cells that lack the coxsackie-adenovirus receptor (CAR), the Ad5/dendron conjugates demonstrated excellent gene propagation rates. Furthermore, the branches allow for the introduction of additional functionalities within the dendron center via in situ postmodifications despite being coupled to the Ad5 surface. The surfaces covered by such branches were tested over blood protein interaction capability, which is required for forecasting how they function in the circulatory system. A recently developed approach for adding biologically active moieties across the Ad5 membrane while not chemically altering viral particles is shown in this research.[34]

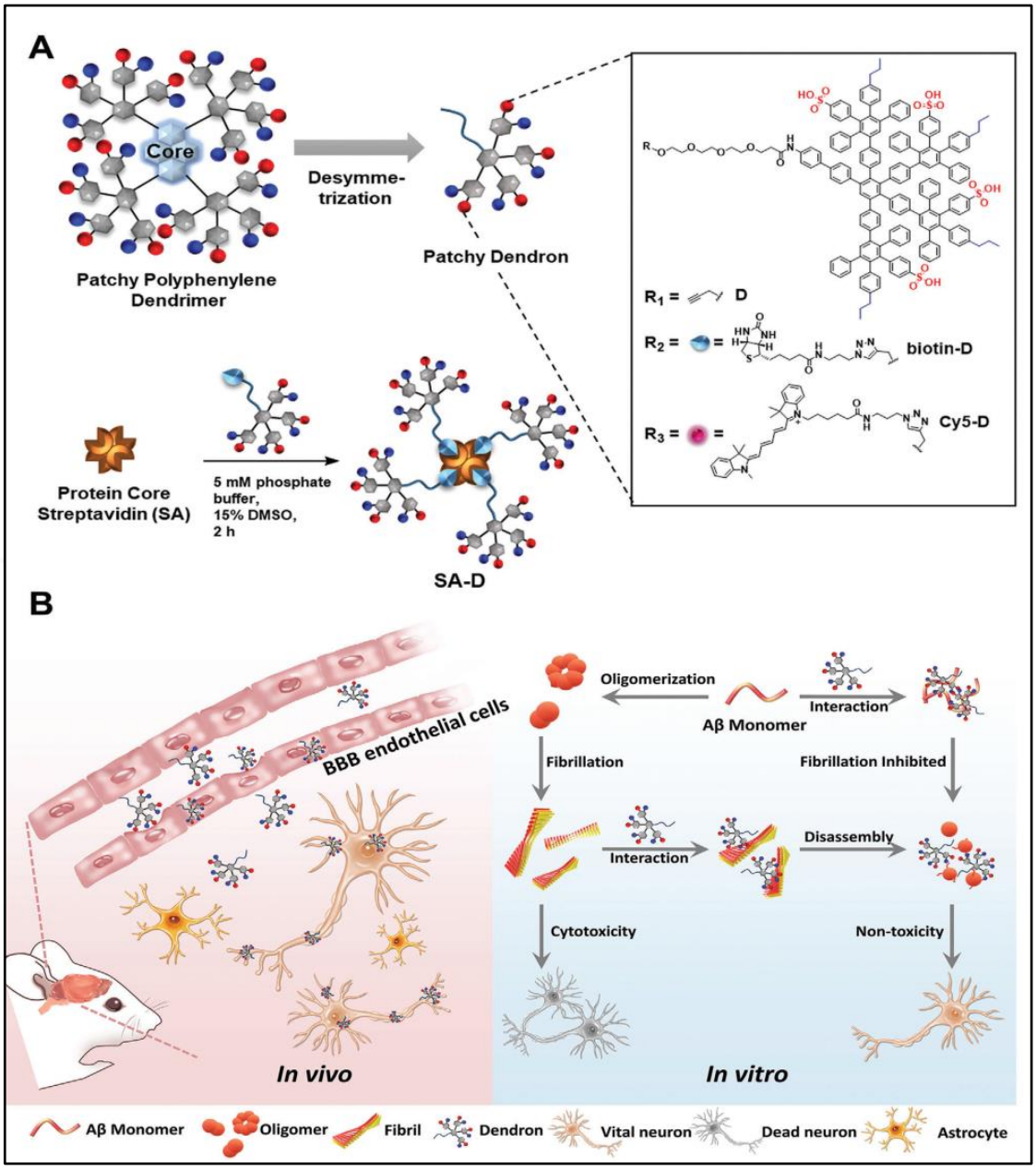

Figure 1.19. The graphical abstract for the research. The absorption of amphiphilic PPDs was found to be predominantly facilitated by nerve and vascular cells. By combining with Aβ (1-42) peptide, their antiamyloidogenic actions in vivo and in vitro were investigated. The formation of filaments was suppressed, and the generated Aβ fibrils disintegrated.[35]

Random fibrillation of amyloid-beta (A$\boldsymbol{\beta}$) deposits neurologically hazardous plaques made of amyloid and has been linked to dementia and Alzheimer's disease. The blockage of A$\boldsymbol{\beta}$ monomer folding and dispersion of produced filaments has been deemed a viable method for therapy. In 2021, Xiang et al. found that amphiphilic polyphenylene

dendrons (APDs) disrupt A$\boldsymbol{\beta}$ aggregation and decrease A$\boldsymbol{\beta}$-cell contacts. APDs, with successive adversely polarized sulfonic acid and hydrophobic n-propyl exterior pairs, attach to the backbone of A$\boldsymbol{\beta}$ agglomerates, preventing fibrillation and disassembling pre-formed fibrils (Figure 1.19). APDs show vascular cell absorption on the endosomes compatible with endothelium and nerve cells and considerable reduction in A$\boldsymbol{\beta}$-stimulated neuronal apoptosis in vitro. Furthermore, molecules are carried throughout the brain and effectively pass the blood-brain barrier following systematic therapy in mice, demonstrating their strong ability to block A$\boldsymbol{\beta}$ fibrillation in vivo. This might be crucial in designing treatment options against Alzheimer's disorder.[35]

1.4.Porosity in PPDs

Although many PPD derivatives have been synthesized, most showed limited porosity and a low S_{BET}-specific surface area- due to dense branching and strong π-π interaction, which cause a dense packing of dendrimers in the solid state.

In the research in 2018, Serenko and colleagues employed polyphenylene dendrimers with different macromolecular structures within the main parts: first- and second-generation dendrimers constructed around tetrakis(4-ethynylphen-1-yl)methane (G1-t and G2-t) (Figure 1.22). On the other hand, the researchers utilized first- and third-generation dendrimers derived from 1,3,5-triethynylbenzene (G1-b and G3-b) (Figure 1.23).[36]

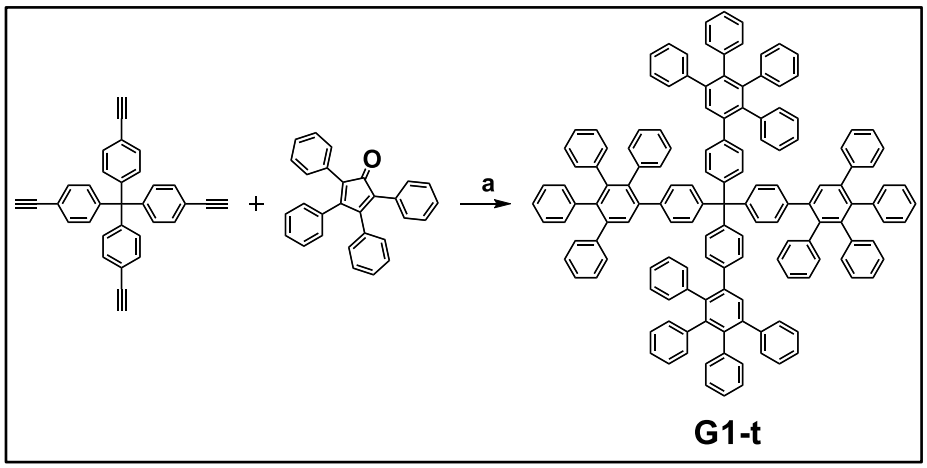

Figure 1.20. Synthesis of G1-t: a) o-xylene, 170 ^{o}C.[36]

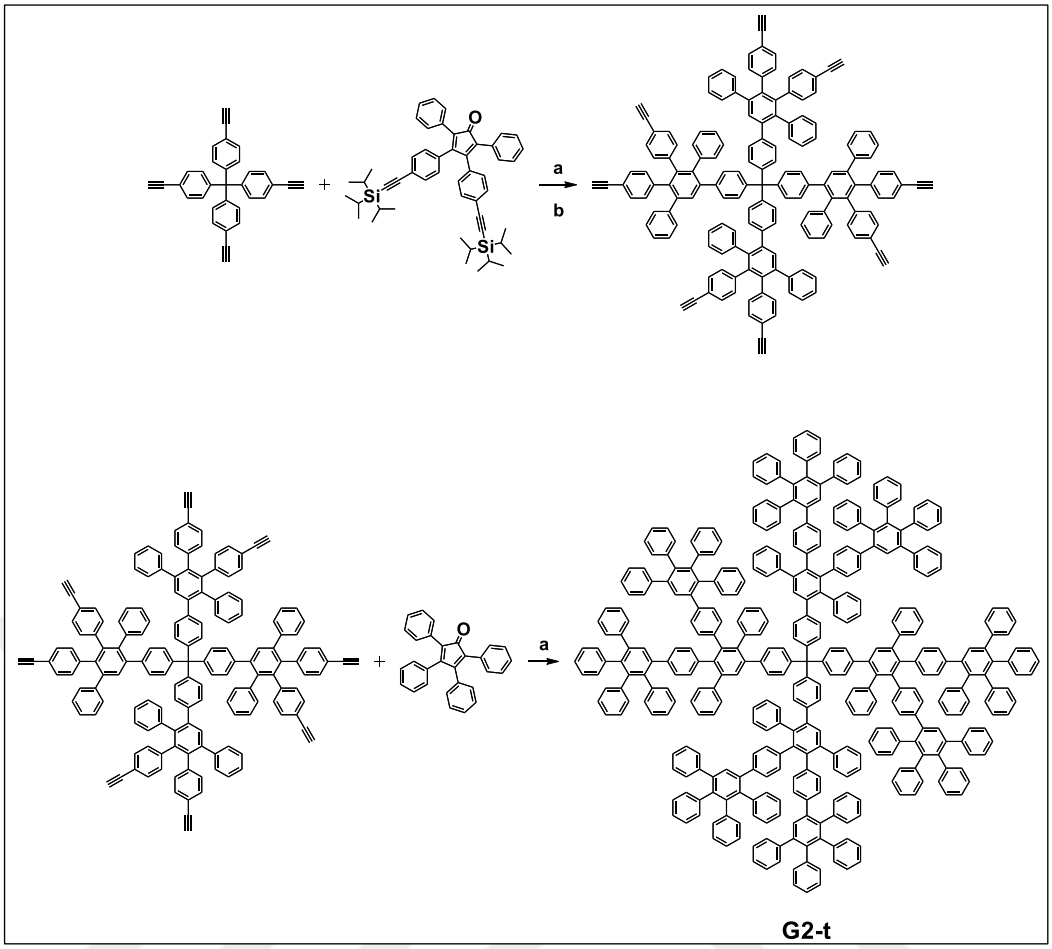

Figure 1.21. Synthesis of G2-t: a) o-xylene, 170 ^{o}C; b) TBAF, THF, R.T., 2 h.[36]

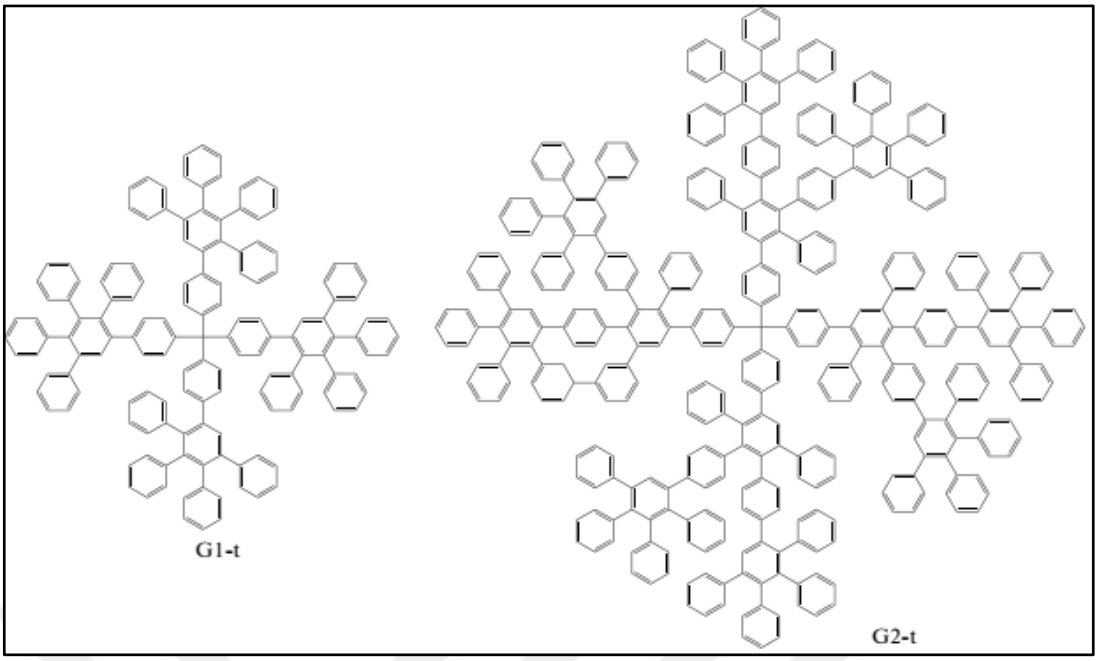

Figure 1.22. The structure of PPDs: G1-t and G2-t.[36]

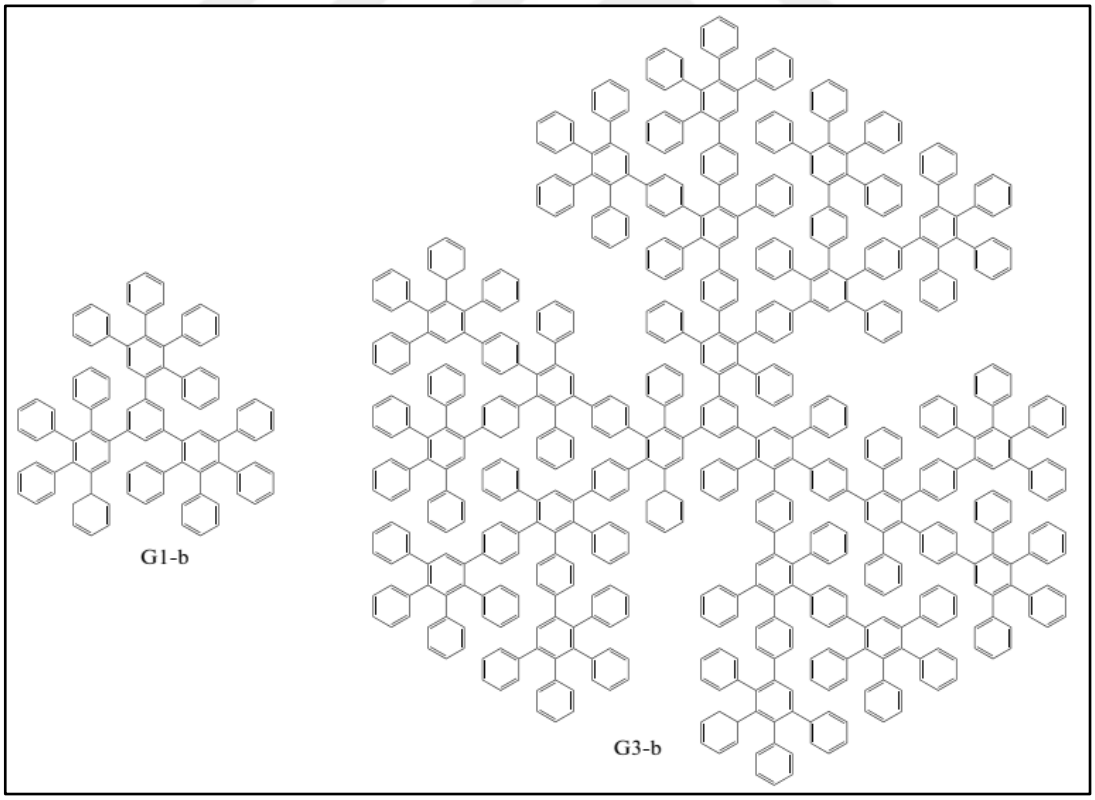

Figure 1.23. The structure of PPDs: G1-b and G3-b.[36]

Table 1.1. Adsorption characteristics of the dendrimers.[36]

Dendrimer	Pore volume, cm^3/g	Specific surface area*, m^2/g		
G1-t	0.133	28	26	30
G2-t	0.128	33	27	36
G1-b	0.229	108	40	69
G3-b	0.622	167	80	85

*Calculated from the sorption isotherms using the BET, BJH, and t-Plot methods.

Table 1.1 shows that the dendrimers have a limited specific surface area. G3-b possesses the largest specific surface area (167 m^2/g), whereas G1-t encompasses the smallest (28 m^2/g). This t-plot analysis based on sorption results demonstrated that G1-t and G2-t polymers lack of microporosity. The G1-b and G3-b dendrimers contain 0.030 and 0.033 cm^3/g micropore volumes with pore diameters of 0.35-1.50 nm, accounting for 13% and 5% for the entire pore volume, respectively. The existence of micropores results in a greater specific surface area for G1-b and G3-b compared to G1-t and G2-t, indicating less dense molecular packing. Nevertheless, the minimal micropore percentage found in both compounds leads to small specific surface area outcomes (108 and 167 m^2/g).[36]

Consequently, in highly branched first- to third-generation dendrimers with stretched spatial structures, self-assembly into nano- and microsized fragments with distinct forms and a minimal specific surface area becomes comparable and independent of the dendrimer's chemical arrangement. Dendrimeric macromolecules' microporous organization is dictated through the macromolecule's stereometry. The micropores are not present in first- and second-generation polyphenylene dendrimers as well as polypyridylphenylene dendrimers composed of tetrakis(4-ethynylphen-1-yl)methane. However, micropores are present in first- and third-generation dendrimers based on 1,3,5-triethynylbenzene, accounting for 13% and 5% of the overall pore volume, respectively.[36]

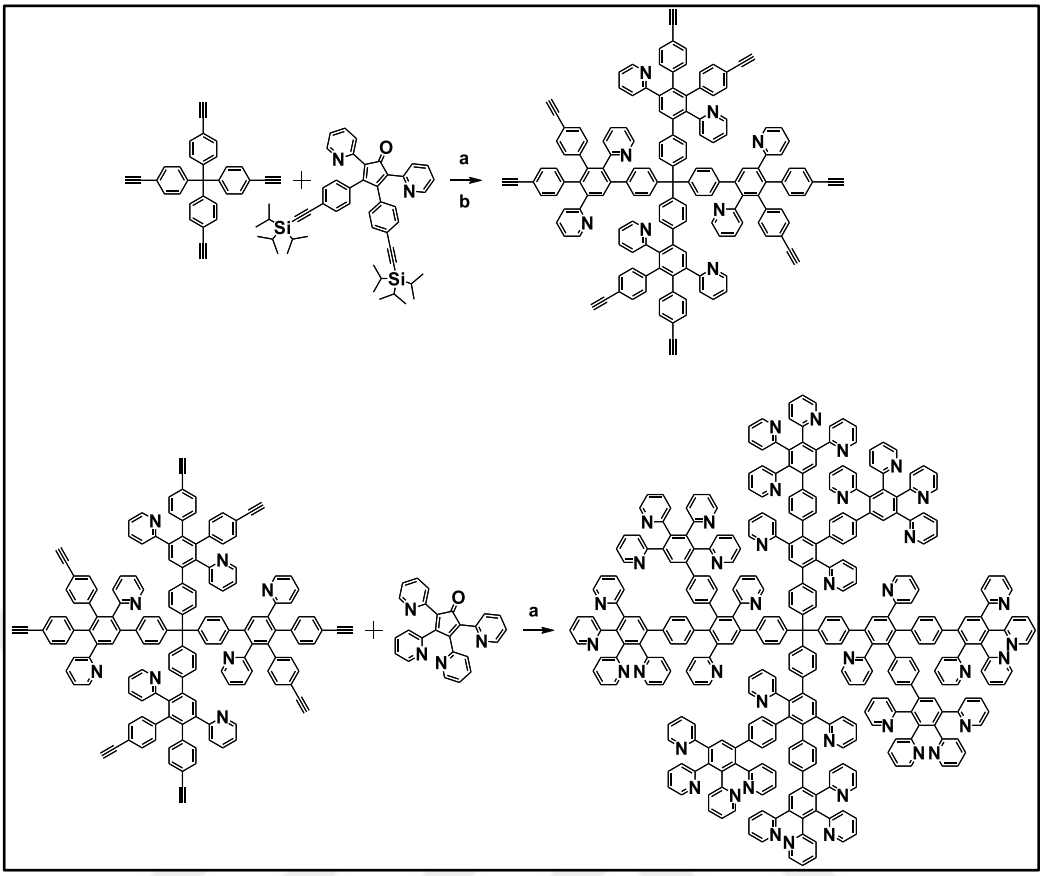

Figure 1.24. Synthesis of second generation pyridylphenylene dendrimer: a) o-xylene, 170 ^{o}C; b) TBAF, THF, R.T., 2 h.[37]

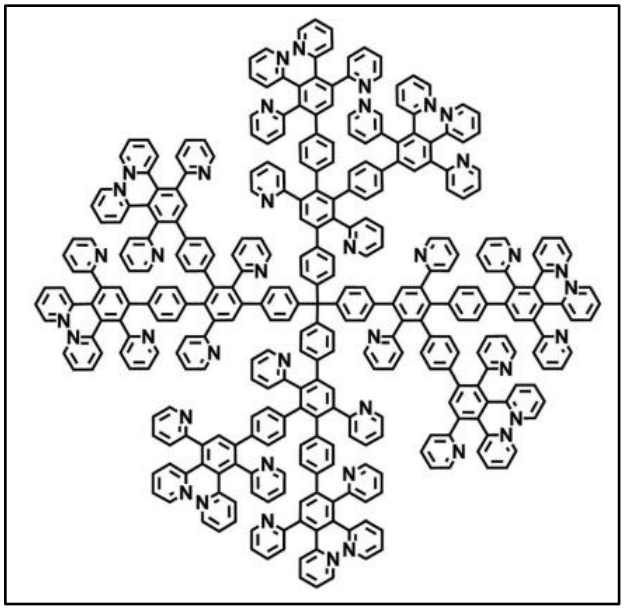

Figure 1.25. The structure of second generation pyridylphenylene dendrimer.[37]

In 2017, Serenko et al. conducted a sorption and surface characteristics investigation using the three generations of pyridyl fragmented polyphenylene dendrimers (Figure 1.24 and Figure 1.25). A BET investigation of N_2 adsorption/desorption isotherms at 77 K produced specific surface area measurements that were not more than 100 m^2 g^{-1}, although mathematical estimations projected significant volumes of pores and surface areas. Molecular dynamics simulations indicated that the discrepancy stemmed from the compact arrangement of dendrimers within the bulk.[37]

1.5. Porous Materials

Porous materials are solids that hold specific linked voids or pores throughout the material's framework.[38] The passage, exchange, adsorption, physisorption, and chemisorption properties of certain liquids or gases through the material are directly facilitated by these voids or pores.[38] These voids, regarded as pores, possess a variety of sizes, shapes, and distributions, and these properties play a vital role in defining the characteristics and potential application areas of porous materials.[39] Porous materials have many subcategories, including zeolites, silicates, activated carbons, porous polymers and metal-organic frameworks (MOFs).[38] These materials are categorized into three types according to the different sizes of pores.[39] Pore diameters are classified as follows: macropores have pore sizes larger than 50 nm, mesopores between 2 and 50 nm, and micropores less than 2 nm.[39] The configuration of void sizes, shapes, and volumes is directly related to the ability of porous materials to perform the specified function in a particular application.[39] The specific surface areas of porous materials can be measured using a technique called gas adsorption measurement.[39] N_2 gas is used mainly for this purpose. Using this approach, N_2 "adsorption-desorption isotherm" can be collected at 77 K. The isotherm includes the concentration of adsorbed/desorbed gas on the x-axis and relative pressure on the y-axis. Afterward, the surface area is determined by calculating the quantity of gas absorbed at monolayer and multilayer, according to the Langmuir and Brunauer-Emmett-Teller (BET) theories, respectively. Additionally, the adsorption/desorption isotherms make it possible to characterize the aperture, size, volume and shape of the pores using DFT calculations.[40]

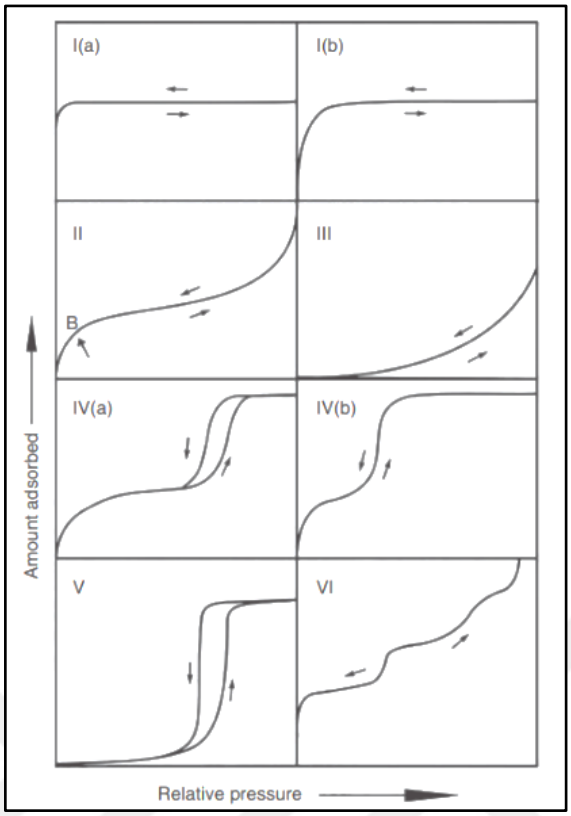

Figure 1.26. The typical isotherms to characterize pore size and shape in porous materials.[40]

Six different isotherm types that are common for particular pore types and geometries are shown in Figure 1.16. Microporous solids, particularly MOFs, exhibit high absorption at low-pressure range where micropores are filled, as shown by Type I isotherms. The two types of microporous materials that are classified under this kind of isotherm are type I(a), which consists of predominantly small pores, and type I(b), which consists of broader micropores combined with thin mesopores. Type III isotherms characterize non-porous or macroporous materials, whereas type II isotherms are linked to non-porous or micro/meso-porous materials. Moreover, mesoporous structures can be recognized by employing type IV isotherms. Next, in cases where the surface of a microporous or mesoporous material is hydrophobic, the type V isotherm is frequently observed. Last, the type VI isotherm represents the homogenous non-porous structure with layer-by-layer adsorption.[40]

1.6 Conjugated Microporous Polymers (CMPs)

There are two types of porous organic polymers: the first is made up of covalent organic frameworks (COFs) and covalent triazine frameworks (CTFs), which possess significant reversible properties within forming bonds and thus exhibit long-range order (crystalline structure); the second type is amorphous porous organic polymers, and these polymers can be constructed using the chemistry that provides rapid and irreversible bond growth, such as conjugated microporous polymers (CMPs), hyper-crosslinked polymers (HCPs), and porous aromatic frameworks (PAFs) (Figure 1.27).[41] Among many other (POPs), in this thesis, CMPs were chosen and synthesized dendrimer-based amorphous porous polymers via Suzuki polycondensation.

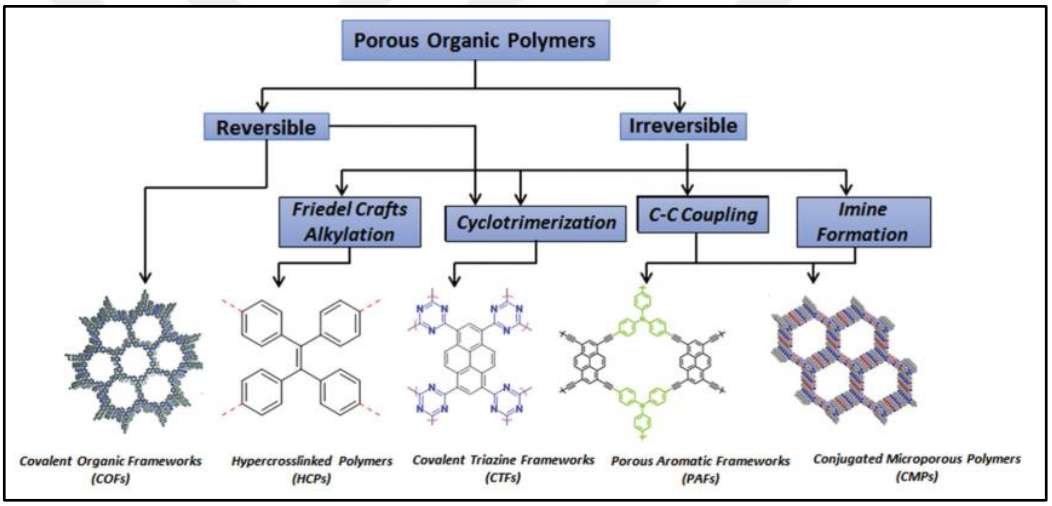

Figure 1.27. Porous organic polymer framework categories and the processes forming these molecules.[41]

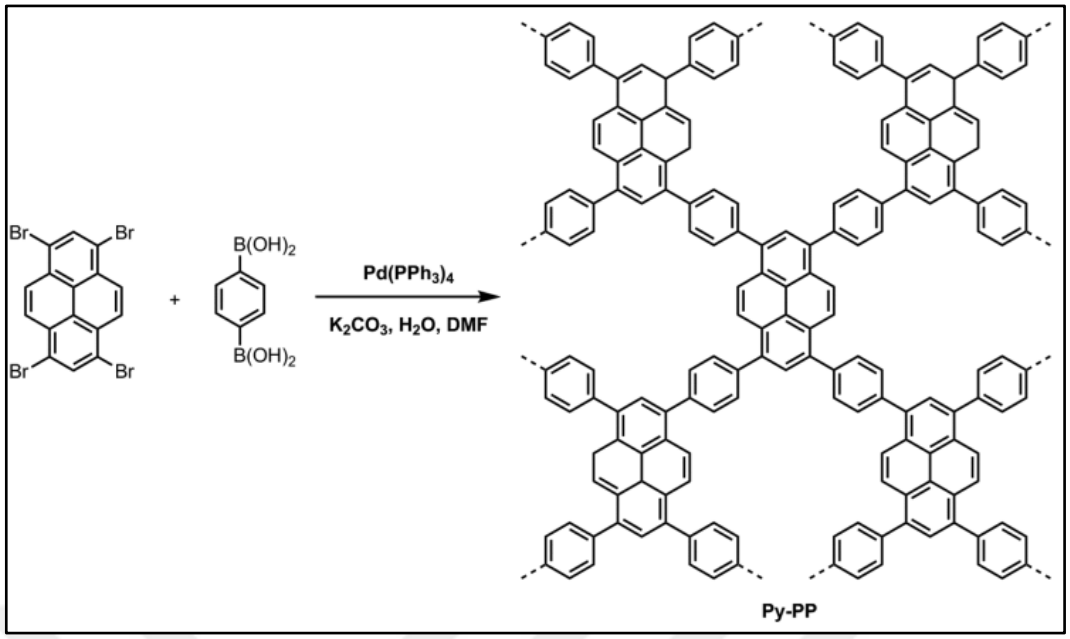

Figure 1.28. Suzuki coupling reaction to synthesize Py-PP, a CMP hosting pyrene.[42]

As a result of their rapid and irreversible bond synthesis, conjugated microporous polymers (CMPs) are one of the well-known family of POPs and do not have long-range order. Their distinct π-conjugated structure offers robust micropores, as well as their easy structural modification via the design of monomers and the versatile synthetic strategies like the Suzuki coupling reaction, Sonogashira-Hagihara reaction, Yamamoto reaction, and phenazine ring integration to connect the building blocks have all drawn significant attention and make CMPs as promising materials for a variety of application. CMPs have a large surface area, high electrical conductivity, and thermal stability as a result of their intrinsic properties, which allow them for a range of uses, such as sensing, clean energy applications, separation, photovoltaic devices, light-harvesting, photocatalysis, and catalysts.[41] Poly tetraphenyl pyrene (Py-PP) was synthesized using a Suzuki coupling reaction, showing a BET surface area of 1070 m^2 g^{-1} (Figure 1.28). Due to its hydrophobic properties, the identical network also demonstrated a substantial absorption of diesel (1200 wt%) from water.[42] Understanding CMP is crucial for our synthetic polymerization strategy, which was adapted for synthesizing porous dendritic polymers (PDendPs) through the Suzuki coupling reaction.

CHAPTER 2

CHEMIRESISTORS FOR VOLATILE ORGANIC COMPOUNDS

2.1. An Overview

Because of the abundance of poisonous, flammable, and dangerous gases in the environment, industry, and even homes, there is a growing interest in developing high-performance gas sensors.[43] To meet this demand, a variety of chemical sensors have been developed and built to detect and monitor these gases.[44] Colorless and poisonous gases not only have the potential to irritate the human respiratory system, but they may also constitute a substantial hazard to the environment, especially at high concentrations.[45] Because of their wide variety of applications, including manufacturing, purification, and refrigeration, these gases have received a lot of attention in the literature.[46] Gas sensors are often made from sophisticated functional materials such as metal oxides, composites, polymers, and carbon-based materials like CNTs and graphene.[43] Conventional sensor technologies usually lack sensitivity and selectivity, have long reaction times, poor recovery, and need high operating temperatures.[47] Recognizing and minimizing these constraints is critical for increasing the efficacy and utility of the sensors.[47]

2.2 Literature Study

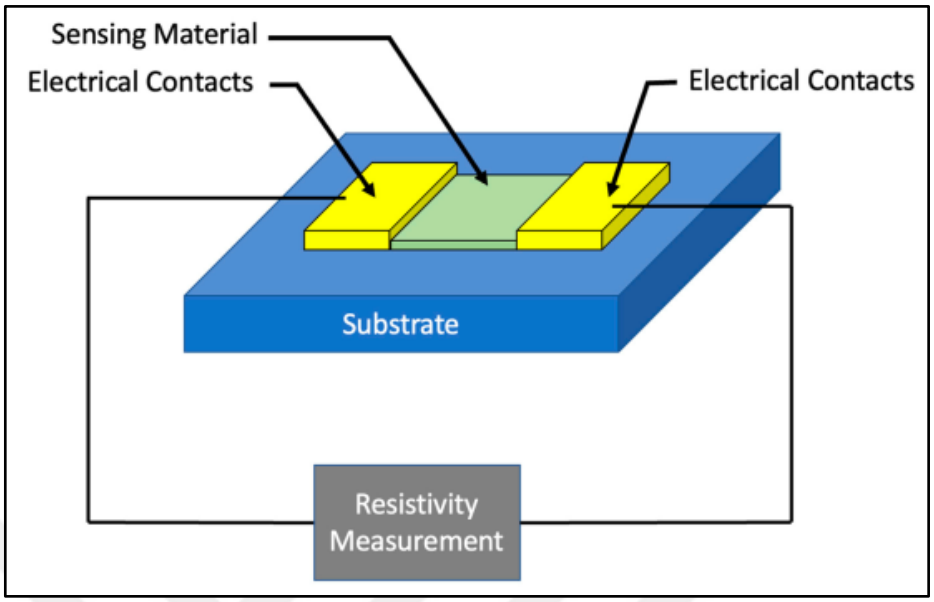

Figure 2.1. Schematic for a simple chemiresistor.[48]

Chemiresistive gas sensors run depending on the changes in electrical resistance of a sensing material in response to the presence of a target volatile organic compound in the atmosphere.[49] Such sensors are often employed to monitor and detect volatile organic compounds (VOCs) in a variety of applications, including environmental surveillance, safety in industries, and ventilation control.[49] These are especially outstanding for detecting VOCs consisting of benzene, toluene, xylene, and formaldehyde, which could lurk in various industrial and household products and adversely affect human well-being.[50] Chemiresistive gas sensors are often made of two electrodes and a sensing material like metal oxides, conductive polymers, and carbon-based materials such as CNTs and graphene.[51] The commonly used sensing materials for chemiresistors are inorganic, organic, and organic-inorganic composites (Figure 2.1).[43,48] The types of functional materials can be considered as noble metals, metal oxides or sulfides, carbon nanotubes, graphene and graphene oxide, conducting polymers, organic-inorganic composites.[43] Among metal oxides, SnO_2, TiO_2, In_2O_3, WO_3, ZnO, Fe_2O_3, CuO, of carbon-based materials, graphene and graphene oxide carbon nanotubes have been frequently used.[43] Polyaniline, polypyrrole, poly(3,4-ethylenedioxythiophene) (PEDOT) are the most preferred conducting polymers.[43]

Once volatile organic molecules can be found in the air, they interact with the sensing material, creating a shift in electrical resistance, which may then be quantified and linked to the quantity of the volatile organic chemical in the air.[51] Chemiresistors have many advantages, including low-cost, shrinkable, and fast-response.[47] Furthermore, chemiresistive gas sensors are noted for their remarkable selectivity, allowing them to detect and differentiate between many volatile organic molecules.[52] These additionally have the advantage of being extremely sensitive, detecting even minute levels of VOCs in the air.[52]

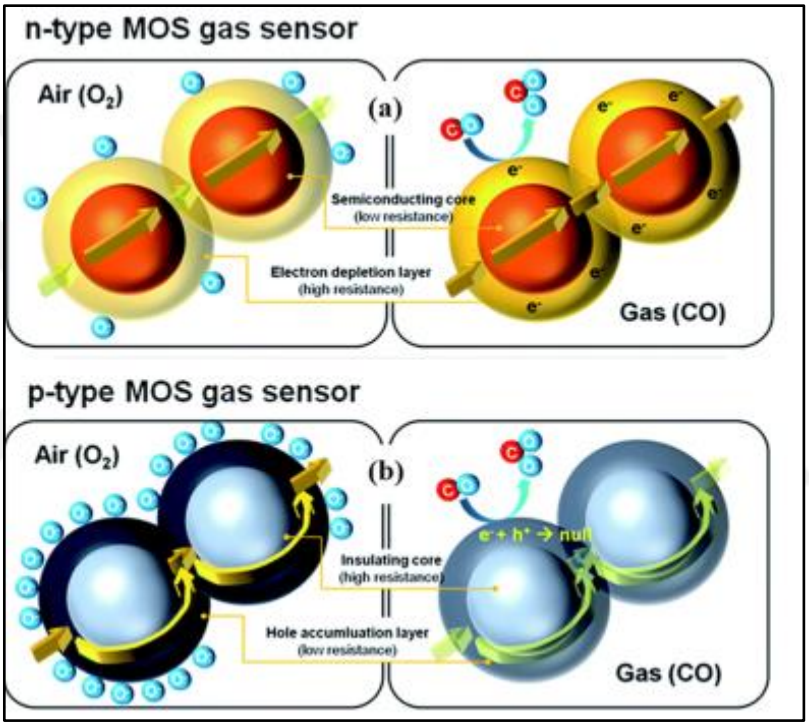

Figure 2.2. The MOS-based sensing approach for n-type and p-type chemiresistors.[49]

Chemiresistors are in high demand in chemistry and materials science for detecting and measuring changes in chemical composition or concentration.[48] These sensors are categorized into two types, including n-type and p-type chemiresistors regarding the sensing materials employed in the applications (Figure 2.2).[49] The electrical working principles of n-type and p-type materials differ due to the effective charge carriers responsible for conductivity.[49] To explain in detail, the excess of electrons plays a vital role as the effective charge carrier in the n-type semiconductor systems, thereby allowing them to transport electricity via the flow of electrons.[49] In reverse, the overabundance of holes is the predominant charge carrier in the p-type chemiresistors,

which results in the conduction of electricity via holes.[53] To put it simply, n-type sensing systems employ numerous negatively charged electrons, whereas p-type chemiresistors have excess positively charged holes.[53] The comprehension of this variation in electrical characteristics and major charge carriers is critical for the effective operation of chemiresistor systems.[53] The interaction of chemical vapours shows a distinction between n-type and p-type sensing materials used in chemiresistors.[49] In the n-type gas sensors, the electrical resistance decreases with their interaction with reducing gases because these systems are more receptive to these volatile compounds due to their plethora of electrons that facilitate simple contact with them.[49] In contrast, the electrical resistance increases when subjected to oxidizing gases.[49] Comparatively, p-type chemiresistors experience the opposite output.[49] Figure 2.2 provides a graphical illustration of this phenomenon.[49] In general, the electrical behavior, effective charge carrier, and receptivity to different target gases of n-type and p-type chemiresistor systems determine their main differences.[49]

2.3. Sensing Materials

Advances in material research have had a significant influence on the fabrication of sensors, notably chemiresistors.[43] These breakthroughs have resulted in the discovery and application of nanomaterials such as noble metals, silicon, and metal oxide nanoparticles, conducting polymers, carbon nanotubes, and metal nanowires.[43] These nanostructures possess distinct physical and chemical characteristics, making them perfect options for chemiresistors.[48] Their increased chemical response, even at ambient temperature, enables sensitive recognition of target analytes or gases.[48] These nanomaterials may be produced and tailored for sensing efficiency.[54] Moreover, research on gas sensors has demonstrated the promise of nanomaterials in sensing applications.[54] In summary, the utilization of nanomaterials in chemiresistors has enormous promise for creating high-performance sensors.[48] Herein, many examples of literature on sensing materials were provided in this section for further understanding of the structure-properties relationship.

A summary of the sensing materials commonly used for chemiresistor applications was provided in Table 2.1. As understood from the table, metal oxides have a general drawback, like high operating temperature, which makes their applicability stringent as a chemically-resistant tool. On the other hand, carbon-based materials such

as graphene, RGO, GQDs, and conjugated polymers like PPy and PANI operate at room temperature and possess higher sensitivity in the trace amount of target gases. These findings motivated us to work on carbon-based PDendPs as active materials for chemiresistive gas sensing.

Table 2.1. Sensing material commonly used for chemiresistor applications.[55]

Sensing material	**Operating temp.**	**Response (%)**
Graphene	RT	1.87 (1 ppm)
Ni/Ce-SnO_2	215 °C	87 (100 ppm)
Ce-SnO_2	250 °C	84 (100 pmm)
ZnO	500 °C	71 (100 ppm)
ZrO_2	RT	50 (10 ppm)
$La_{1-x}Sr_xCoO_3$	RT	10 (10 ppm)
PPy/PANI	RT	1.19 (2983 ppm)
SnO_2-RGO	RT	2.19 (10 ppm)
PANI/Ni-Pc	RT	50 (150 ppm)

2.3.1. Noble Metals, Metal Oxides, or Sulfides for VOCs sensing

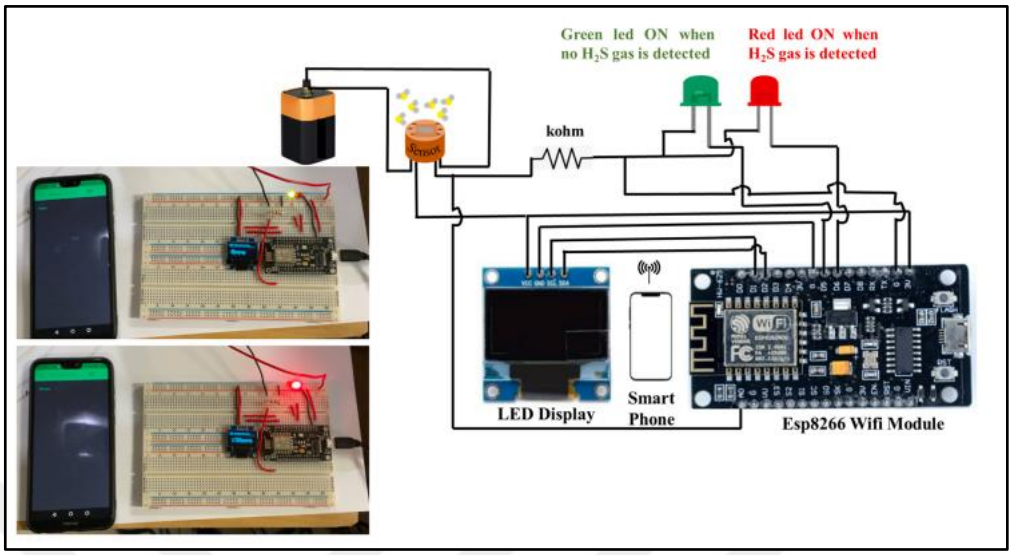

Figure 2.3. Pd-anchored device prototype connected with IoT platform.[56]

Kumar et al. have recently invented a new manufacturing process for H_2S gas sensing models that employ a noble metal-containing metal oxide semiconductor (MOS) strategy. $CuCrO_2$-recognizing thin films were grown on SiO_2/Si surfaces adopting the RF blasting technique. Pd nanoparticles, recognized for their outstanding gas-sensing catalytic characteristics, were subsequently fabricated onto $CuCrO_2$ coatings by applying DC deposition with various sputtering periods of 3, 6, 9, and 12 seconds. The obtained nanorice shape improves the uptake of gases and captures more target analytes. Sputtering Pd through 9 seconds significantly increased H_2S detection compared with other gases. Pd-coated $CuCrO_2$ surface experienced the greatest 72.3% response after exposure to 50 ppm H_2S, with a detection limit of 0.5 ppm. These findings were obtained at the high operating temperature of 150 ^oC. The technology was transferred to construct a sensor component for the working model that includes integration into the Internet of Things. The prototype hyperlinks to Wi-Fi and then to a smartphone via a hotspot on the phone. Therefore, the findings from this study will assist to speed the deployment of IoT-enabled sensors, paving the path towards an environmentally friendly future platform (Figure 2.3).[56]

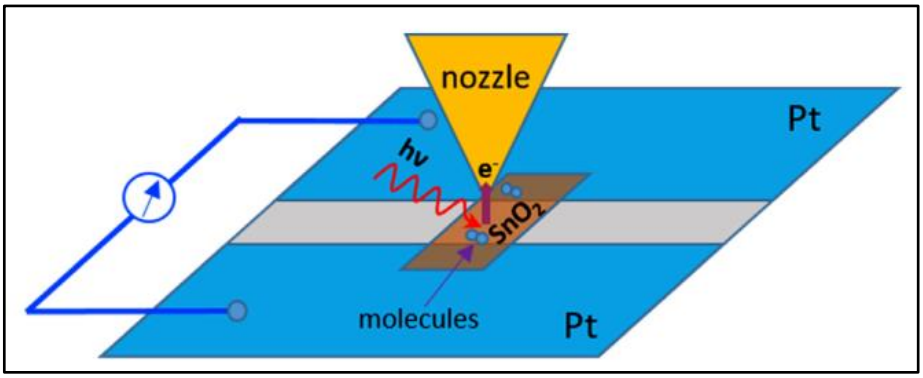

Figure 2.4. A visual representation illustrates the underlying idea of metal-based SnO_2 sensor's in-situ measurement supported by NAP-XPS analysis.[57]

Vorokhta and colleagues provided the findings of a research study through the chemical reactions occurring around the exterior of a SnO_2-based chemiresistor in various atmospheres at relatively high operating temperatures (450 and 573 K). The fundamental approach for nanoscale investigation was Near Ambient Pressure X-ray Photoelectron Spectroscopy (Figure 2.4). The capacitance and DC sensitivities of the SnO_2 layer were measured in situ, giving information regarding macroscale activities for gas detection. The shift monitored in sensor conductivity along with ethanol exposure indicates the chemisorption process between the sensor's surface and ethanol molecule. This phenomenon was proved by the temporary absence of the band stretching result and the discovery of various carbon based moieties from the sensor's exterior within the XPS analysis. Moreover, the NAP-XPS spectra revealed that the nanostructured material tin oxide undergoes a partial reduction even when subjected to clean oxygen at 573 K. The combined exposure of the sensor to O_2/EtOH could not substantially enhance the surface reduction which is most likely caused by the slow rate of the ethanol reduction procedure and the quick oxygen reoxidation kinetics. Nevertheless, the data confirms that the periphery of chemiresistor is progressively polluted with carbon accumulation.[57]

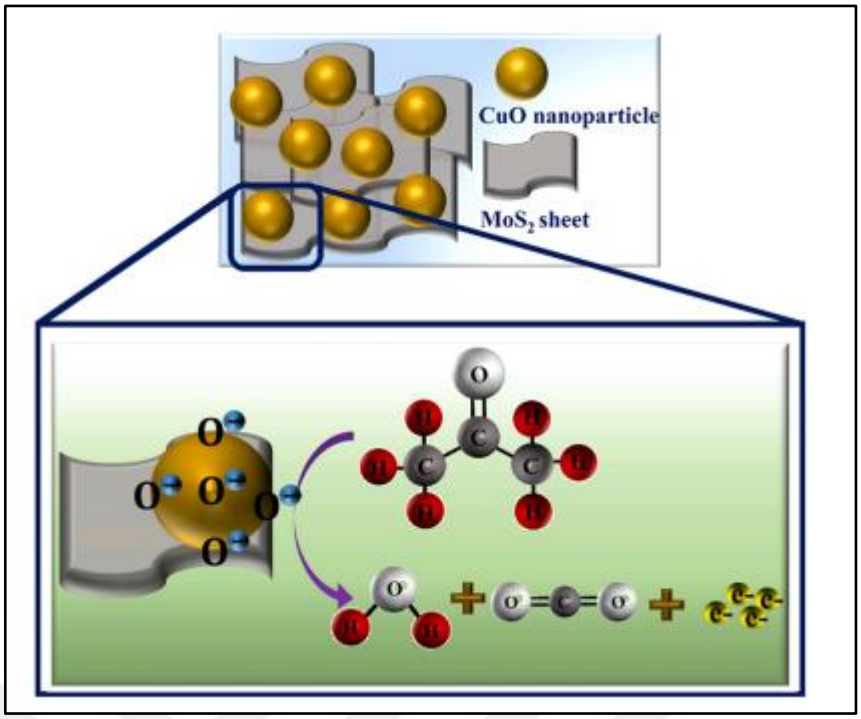

Figure 2.5. The principle of MoS_2-CuO nanocomposite chemiresistor for sensing acetone vapor is schematized in this image.[58]

In 2022, Roy and colleagues established the chemiresistor to sense acetone vapor at ambient temperature using molybdenum disulfide (MoS_2)-copper oxide (CuO) composites (Figure 2.5). The topological and physical properties of the crystalline structure and adhesion of CuO nanoparticles to MoS_2 nanosheets were studied utilizing conventional material characterization methods. The recognition capabilities were thoroughly tested by subjecting the MoS_2-CuO chemiresistor system to changing levels of acetone vapor. The sensor device, which has significant sensitivity, rapid response, recovery time, and a detection limit of 93 ppb, demonstrated an outstanding sensing performance toward acetone. Finally, the device demonstrated excellent reliability, consistency, and stability, indicating significant potential application areas for acetone gas detection in medical care, nature, and industry.[58]

2.3.2. Carbon-based materials for VOCs sensing

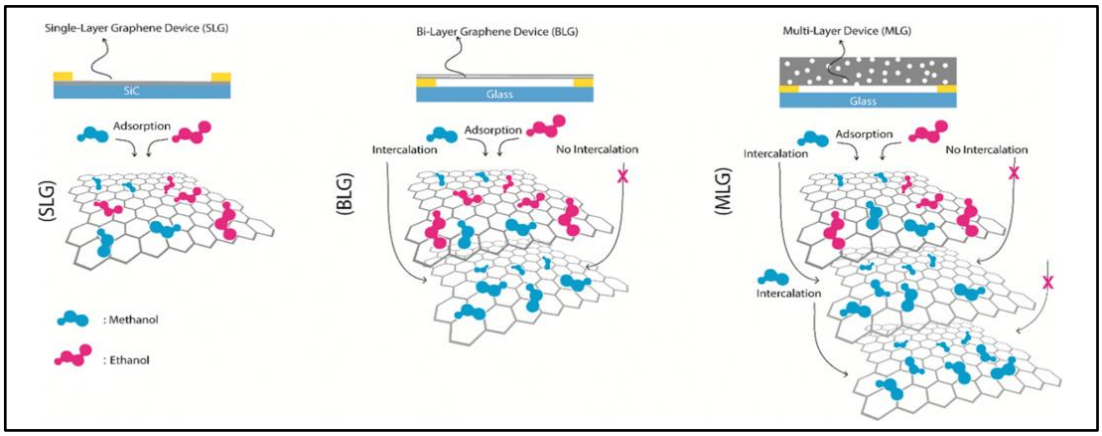

Figure 2.6. The scheme demonstrates MeOH/EtOH detection capacities of chemiresistors SLG, BLG and MLG which are formed in three distinct morphologies.[59]

Along with identical molecular composition and functional groups, primary alcohol is particularly challenging to sense in chemiresistor applications. To overcome this problem, Inanc et al. have prepared single-layer, bi-layer, and multi-layer graphenes with different morphologies to investigate the differential methanol–ethanol features (Figure 2.6). Chemiresistive gas sensors composed of three graphene topologies show distinct MeOH-EtOH reactions due to distinct intercalation of MeOH inside layers of graphene morphologies vs. EtOH. Density functional theory simulations confirm that EtOH molecules adsorb more efficiently on graphene surfaces than MeOH molecules, preventing intercalation in multilayer graphene structures. Increasing the number of graphene layers leads to more MeOH intercalation, resulting in various MeOH-EtOH reactions. The findings from this study imply that selective and sensitive MeOH tests may be developed employing multiple graphene patterns using a multifunctional sensor array configuration.[59]

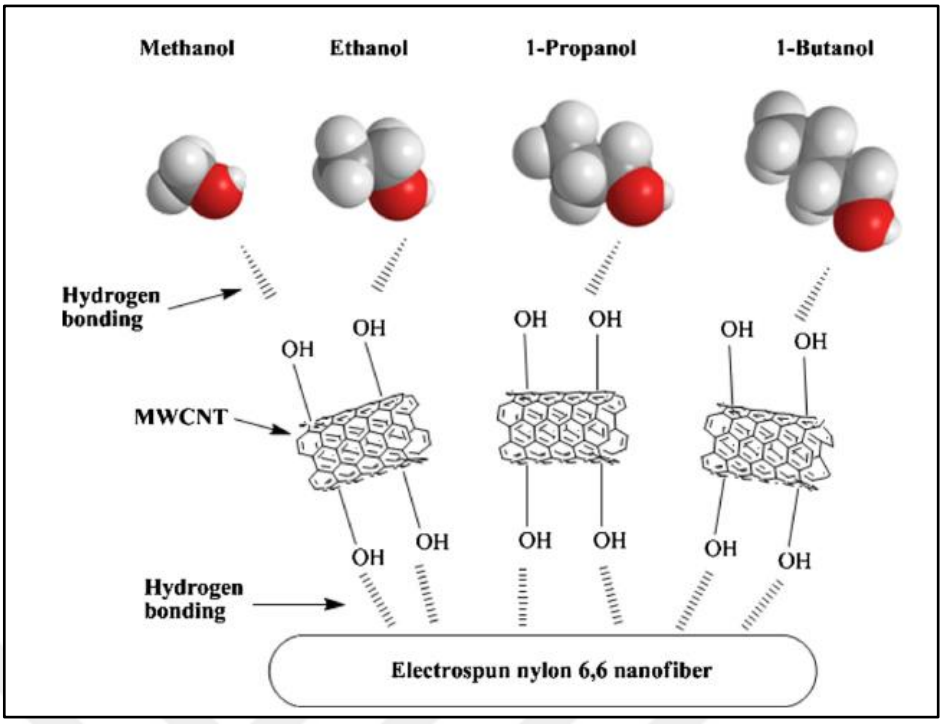

Figure 2.7. The detection strategy to alcohol gases with low molecular weight by a nanocomposite consisting of MWCNT-OH connected electrospun nylon 6,6 nanofibers.[60]

Choi and co-workers generated MWCNT-OH adsorbed electrospun nylon 6,6 nanofibers using the electrospinning and dip coating approach in this study (Figure 2.7). The pristine electrically spun nylon 6,6 nanofibers received 0.056 wt% of MWCNT-OH with an electrical conductivity of 5.24×10^{-3} S cm^{-1}. The sensing characteristics of this chemiresistor were examined regarding its response to small molecular weight alcohol vapors, including methanol, ethanol, 1-propanol, and 1-butanol. This sensor's electrical impedance changed due to weak hydrogen bonding between alcohols, hydroxyl groups upon MWCNT-OH, and amide clusters in nylon 6,6. The constructed sensor demonstrated significant reversibility and repeatability throughout the trials.[60]

2.3.3. Conducting polymers for VOCs sensing

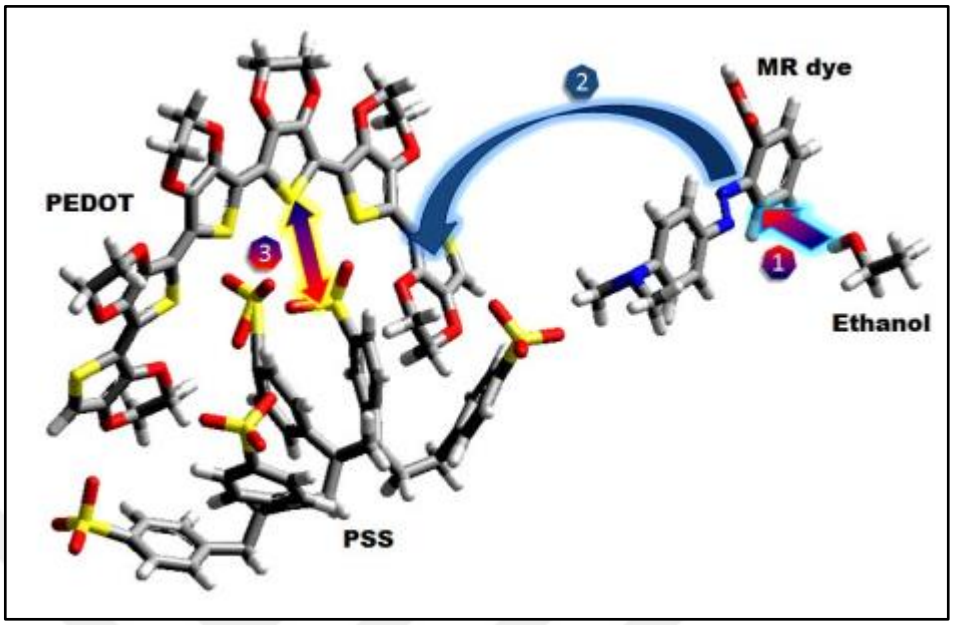

Figure 2.8. A chemiresistor system composed of conjugated polymer complex or composite (PEDOT:PSS) doped with Methyl Red (MR) fluorescent molecule to sense ethanol vapor.[61]

Dos Reis et al. in 2010 coated the conducting mix of poly (3,4-ethylene dioxythiophene) and polystyrene sulfonated acid (PEDOT-PSS) polymers using Methyl Red (MR) dye in the acidic version and acted as the active material of a chemiresistor to sense ethanol vapor (Figure 2.8). Chemical vapor deposition and spin-coating methods were used to produce this Au-Polymers-dye combination for the device. The metal electrodes were deposited onto the surface of the glass initially, followed by the fabrication of an organic thin film with an active surface of around 1.0 mm². This sensor operates based on electrical resistivity with atmospheres including ethanol vapor transported by N_2 gas and vapor. It possesses a sensitivity of 1.15 for a detection limit of 26.25 ppm analyte operating at room temperature. Also, it is reversible with a minimal electrical consumption of 20 μW. Atomic Force Microscopy (AFM) investigated the thin film shape of ~200 nm thickness, revealing a granulometric interface conducive to adsorption. This method of combining PEDOT-PSS doped with MR dye to make a blend film performs well as a chemiresistor.[61]

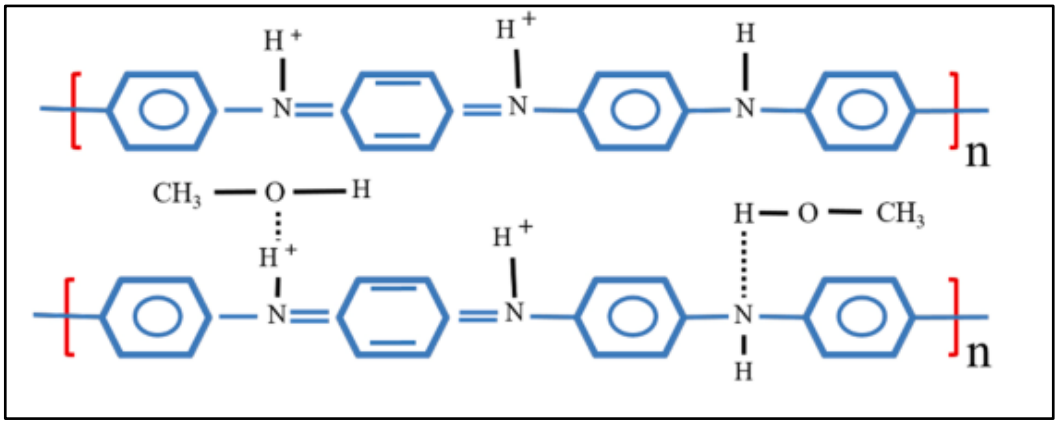

Figure 2.9. PANI and PANI/AC blends for methanol vapor detection mechanism.[62]

Kumar et al. in 2023, towards the production of an innovative chemiresistor operating at room temperature to sense methanol, polyaniline (PANI), and activated charcoal (AC) composites with changing concentrations of activated carbon from 5-10 to 15-20 wt. % prepared for these applications (Figure 2.9). FT-IR analysis was employed for pure and PANI nanocomposites to verify the targeted materials' synthesis. The semi-crystalline structure of PANI nanocomposites was also established by XRD spectra. Moreover, in the changing methanol concentrations in ppm scales, the prepared samples have been applied as a chemoresistive sensor. The concentration of carbon black as an additive in the PANI matrix increases, the sensing material's response increases in terms of the ppm value. The composite of PANI/AC (20 wt.%) had the highest sensitivity to methanol with 42.54% resistivity change, at 200 ppm level. Furthermore, age and humidity did not significantly affect AC-PANI composites' detecting capacities, making it an extremely favorable sensor. Finally, these materials are environmentally friendly, cheap, selective, sensitive, and robust for methanol vapor sensing. Therefore, these features make them a promising choice for the fabrication of industrial methanol sensors.[62]

2.3.4. PPD for VOCs sensing

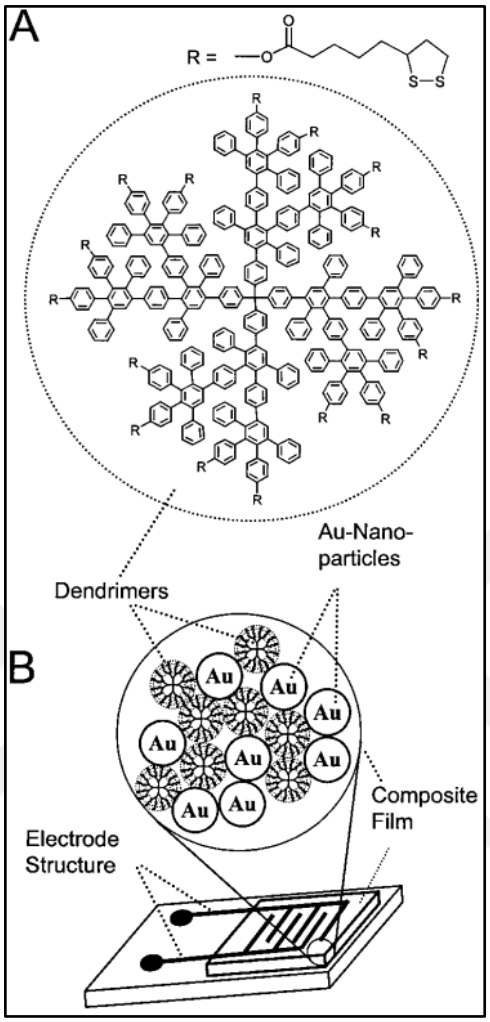

Figure 2.10. A) PPDs utilized for layer-by-layer gold nanoparticle coating B) A graphical illustration of the gold nanoparticle/dendrimer layer framework, as well as the electrode structure utilized to electronically access the film.[63]

Vossmeyer et al. in 2002 applied disulfide-functionalized PPDs on gold nanoparticles to fabricate layer-by-layer composite films (Figure 2.10). Dendrimers crosslinked particles through film accumulation allowed for step-by-step production of dynamically fortified films with exact thickness control. In chemiresistive sensor application device, this film demonstrated significant sensitivity towards toluene and trichloroethylene, which are highly toxic vapors. The material's quick reaction times, great sensitivity to VOCs, and low susceptibility to moisture make them an ideal candidate for applications in sensor technology.[63]

2.4. Target Gases

This part provides descriptions and lists of some significant gases in environmental pollution monitoring, welfare, and the manufacturing sector. Chemiresistor devices for every type of target gas have been explored and employed in many areas.[43] In this thesis, studies based on combustible solvent EtOH as a target gas have been completed using PDendPs as sensing materials.

Volatile organic compounds (VOCs): These substances include carbon-derived organic molecules such as halogenated compounds, aldehydes, alcohols, ketones, aromatic compounds, etc. VOCs are an essential ingredient to air contamination, and their releases from both external and internal sources are escalating as a result of expanding economic growth and urbanization. Excessive amounts of VOCs could lead to health problems or severe illnesses like cancer.[64]

Hydrogen (H_2): The colorless, combustible gas produces exploding combinations with the atmosphere. It is the most plentiful element in the cosmos; if not, it is very uncommon in the Earth's surrounding environment. It can be considered mainly an artificial product that serves as an additive in the chemical sector, gasoline, a power source, and a chiller in electrical power plants.[65]

Ammonia (NH_3): The irritating gas that has an unpleasant odor is utilized in fertilization for intensive cultivation, sanitary goods, textile manufacturing, and refrigeration gas. In excessive amounts, it has the potential to pollute the atmosphere, land, and water, as well as cause serious adverse effects on human health.[66]

Water vapor (H_2O): The planet's major greenhouse gas absorbs greater amounts of heat than carbon dioxide, and its quantification and regulation are critical in many fields, including weather science, health care, business, and farming. However, water vapor is important since it interferes with many gases that may be identified, whether they are contaminants or not. Therefore, the comprehension of humidity is the critical element that defines how moisture affects the sensor's reaction.[67]

Oxygen (O_2): Oxygen is the primary gas required for existence and one of the three principal elements of the planet's atmosphere, along with nitrogen and argon, accounting for around 21% of the total volume. In enclosed places, O_2 concentrations can drop significantly, posing a considerable health risk. It is employed to cure physiological

disorders, industrial and combustion procedures, and the automobile industry; when combined with gasoline, it provides better performance and lowers fuel usage.[68]

Ozone (O_3): This is an atmospheric gas featuring an appealing smell that may cause irritation and damage humans. It is abundant in the ozone layer and screens the sun's ultraviolet radiation, potentially harming life on Earth. In the ground-level atmosphere, it is an indoor contaminant that promotes respiratory malfunction and exacerbates breathing problems.[69]

Carbon monoxide (CO): The combustible gas is produced by burning hydrocarbon-based fuels. Because its propensity for hemoglobin is greater than that of oxygen, since CO levels in the atmosphere exceed, it clings to hemoglobin, impeding O_2 transport in the metabolism. The effects include oxygen deprivation, tissue damage, heart disease, and fatality.[70]

Carbon dioxide (CO_2): The colorless gas is employed as a reagent in photosynthesis by plants to produce oxygen and glucose, and it is formed throughout inhalation in living organisms. Moreover, this can also be generated within the combustion cycle reaction. This is a primary gas causing the formation of greenhouse gases.[70]

Hydrogen sulfide (H_2S): The combustible gas with an unpleasant odor is formed via volcanic activity, organic substance degradation, and fossil fuel burning. Many industrial processes, from food manufacturing to leather tanning and oil refinery, also yield hydrogen sulfide as a by-product. It may cause physiological implications like lung disorders as well as the nervous, heart, kidneys, liver, and hematological systems.[71]

Sulfur dioxide (SO_2): The gas with a suffocating odor represents one of the most significant atmospheric contaminants. Its interactions with various compounds have a broad spectrum of detrimental medical and ecological effects, including pulmonary ailments, eye disabilities, and acid rain. Prolonged SO_2 intake can harm the eyes, lungs, and throat.[72]

Nitric oxide (NO): The poisonous gas can be considered a by-product of the burning of fossil fuels. This gas constitutes one of the most significant contaminants in the air. Its excessive amounts act as a biomarker in a person's respiration, thereby indicating pulmonary inflammation.[73]

Nitrogen dioxide (NO_2): Harsh NO_2 gas is created during the burning of fossil fuels and the oxidization of nitrogen. It can be observed in high-traffic areas and is created

interiors by heating. It is an acidifying contaminant that triggers acid rains and is potentially harmful at minimal concentrations. The contact with it induces illnesses of the respiratory tract, which can lead to mortality.[74]

Methane (CH_4): The combustible gas occurs via the breakdown of several organic substances in the absence of oxygen. The gas is recovered from subsurface mines and is frequently mixed with various hydrocarbons. It can be defined as a type of greenhouse gas emitted mainly by waste dumps degradation, fossil fuel processing, and livestock digestion.[75]

Ethylene (C_2H_4): This opaque gas is used as a chemical sector starting material to manufacture other VOCs and other plastics, such as polyethylene. Additionally, it aids in the maturation of tropical fruits. Ethylene may be considered an indicator hormone that initiates the maturation process of fruits, as well as a cue for the maturity of fruits.[43]

Acetone (C_3H_6O): The transparent, combustible liquid is primarily applied as a solvent in industry. It is a physiological indicator linked to certain biochemical illnesses, such as hyperglycemia.[43]

Ethanol (C_2H_5OH): The combustible gas with low cytotoxicity serves as a different fuel, cleaner, and solvent used for resins and paintings. The ethanol can be processed in the human body, with just a tiny quantity excreted via urine, perspiration, and inhaled air. This indicates a biological indicator associated with alcohol intake.[76]

Formaldehyde (CH_2O): The transparent, poisonous gas can cause cancer. Moreover, it is primarily employed in the creation of polymers as well as other chemicals used to construct manual labor, coverings, and isolating foams, all of which emit molecules of formaldehyde into the surroundings over time.[77]

Chlorine (Cl_2): A gaseous form possesses a powerful odor and is exceedingly hazardous. Chlorine has applications in the chemical and medical sectors to purify water and household cleaning goods. The excess amount of this gas may have a high level of toxicity and irritation.[78]

Benzene (C_6H_6) and Toluene (C_7H_8): These substances are transparent, poisonous, and cancerous chemicals with a distinctive smell that are inherently contained in petroleum-based goods and are then discharged into the surrounding environment after partial combustion in transportation. Chemicals are employed in the manufacturing sector as solvents for pigments, gums, and sealants.[50]

Liquefied petroleum gas (LPG): This fossil fuel, made mostly of gaseous hydrocarbons, is widely used in home and industrial settings to create electricity and operate heaters. This also has applications as a vehicle fuel. This is a highly explosive gas.[79]

CHAPTER 3

EXPERIMENTAL METHODS

3.1. General Methods

All reagents were purchased from commercial suppliers (Sigma-Aldrich, Fluorochem, and Merck) and used without further purification unless otherwise noted. All dendrimers were synthesized according to literature procedures and isolated by column chromatography using common organic solvents as eluent and precipitation in different solvent or solvent mixtures.[83] Nitrogen (N_2) sorption isotherms were measured at 77 K using a Micromrititcs 3flex gas sorption analyzer. Before measurement, the samples were degassed under vacuum at 130 °C for 12 h. The Brunauer-Emmett-Teller (BET) method was used to calculate the specific surface areas. TGA analysis was done on a Perkin Elmer Diomand TG/DTA. ^{1}H NMR spectra were collected using a MERCURYplus-AS 400 and a Varian NMR 400 MHz Nuclear Magnetic Resonance Spectrometer. Chemical shifts were calibrated using residual solvents signals ($CDCl_3$: δ (H)= 7.26) or TMS. FT-IR spectra were recorded using a Perkin–Elmer Spectrum 100 at R.T. All samples were prepared as KBr pellets. SEM images were collected using FEI QUANTA 250 FEG scanning electron microscope. EDX analysis was performed using ZEISS EVO10. XRD measurements were performed on a Bruker D8 Advance.

3.2. Synthetic Methods

3.2.1. Synthesis of 1,3,5-tris-(1-trimethylsilylethynyl)benzene:

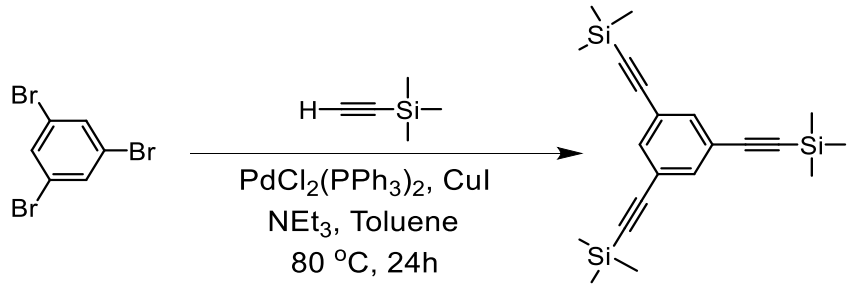

Figure 3.1. Synthesis of 1,3,5-tris-(1-trimethylsilylethynyl)benzene.

Synthesized according to the reported procedure in the literature.[80] 1,3,5-tribromobenzene (3.0 g, 9.53 mmol), bis(triphenylphosphine)palladium chloride (0.20 g, 0.29 mmol), and copper(I)iodide (011 g, 0.57 mmol) were dried and degassed into a 100 ml Schlenk tube and dissolved in a mixture of THF:NEt_3 (15 ml: 10 ml) under argon atmosphere. Upon heating the reaction mixture to 60 °C, trimethylsilylacetylene (4.6 mL, 3.27 g, 33.4 mmol) was added. The resulting mixture was then heated to 80 °C and stirred at this constant temperature for 24 hours. After the reaction had cooled to room temperature, the volatile components were removed under reduced pressure. The resulting light yellow solid product was purified via column chromatography using hexane eluent as eluent and was subsequently used in the following step.

3.2.2. Synthesis of 1,3,5-Triethynylbenzene:

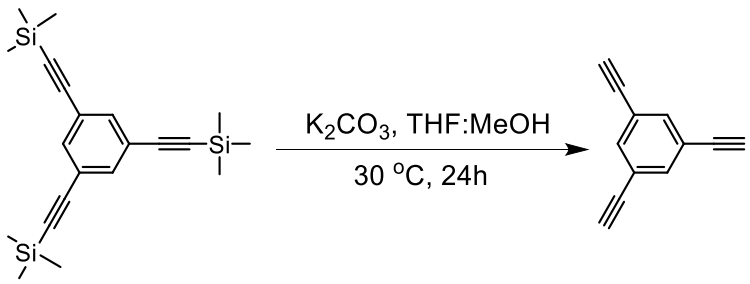

Figure 3.2. Synthesis of 1,3,5-triethinylbenzene.

In a 100 ml round bottom flask, the obtained 1,3,5-tris-(1-trimethylsilylethinyl)benzene was added and dissolved in a mixture of THF (15 mL) and methanol (15 mL). Potassium carbonate (7.71 g, 55.8 mmol) was added to the reaction mixture and stirred at room temperature for 2 hours. The resulting reaction mixture was concentrated under reduced pressure and then extracted with water and ethyl acetate. The organic phase was collected and dried with sodium sulfate, and the volatiles were removed under reduced pressure. The final product was isolated as a light yellow solid after purification via silica gel column chromatography, yielding 0.92 g, which affords a total yield of 58% obtained after two steps.[80]

3.2.3. Synthesis of 4,4'-bis(tri isopropyl silylethynyl) benzyl:

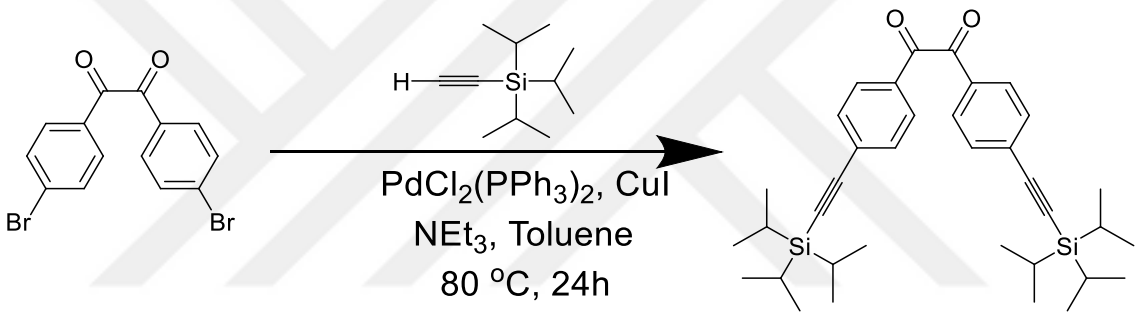

Figure 3.3. Synthesis of 4,4'-bis(tri isopropyl silylethynyl) benzyl.

Synthesized following the common procedure in the literature.[81] 1,2-bis(4-bromophenyl)ethane-1,2-dione (0.49 g, 1.32 mmol), bis(triphenylphosphine)palladium chloride (0.11 g, 0.15 mmol) and copper(I)iodide (0.06 g, 0.30 mmol) were dissolved into a 100 ml Schlenk tube with dry and degassed toluene: NEt_3 (10 ml: 10 ml) under argon atmosphere. After heating the reaction mixture to 80 °C, triisopropylsilylacetylene (0.94 mL, 0.65 g, 6.60 mmol) was added. The final mixture was maintained at 80 °C and stirred for a period of 24 hours. After the reaction was cooled down to room temperature, the volatiles were removed under reduced pressure. The resulting product was purified using silica gel column chromatography to afford a light yellow solid (0.60 g, 55%).

3.2.4. Synthesis of 2,5-diphenyl-3,4-bis(4-((triisopropylsilyl)ethynyl)phenyl)cyclopenta-2,4-dien-1-one:

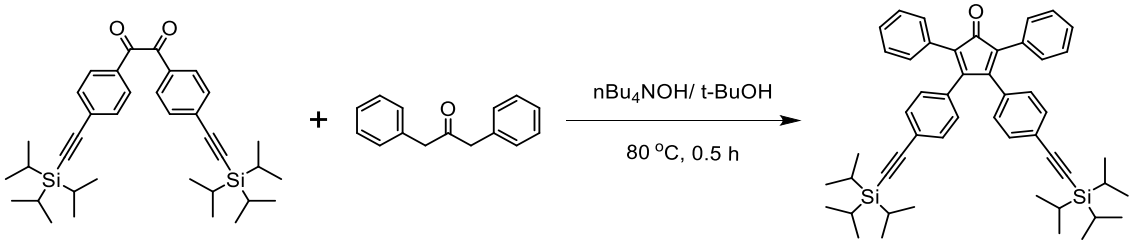

Figure 3.4. Synthesis of 2,5-diphenyl-3,4-bis(4-((tri isopropylsilyl) ethynyl) phenyl) cyclopenta-2,4-dien-1-one.

The synthesis was performed following a modified version of the reported procedure in the literature.[82] To a round-bottomed flask, 4,4'-bis(triisopropylsilylethinyl) benzyl (660 mg, 1.16 mmol) and 1,3-diphenylpropan-2-one (220 mg, 1.05 mmol) were dissolved in *t*-BuOH (5 mL) and heated to 80 °C. 300 µl of 40% TBAH solution (in MeOH: commercial product) -diluted with 1 ml of *t*-BuOH- was added dropwise and stirred at this temperature for 30 minutes. The reaction was quenched with 5 ml MeOH and the mixture was allowed to precipitate at 4°C overnight. The precipitate was purified by filtration and washed with cold MeOH. After removing the residual solvent under reduced pressure, the product was obtained as a purple-red solid (0.6 g, 76%).

3.2.5. Synthesis of GNRD-G1ap:

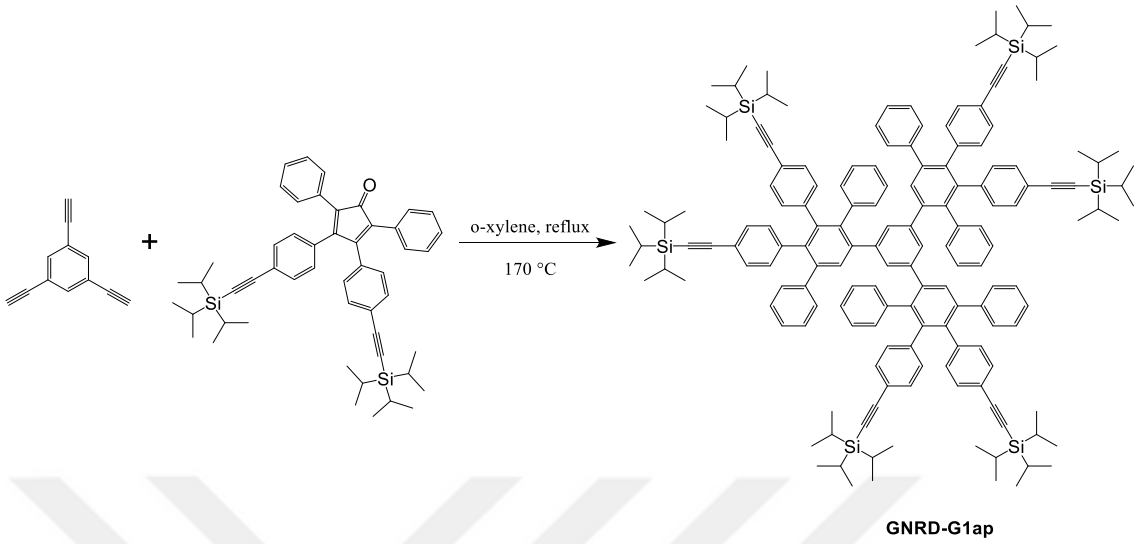

Figure 3.5. Synthesis of GNRD-G1ap.

The synthesis was performed following a modified version of the reported procedure in the literature.[83] In a round-bottomed flask, 2,5-diphenyl-3,4-bis(4-((triisopropylsilyl)ethynyl)phenyl) cyclopenta-2,4-diene-1-one (625 mg, 0.84 mmol) dissolved in o-xylene (20 mL) was evacuated and filled with argon gas three times and then heated to 100 °C. To this mixture, a solution of 1,3,5-triethynylbenzene (35 mg, 0.23 mmol) in 3 ml of o-xylene was added dropwise, the temperature was then increased up to 170 °C. After the overnight reaction, o-xylene was evaporated under reduced pressure, and the remaining mixture was purified by column chromatography in a hexane-DCM system. The remaining solid was dissolved with DCM and precipitated with MeOH. The product was then afforded as a yellow-white solid (0.33 g, 62%).

3.2.6. Synthesis of GNRD-G1a:

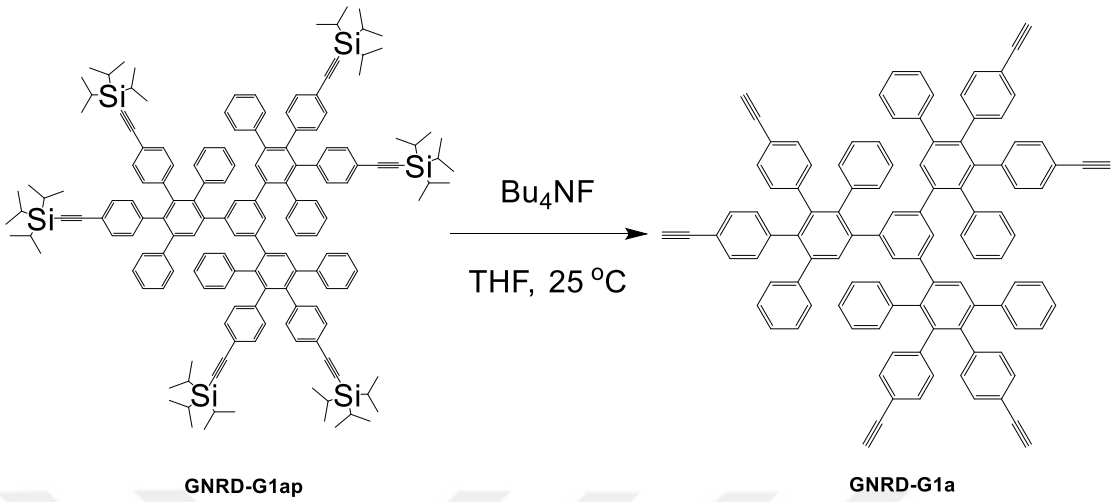

Figure 3.6. Synthesis of GNRD-G1a.

The synthesis was performed following a modified version of the reported procedure in the literature.[83] To a round-bottomed flask, GNRD-G1ap (300 mg, 0.13 mmol) was dissolved in THF (5 ml). Bu_4NF (2.35 ml, 2.35 mmol from 1M Bu_4NF solution in THF) was added to this solution. After 2 h stirring at room temperature, the reaction was quenched with ~5 ml DCM, and the organic phase was washed with water and dried over Na_2SO_4. After evaporating the solvent under reduced pressure, the crude product was washed with DCM and purified by reprecipitation in MeOH. The product was then afforded as a yellow-white solid (150 mg, 86%).

3.2.7. Synthesis of GNRD-G2ap:

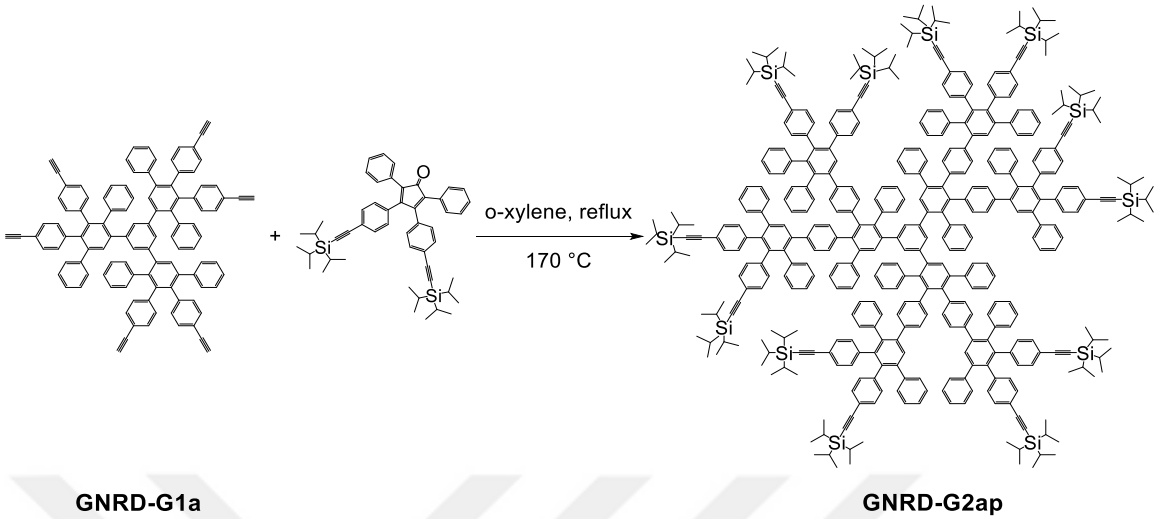

Figure 3.7. Synthesis of GNRD-G2ap.

Modified according to the reported methodology in the literature.[83] In a round-bottomed flask, 2,5-diphenyl-3,4-bis(4-((triisopropylsilyl) ethynyl)phenyl) cyclopenta-2,4-diene-1-one (675 mg, 0.90 mmol) dissolved in o-xylene (20 mL) was evacuated and filled with argon gas three times and then heated to 100 °C. To this mixture, a solution of GNRD-G1a (150 mg, 0.11 mmol) in 3 ml of o-xylene was added dropwise, the temperature was then increased up to 170 °C. After the overnight reaction, o-xylene was evaporated under reduced pressure; the remaining mixture was purified by column chromatography in the hexane-DCM system. The remaining solid was dissolved with DCM and precipitated with MeOH. The product was then afforded as a yellow-white solid (0.2 g, 32%).

3.2.8. Synthesis of GNRD-G2a:

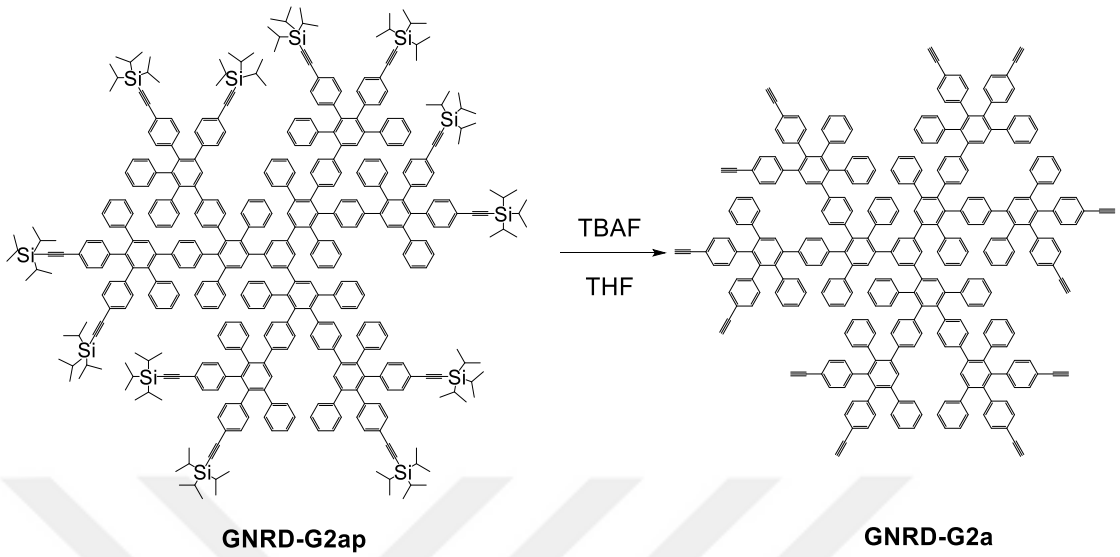

Figure 3.8. Synthesis of GNRD-G2a.

Modified in accordance with the reported methodology in the literature.[83] To a round-bottomed flask, GNRD-G2ap (200 mg, 0.04 mmol) was dissolved in THF (5 ml). To this solution, Bu_4NF (1.27 ml, 1.27 mmol from 1M Bu_4NF solution in THF) was added. After 2 h stirring at room temperature, the reaction was quenched with ~5 ml DCM, and the organic phase was washed with water and dried over Na_2SO_4. After evaporating the solvent under reduced pressure, the crude product was washed with DCM and purified by reprecipitation in MeOH. The product was then afforded as a yellow-white solid (0.1 g, 75%).

3.2.9. Synthesis of CP-Br:

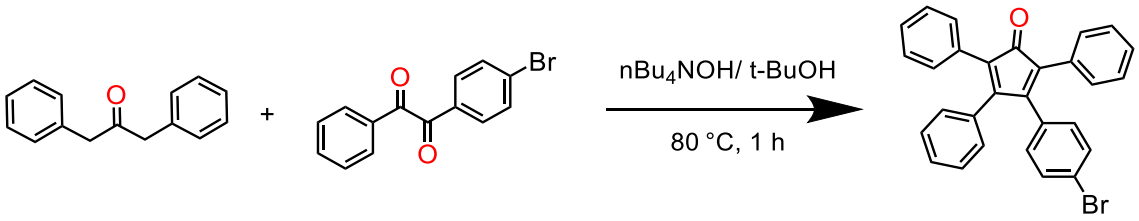

Figure 3.9. Synthesis of CP-Br.

Modified in accordance with the reported methodology in the literature.[82] To a round-bottomed flask, 1-(4-bromophenyl)-2-phenylethane-1,2-dione (720 mg, 2.49 mmol) and 1,3-diphenylpropan-2-one (480 mg, 2.29 mmol) were dissolved in *t*-BuOH (5 mL) and heated to 80 °C with reflux. 640 µl of 40% TBAH solution (in MeOH: commercial product) -diluted with 1 ml of *t*-BuOH- was added dropwise and stirred at this temperature for 1 hour. The reaction was quenched with 5 ml MeOH and precipitated at 4 °C overnight. The precipitate was purified by filtration with cold MeOH. The product was obtained as a purple-red solid after drying under vacuum (0.9 g, 86%).

3.2.10. Synthesis of G1:

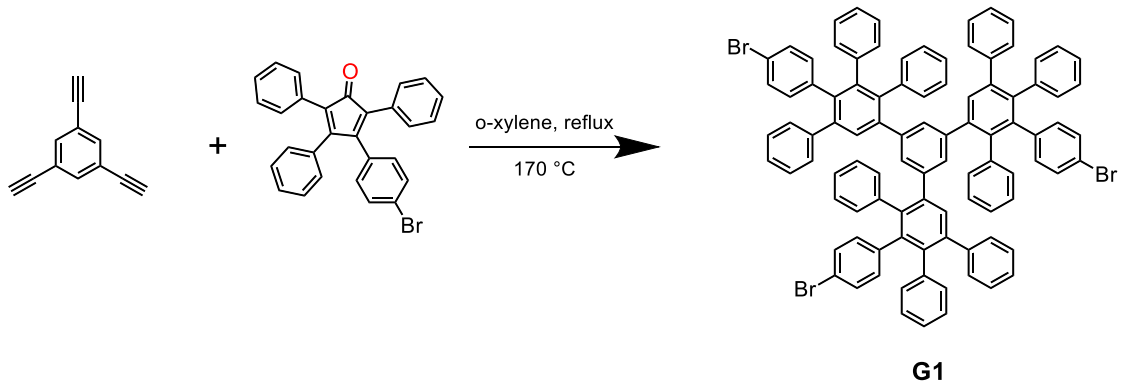

Figure 3.10. Synthesis of G1.

In a round-bottomed flask, CP-Br (300 mg, 0.65 mmol) dissolved in o-xylene (20 mL) was evacuated and filled with argon gas three times and then heated to 100 °C. To this mixture, a solution of 1,3,5-triethynylbenzene (16.2 mg, 0.11 mmol) in 3 ml of o-

xylene was added dropwise, the temperature was then increased up to 170 °C. After the overnight reaction, o-xylene was evaporated under reduced pressure, the remaining mixture was purified by column chromatogtaphy in DCM system. The remaining solid was dissolved with DCM and precipitated with MeOH. The product was then afforded as a white solid (0.15 g, 97%).

3.2.11. Synthesis of G2:

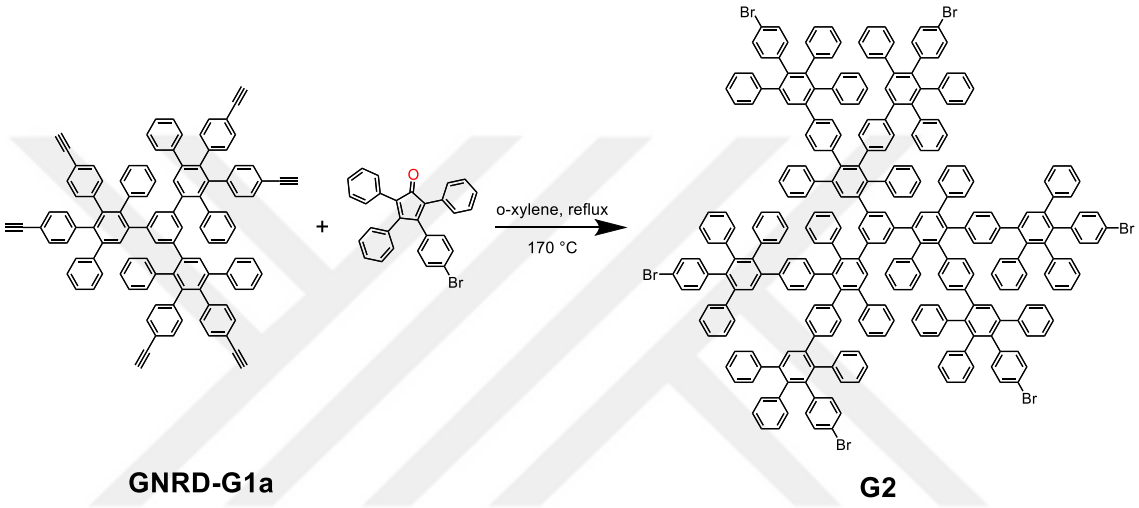

Figure 3.11. Synthesis of G2.

In a round-bottomed flask, CP-BR (250 mg, 0.54 mmol) dissolved in o-xylene (20 mL) was evacuated and filled with argon gas three times and then heated to 100 °C. To this mixture, a solution of GNRD-G1a (96 mg, 0.07 mmol) in 3 ml of o-xylene was added dropwise, the temperature was then increased up to 170 °C. After the overnight reaction, o-xylene was evaporated under reduced pressure, the remaining mixture was purified by column chromatogtaphy in DCM system. The remaining solid was dissolved with DCM and precipitated with MeOH. The product was then afforded as a yellow-white solid (0.16 g, 58%).

3.2.12. Synthesis of G3:

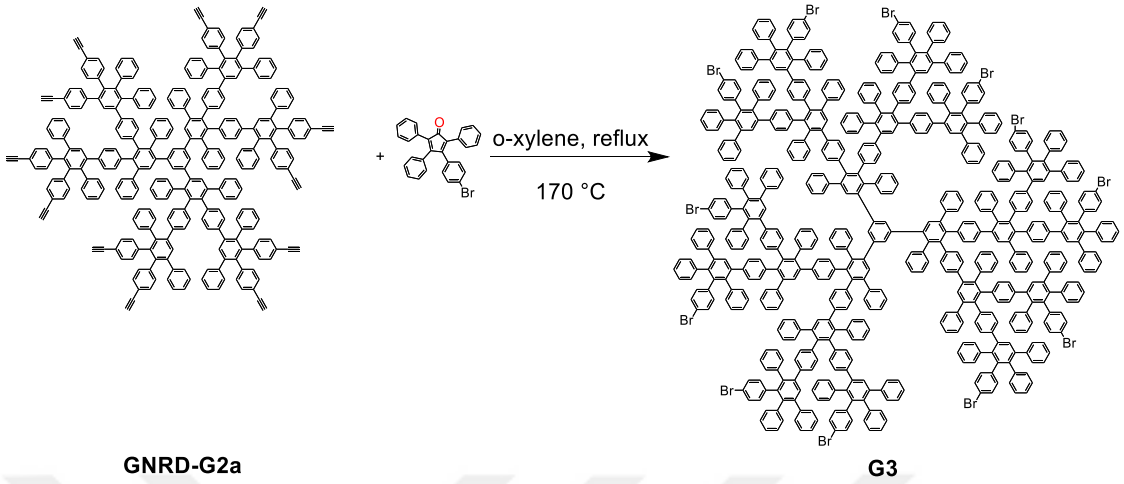

Figure 3.12. Synthesis of G3.

In a round-bottomed flask, CP-BR (247 mg, 0.53 mmol) dissolved in o-xylene (20 mL) was evacuated and filled with argon gas three times and then heated to 100 °C. To this mixture, a solution of GNRD-G2a (67 mg, 0.02 mmol) in 3 ml of o-xylene was added dropwise, the temperature was then increased up to 170 °C. After the overnight reaction, o-xylene was evaporated under reduced pressure, the remaining mixture was purified by column chromatogtaphy in DCM system. The remaining solid was dissolved with DCM and precipitated with MeOH. The product was then afforded as a yellow-white solid (0.1 g, 65%).

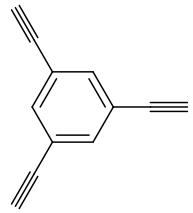

1,3,5-triethynylbenzene

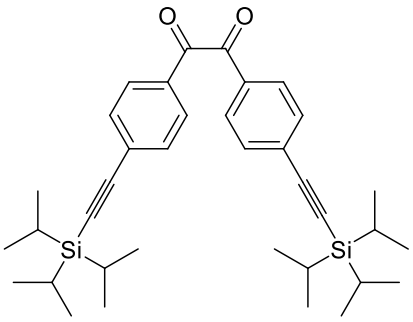

4,4'-bis(tri isopropyl silylethynyl) benzyl

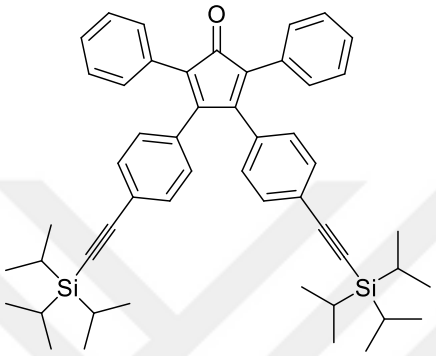

2,5-diphenyl-3,4-bis(4-((triisopropylsilyl)ethynyl)phenyl) cyclopenta-2,4-dien-1-one

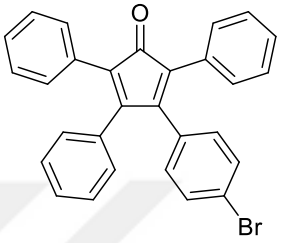

CP-Br

Figure 3.13. All synthesized reactants.

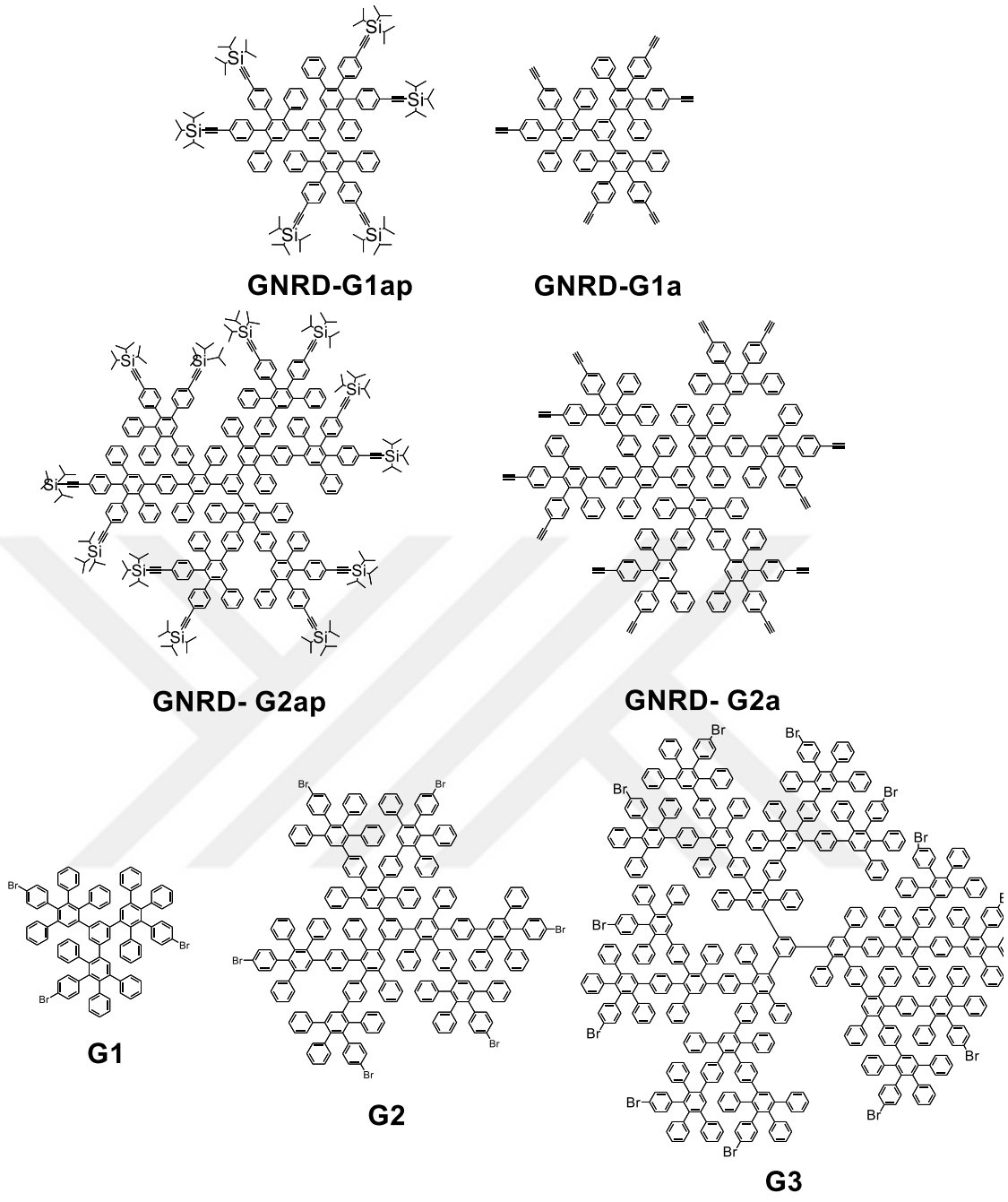

Figure 3.14. All synthesized dendrimers.

3.3. General Method for the Synthesis of PDendPs via Suzuki polycondensation

3.3.1. Polymer synthesis

The mixture of PPD, 1,4-bis(4,4,5,5-tetramethyl-1,3,2-dioxaborolan-2-yl)benzene, and $Pd(PPh_3)_4$ was evacuated and filled with argon gas three times. The pre-degassed DMF (and o-xylene), and an aqueous solution of K_2CO_3 were added to the reaction mixture, respectively, and then gradually heated to 150 °C for 4 days. After washing PDendPs with appropriate solvents, the polymers were obtained as a grey powder.

3.3.2. G1 Polymerization- P1DendP:

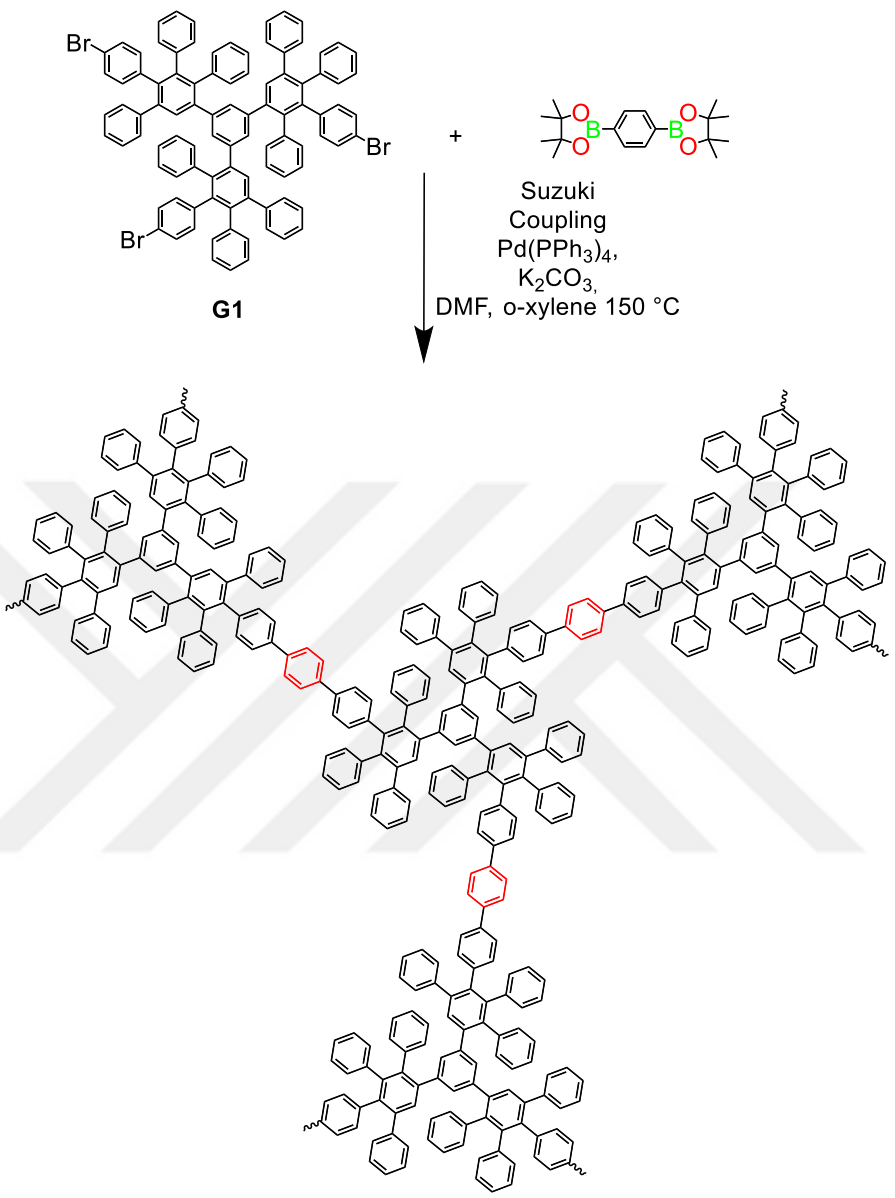

Figure 3.15. Synthesis of P1DendP.

In a Schlenk tube, G1 (80 mg, 0.055 mmol), 1,4-bis(4,4,5,5-tetramethyl-1,3,2-dioxaborolan-2-yl)benzene (27 mg, 0.082 mmol) and $Pd(PPh_3)_4$ (20 mg, 0.017 mmol) was evacuated and filled with argon gas three times. To the reaction mixture, pre-degassed 3 ml DMF, 3 ml o-xylene and K_2CO_3 (2M/H_2O, 1.1 mL, 2.2 mmol) was added and then, heated to 150 ^oC for 4 days. The reaction mixture was washed with DMF, distilled water, THF, acetone, 1M HCl, and MeOH, respectively. The product was then afforded as a grey powder (64 mg, 83%).

3.3.3. G2 Polymerization- P2DendP:

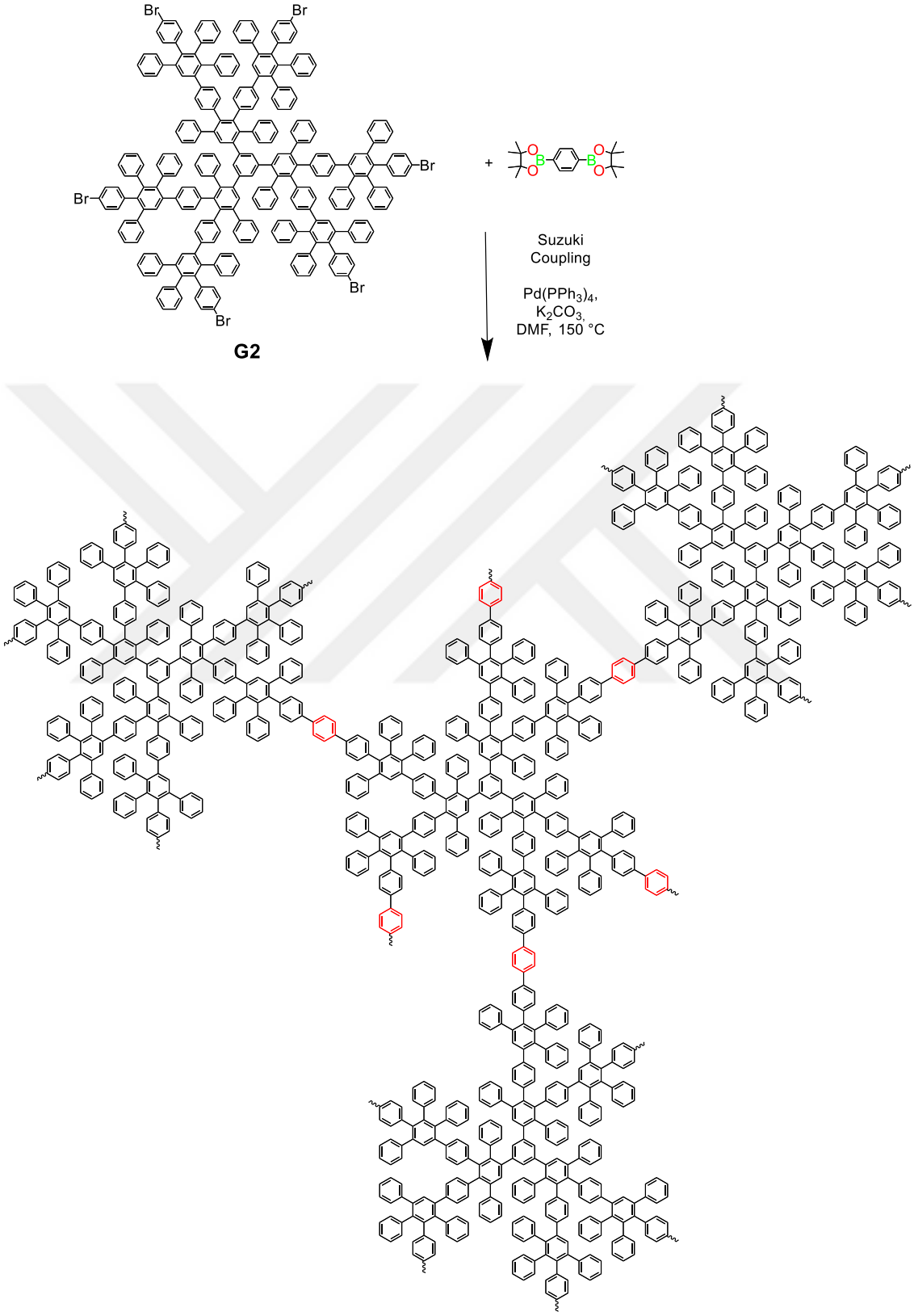

Figure 3.16. Synthesis of P2DendP.

In a Schlenk tube, G2 (85 mg, 0.021 mmol), 1,4-bis(4,4,5,5-tetramethyl-1,3,2-dioxaborolan-2-yl)benzene (21 mg, 0.064 mmol) and $Pd(PPh_3)_4$ (20 mg, 0.017 mmol) was evacuated and filled with argon gas three times. To the reaction mixture, pre-degassed 6 ml DMF and K_2CO_3 (2M/H_2O, 1.1 mL, 2.2 mmol) were added and then heated to 150 ^oC for 4 days. The reaction mixture was washed with DMF, distilled water, THF, acetone, 1M HCl and MeOH, respectively. The product was then afforded as a grey powder (66 mg, 79%).

3.3.4. G3 Polymerization- P3DendP:

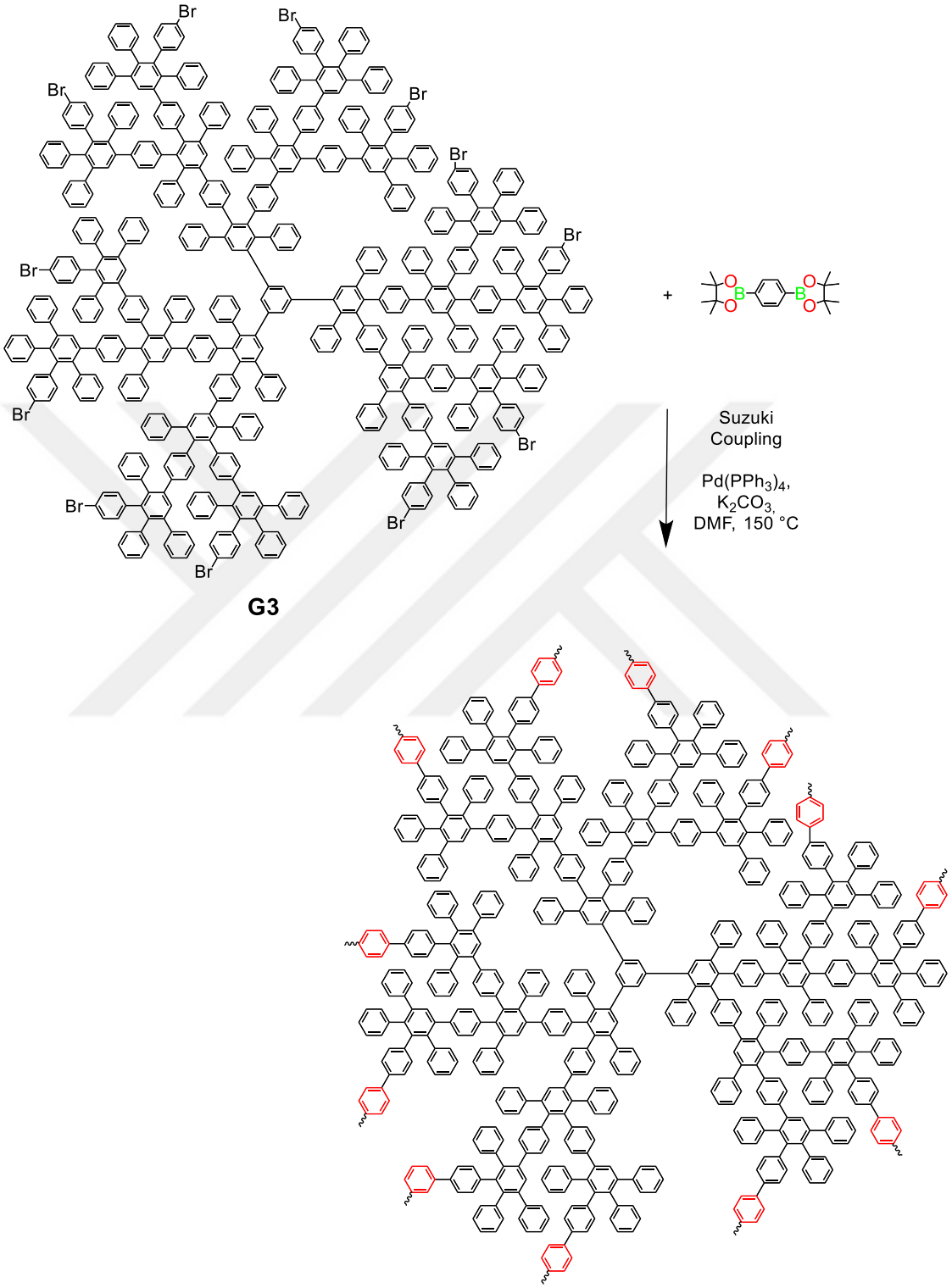

Figure 3.17. Synthesis of P3DendP.

In a Schlenk tube, G3 (50 mg, 0.00555 mmol), 1,4-bis(4,4,5,5-tetramethyl-1,3,2-dioxaborolan-2-yl)benzene (15 mg, 0.09 mmol) and $Pd(PPh_3)_4$ (20 mg, 0.017 mmol) was evacuated and filled with argon gas three times. To the reaction mixture, pre-degassed 6 ml DMF and K_2CO_3 (2M/H_2O, 1.1 mL, 2.2 mmol) were added and then heated to 150 ^oC for 4 days. The reaction mixture was washed with DMF, distilled water, THF, acetone, 1M HCl, and MeOH. The product was then afforded as a grey powder (40 mg, 79%).

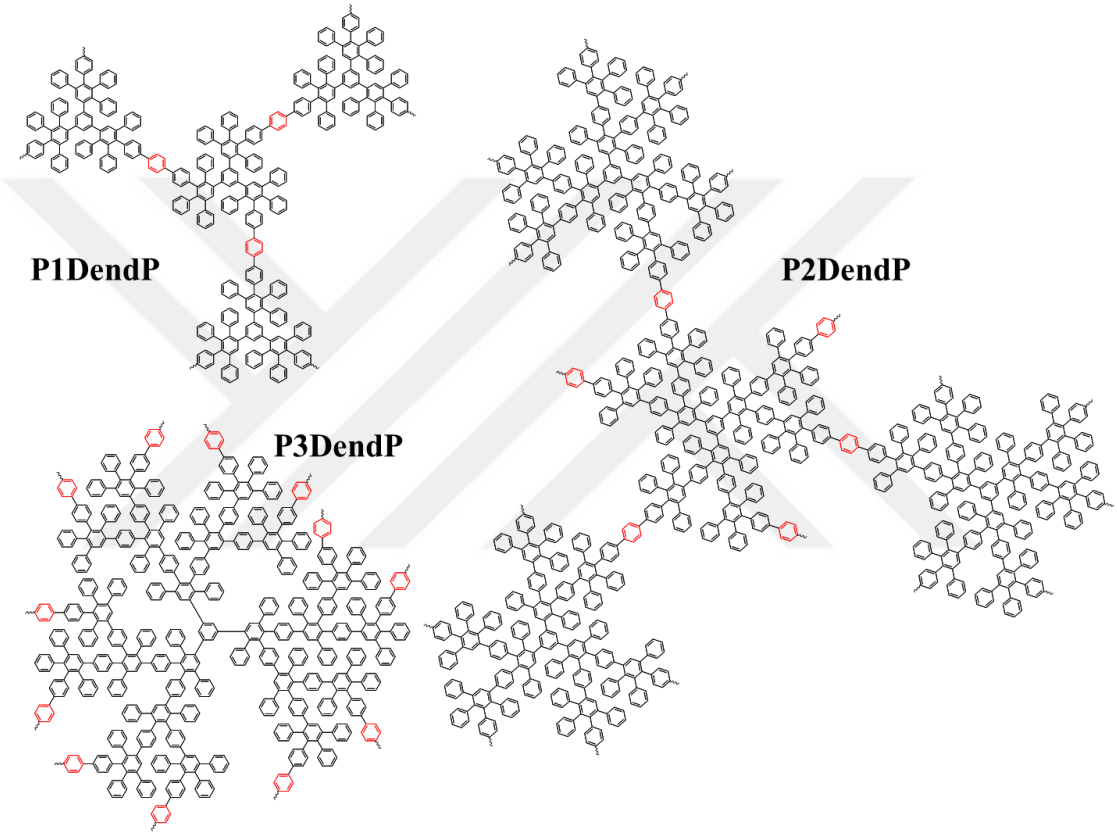

Figure 3.18. Synthesized dendritic polymers: P1DendP, P2DendP, P3DendP.

3.4. Characterization Data for Synthesized Compounds

All synthesized reactants and dendrimers were characterized by ^{1}H NMR spectroscopy. Below are the NMR data for all reactants and dendrimers synthesized.

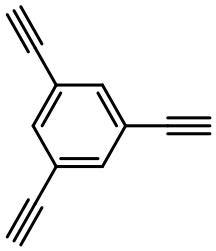

Figure 3.19. 1,3,5-triethynylbenzene.

1,3,5-Triethynylbenzene: ^{1}H NMR (300 MHz $CDCl_3$) δ 7.54 (s, 3H), 3.08 (s, 3H).

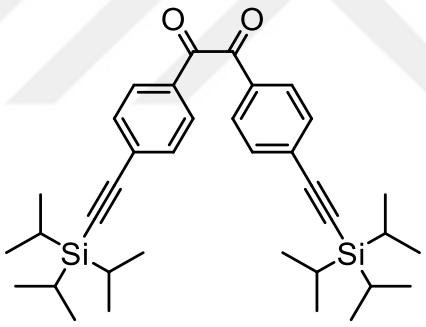

Figure 3.20. 4,4'-bis(tri isopropyl silylethynyl) benzyl.

4,4'-bis(tri isopropyl silylethynyl) benzyl: ^{1}H NMR (300 MHz, $CDCl_3$) δ 7.92 (d, J = 8.6 Hz, 4H), 7.60 (d, J = 8.6 Hz, 4H), 1.15 (m, 42H).

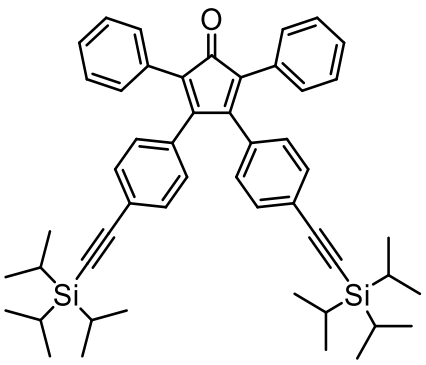

Figure 3.21. 2,5-diphenyl-3,4-bis(4-((triisopropylsilyl)ethynyl)phenyl)cyclopenta-2,4-dien-1-one.

2,5-diphenyl-3,4-bis(4-((triisopropylsilyl)ethynyl)phenyl)cyclopenta-2,4-dien-1-one: ^{1}H NMR (400 MHz $CDCl_3$) δ 7.37-7.26 (m, 9 H), 7.19-7.15 (m, 5 H), 6.85 (d, J = 8.4 Hz, 4 H), 1.10-1.09 (m, 42 H).

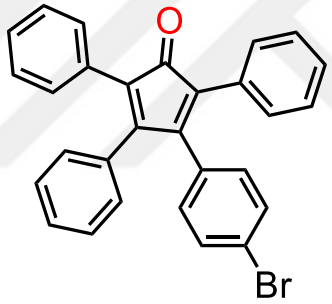

Figure 3.22. CP-Br.

CP-Br: ^{1}H NMR (400 MHz $CDCl_3$) δ 7.30-7.25 (m, 4 H), 7.24 (d, J=2.0 Hz, 2 H), 7.23-7.17 (m, 9 H), 6.91 (d, J = 7.2 Hz, 2 H), 6.78 (d, J = 8.8 Hz, 2 H).

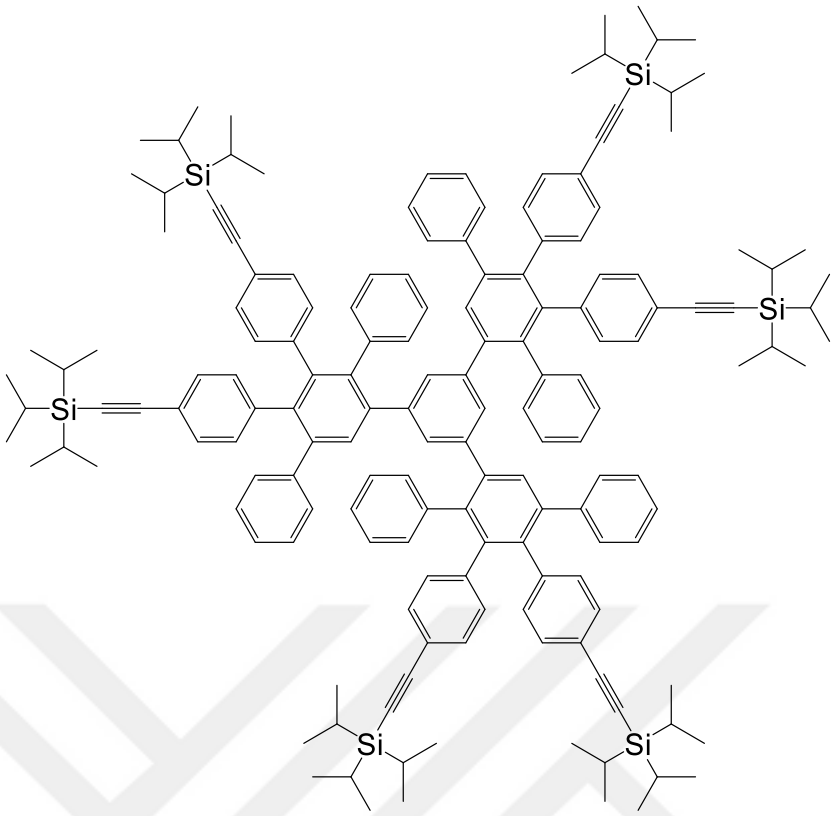

Figure 3.23. GNRD-G1ap.

GNRD-G1ap: ^{1}H NMR (400 MHz $CDCl_3$) δ 7.16-7.09 (m, 12H, arom.), 7.06-6.95 (m, 18H, arom.), 6.88-6.74 (m, 12H, arom.), 6.71-6.69 (m, 6H, arom.), 6.66-6.55 (m, 12H, arom.), 1.06-1.05 (m, 126 H, aliphatic).

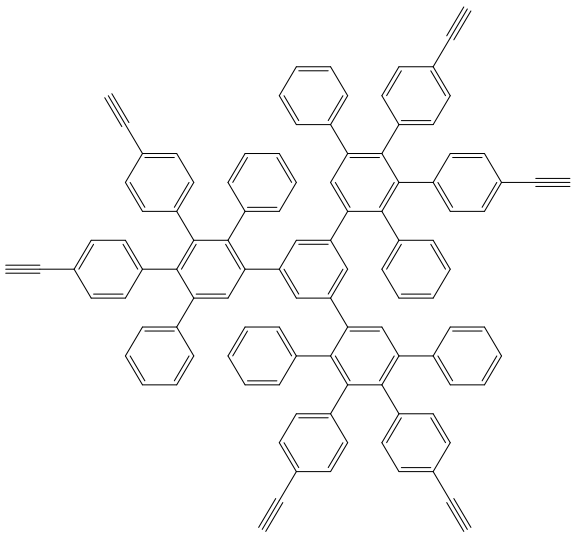

Figure 3.24. GNRD-G1a.

GNRD-G1a: ^{1}H NMR (400 MHz $CDCl_3$) δ 7.16-7.14 (m, 9H, arom.), 7.03-7.00 (m, 12H, arom.), 6.95 (d, J=8.4 Hz, 6H, arom.), 6.82-6.76 (m, 12H, arom.), 6.72-6.68 (m, 9H, arom.), 6.60 (d, J=8.4 Hz, 6H, arom.), 6.54 (d, J=8.4 Hz, 6H, arom.), 2.95 (s, 3H, C≡C-H), 2.92 (s, 3H, C≡C-H).

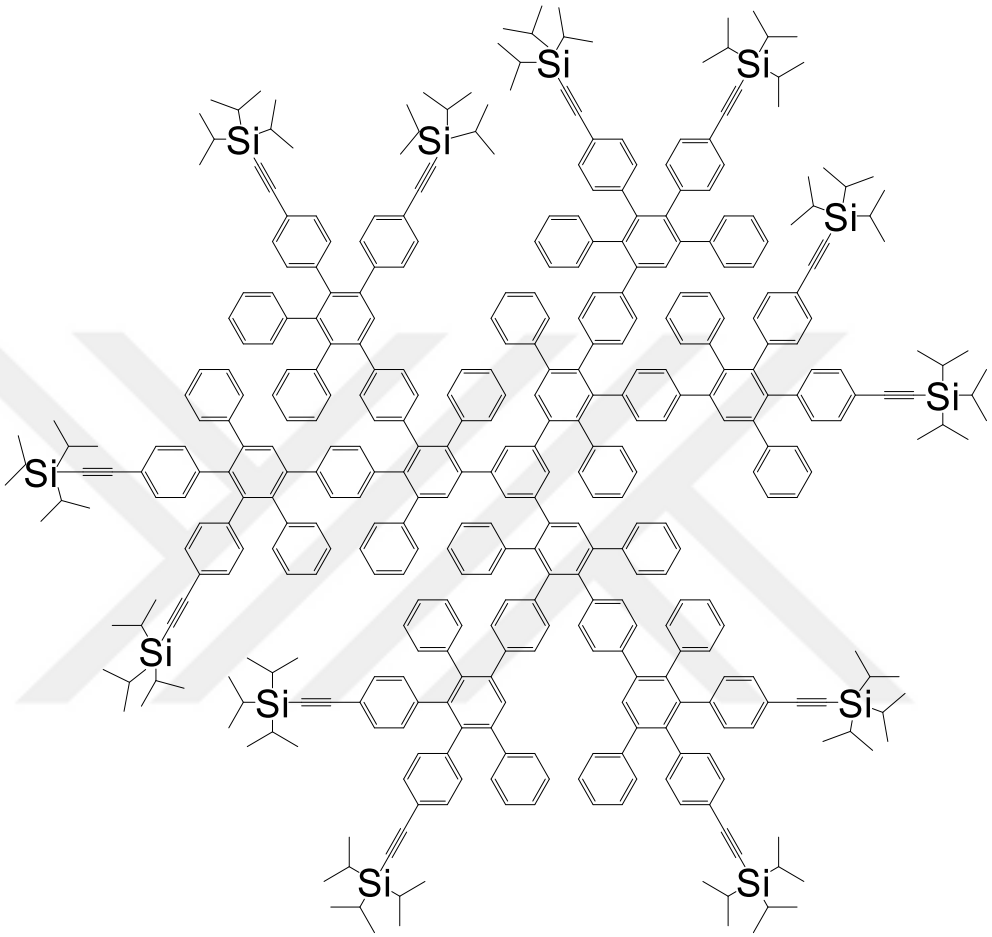

Figure 3.25. GNRD- G2ap.

GNRD-G2ap: ^{1}H NMR (400 MHz $CDCl_3$) δ 7.40 (s, 3H, arom.), 7.37 (s, 3H, arom.), 7.18-7.11 (m, 24H, arom.), 7.10-7.02 (m, 30H, arom.), 7.00-6.62 (m, 114H, arom.), 1.06-1.06 (m, 252H, aliphatic).

Figure 3.26. GNRD- G2a.

GNRD-G2a: ^{1}H NMR (400 MHz $CDCl_3$) δ 7.44 (s, 3H, arom.), 7.40 (s, 3H, arom.), 7.19-7.13 (m, 24H, arom.), 7.10-7.05 (m, 24H, arom.), 7.01-6.97 (m, 18H, arom.), 6.89-6.80 (m, 24H, arom.), 6.78-6.72 (m, 18H, arom.), 6.70-6.62 (m, 33H, arom.), 6.60-6.55 (m, 12H, arom.), 6.47 (d, J=8.8 Hz, 9H, arom.), 6.36 (d, J=7.2 Hz, 6H, arom.), 2.97 (s, 6H, C≡C-H), 2.95 (s, 6H, C≡C-H).

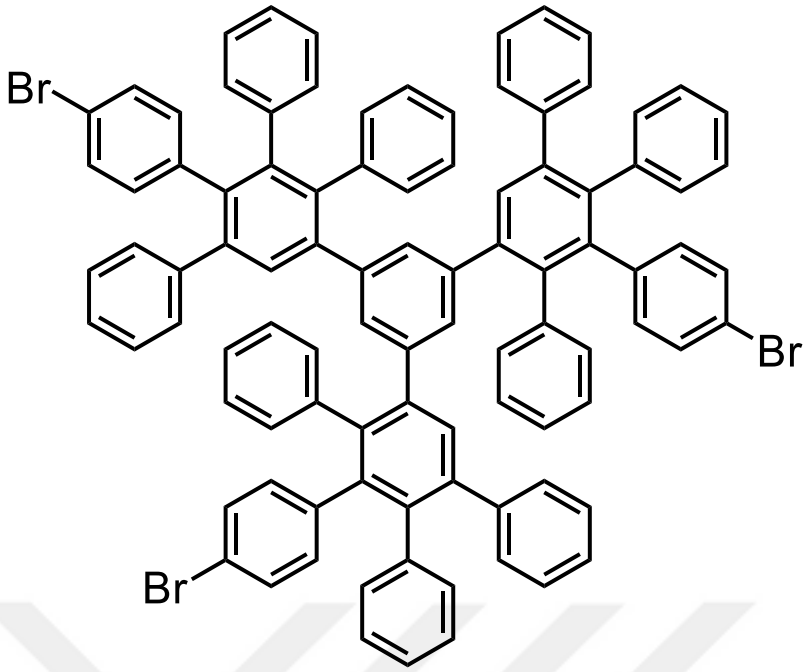

Figure 3.27. G1.

G1: ^{1}H NMR (400 MHz $CDCl_3$) δ 7.20-7.12 (m, 9H, arom.), 7.08-6.99 (m, 9H, arom.), 6.96-6.90 (m, 6H, arom.), 6.86-6.75 (m, 21H, arom.), 6.71 (s, 3H, arom.), 6.66 (d, J=8.4 Hz, 6 H), 6.60-6.53 (m, 9 H).

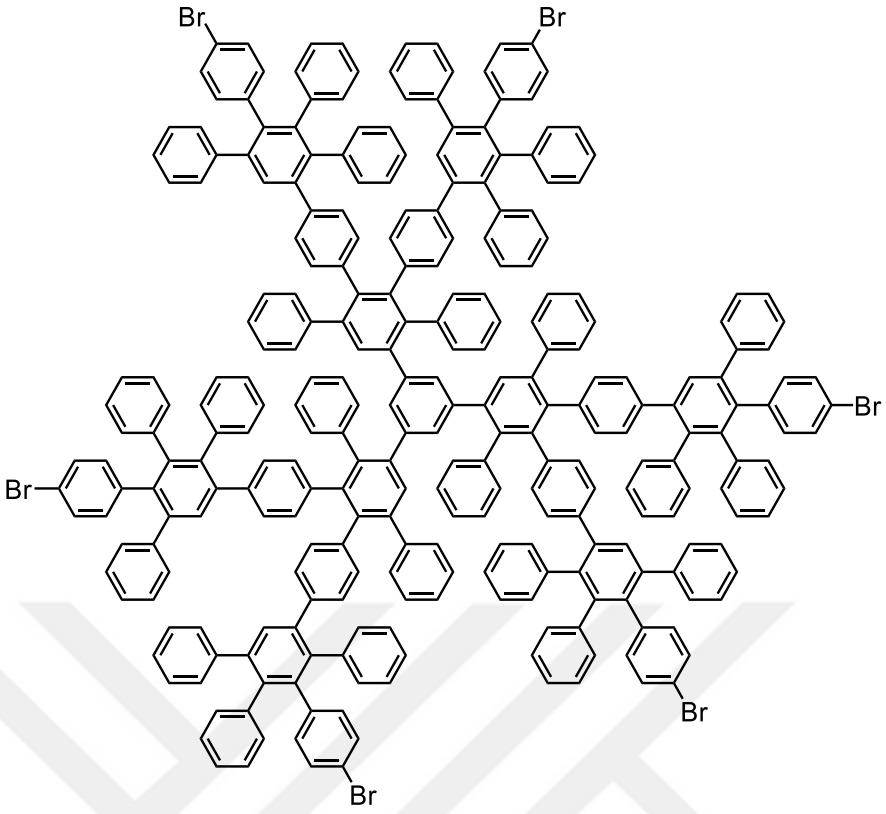

Figure 3.28. G2.

G2: ^{1}H NMR (400 MHz $CDCl_3$) δ 7.42 (dd, J=16.4 Hz, 6H, arom.), 7.18-7.10 (m, 42H, arom.), 7.05-6.92 (m, 36H, arom.), 6.88-6.78 (m, 42H, arom.), 6.72-6.66 (m, 30H, arom.), 6.61-6.57 (m, 12 H, arom.), 6.48 (d, J=7.2 Hz, 6 H, arom.), 6.37 (d, J=8 Hz, 6 H, arom.).

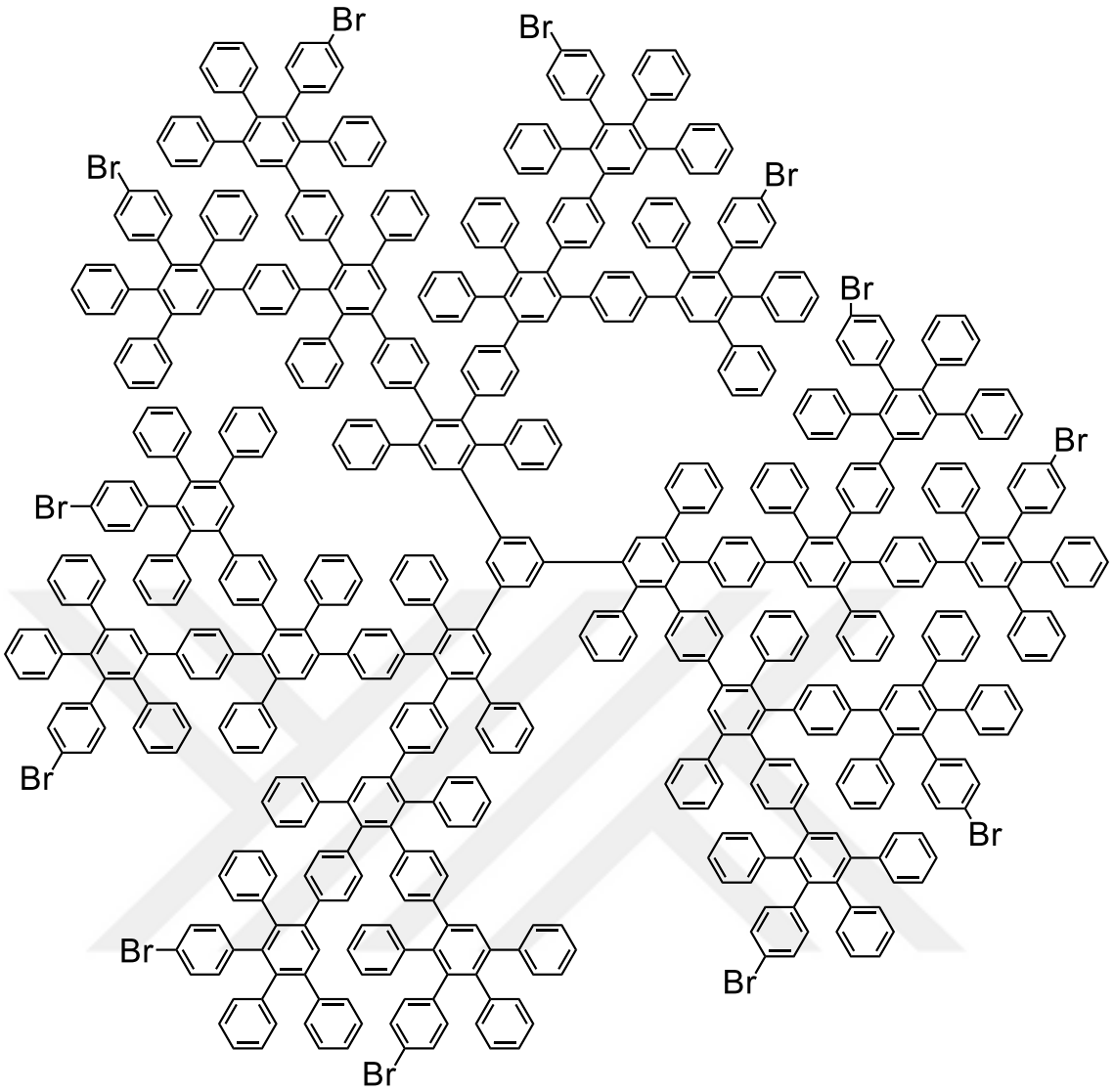

Figure 3.29. G3.

G3: ^{1}H NMR (400 MHz $CDCl_3$) δ 7.49-7.30 (m, 15H, arom.), 7.24-7.07 (m, 78H, arom.), 7.07-7.00 (m, 30H, arom.), 7.00-6.91 (m, 45H, arom.), 6.91-6.76 (m, 96H, arom.), 6.75-6.65 (m, 60H, arom.), 6.64-6.54 (m, 45H, arom.), 6.53-6.30 (m, 45 H, arom.)

3.5. The Brunauer-Emmett-Teller (BET) Calculations for the Specific Surface Areas

BET equation needs a linear plot of $1/[Q(P/P_0)-1]$ vs. relative pressure (P/P_0). Slope(s) and intercept(i) are used to calculate W_m value (weight of monolayer), which is equal to $\frac{1}{s+i}$. S_t (total surface area) will be derivated as; $S_t=\frac{Wm.N.Acs}{M}$, where N = Avogadro's number ($6.023x10^{23}$), M = Molecular weight of Adsorbate, A_{cs} = Adsorbate cross-sectional area ($16.2Å^2$ for Nitrogen). S (specific surface area) is calculated with $S=\frac{St}{w}$, where w is the sample weight.

3.6. Gas Sensing Properties of Porous Dendritic Polymers

3.6.1. Device Fabrication

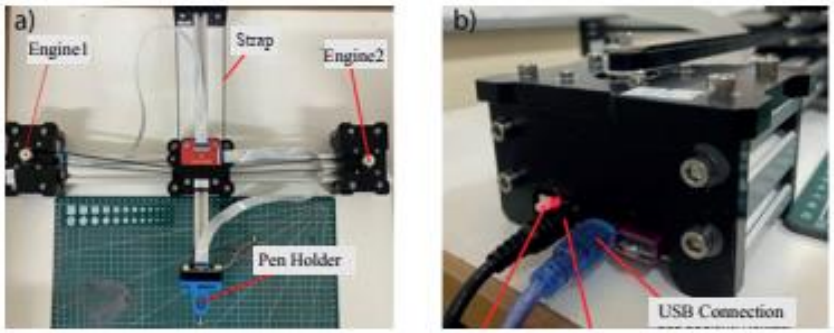

Figure 3.30. (a) 2D Printer, (b) Connection point of 2D printer.

A 2D printer was used to produce the device geometry, displayed in Figure 3.30, to prepare the sensor device. Paper substrate was our preferred option due to its plentiful raw material, physical flexibility, biodegradability, biocompatibility, and economical disposable qualities. The substrates for the chemiresistors were made by coating graphite electrodes over paper substrate utilizing a 2D printer. The conductivity in the chemiresistor was provided by electrode pairs found in all devices. It is common knowledge that 2D printers are frequently used to produce electrical gadgets.[84-87] As seen in Figure 3.30, a 2D printer of the "VG-4X" type from the VigoTec firm was utilized to

generate uniform sensor devices. The printer in the picture can move left and right with motors and belts. The springs in the pen holder control the pen's height relative to the surface.

3.6.2. Gas Sensing Measurements

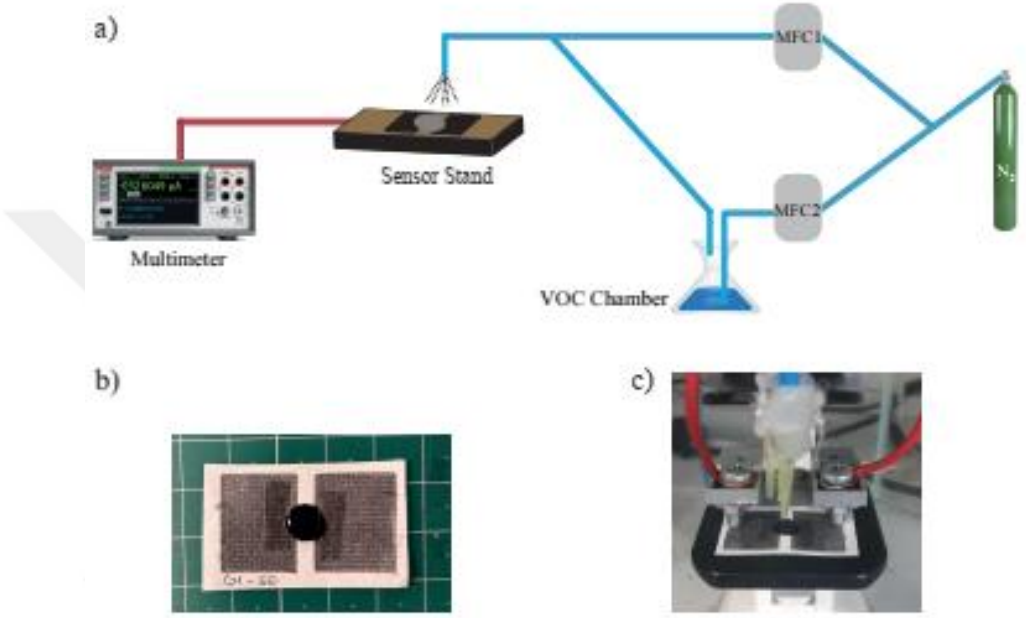

Figure 3.31 (a) Illustrated gas sensing setup, (b) sensing device, (c) measurement stand.

Figure 3.31 illustrates the sensing system used in the VOC detection tests. The electrodes of the sensor surface between them are linked in series with the power supply and multimeter. The sensor setup is concealed in a glass reservoir to protect it from external effects like wind while permitting it to interact with the air. The N_2 gas in the tank is transported promptly to the sensor device, whereas the organic component ethanol in the VOC chamber is evaporated by heating and transmitted to the sensor device via pipelines attached to the chamber utilizing N_2 as carrier gas. Figure 3.31a indicates how the gas flow is regulated by MFC1 (Mass Flow Controller) and MFC2 for N_2 and ethanol, respectively. For ethanol gas detection, the identical measuring system was utilized for all polymers (P1DendP, P2DendP, and P3DendP).

3.6.3. HPPM Measurements

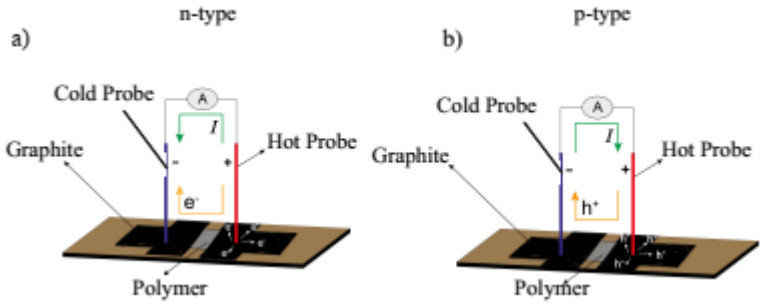

Figure 3.32. Schematic illustration of the HPPM measurements, (a) n-type, (b) p-type.

The measurement determines the potential difference between two spots on the surface. The multimeter's (+) probe is hot, while the other probe stays cold. Temperature causes the dominant charge carriers to migrate on the electrodes where the (+) and (-) probes touch, resulting in a potential difference between the two sites. The best method for determining the type of conductivity is to observe at the direction in which current and charge carrier flow. Since holes are the primary charge carriers in p-type materials, current flow is directed in the same direction as the direction in which holes move. Nevertheless, the current will move in the opposite direction of electron migration since electrons are the primary charge carriers in n-type materials. As a result, current flows in distinct paths in materials with varying conductivity. A negative voltage value on the multimeter reveals a p-type character, whereas a positive voltage value suggests an n-type character.

3.6.4. Computational Methodology

To examine the interaction between ethanol and PDendPs, the Vienna ab initio Simulation Package (VASP) was used for first-principle calculations. The exchange-correlation function of the Perdew-Burke-Ernzerhof model has been executed as a Generalized Gradient Approximation.[88-89] As projector-augmented wave potentials, single-atom pseudopotentials were employed.[90] In the Grimme damping function technique via the DFT-D2 methodology, the van der Waals adjustment was used to

estimate the weak dispersion forces.[88] The Bader charge technique calculated how charge moves between ethanol and PDendPs. The total energy optimizations used a kinetic energy cutoff of 500 eV and a convergence threshold of 10^{-5} eV. To avoid interactions between surrounding layers in-plane and out-of-plane, a vacuum separation of 16 Å was chosen. A 1×1×1 k-point mesh was implemented to sample real space for compositional optimizations and density state computations.

CHAPTER 4

RESULTS & DISCUSSION

PPDs and PDendPs hold unique physical and chemical properties. However, reaching specific surface areas of S_{BET} up to 100 m^2/g makes it very challenging to synthesize and derivatize these important materials. Because of this, the development of a new and straightforward method to obtain various analogs of PPDs and PDendPs with higher specific surface areas is in high demand. The thesis study's primary motivation is to construct a new and applicable method for synthesizing PPDs and PDendPs. These porous dendritic polymers have good potential to be employed as a chemiresistors. For future perspective, this study commits a novel approach in the bottom-up solution synthesis of well-defined porous graphene nanoribbons (pGNRs).

4.1. Synthesis of PPDs and PDendPs

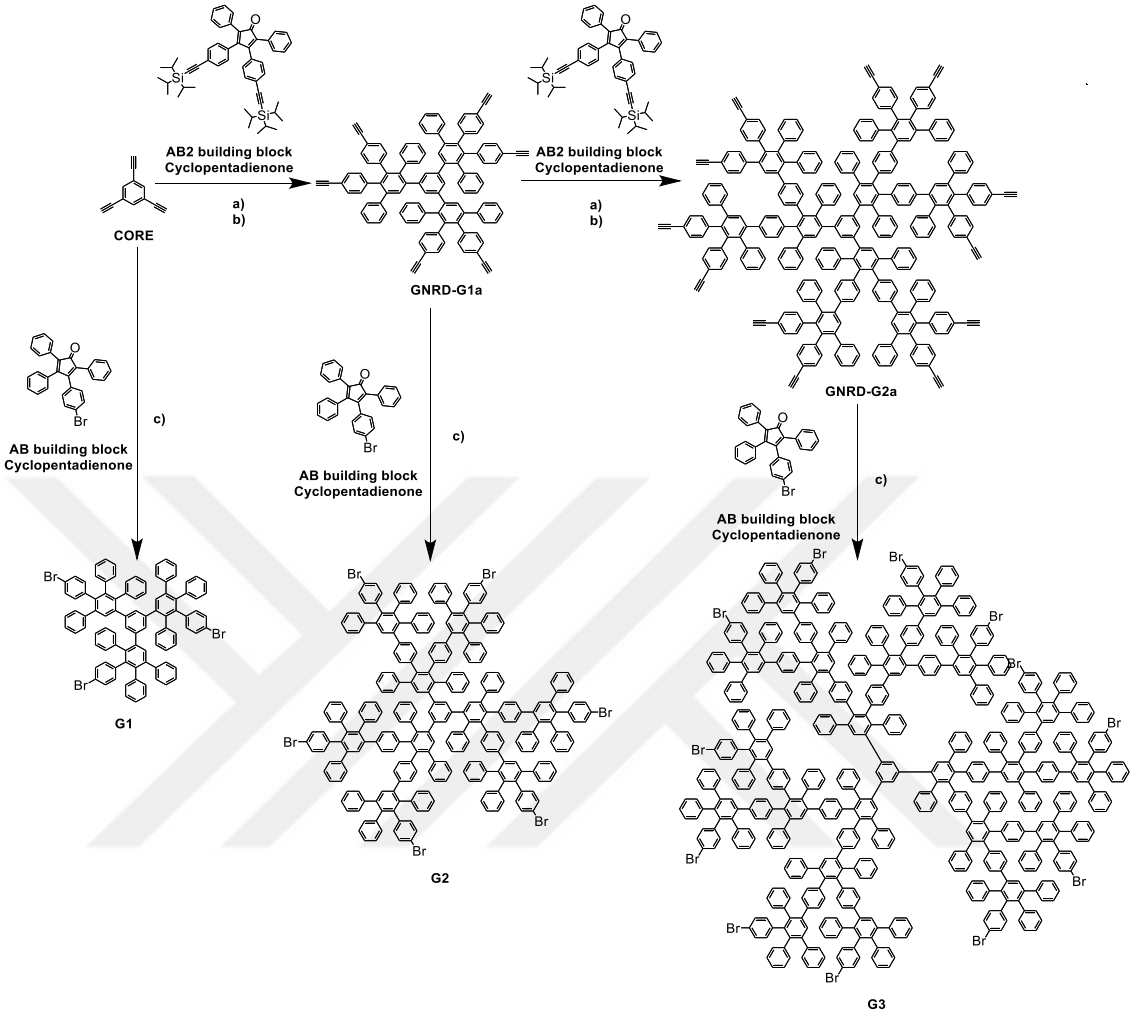

Figure 4.1. Synthesis of polyphenylene dendrimers: GNRD-G1a, GNRD-G2a, G1, G2, and G3: a) AB2 building block, o-xylene, 170 ^{o}C; b) TBAF, THF, R.T., 2 h; c) AB building block, o-xylene, 170 ^{o}C.

In the divergent method of dendrimer synthesis, the tritopic phenyl core shown in Figure 4.1 performed two distinct Diels-Alder reactions, yielding GNRD-G1a with double-sillylated cyclopentadienone (CP-bis-sillyl: AB2 building block) and G1 with mono-brominated cyclopentadienone (CP-Br: AB building block). Furthermore, by submitting GNRD-G1a to Diels-Alder reactions with CP-bis-sillyl and CP-Br, two PPDs were produced: GNRD-G2a and G2. Ultimately, G3 was synthesized from GNRD-G2a using a Diels-Alder reaction and CP-Br. Monobrominated cyclopentadienone (CP-Br:

AB building block) was chosen to avoid probable steric issues within polymerization reactions.

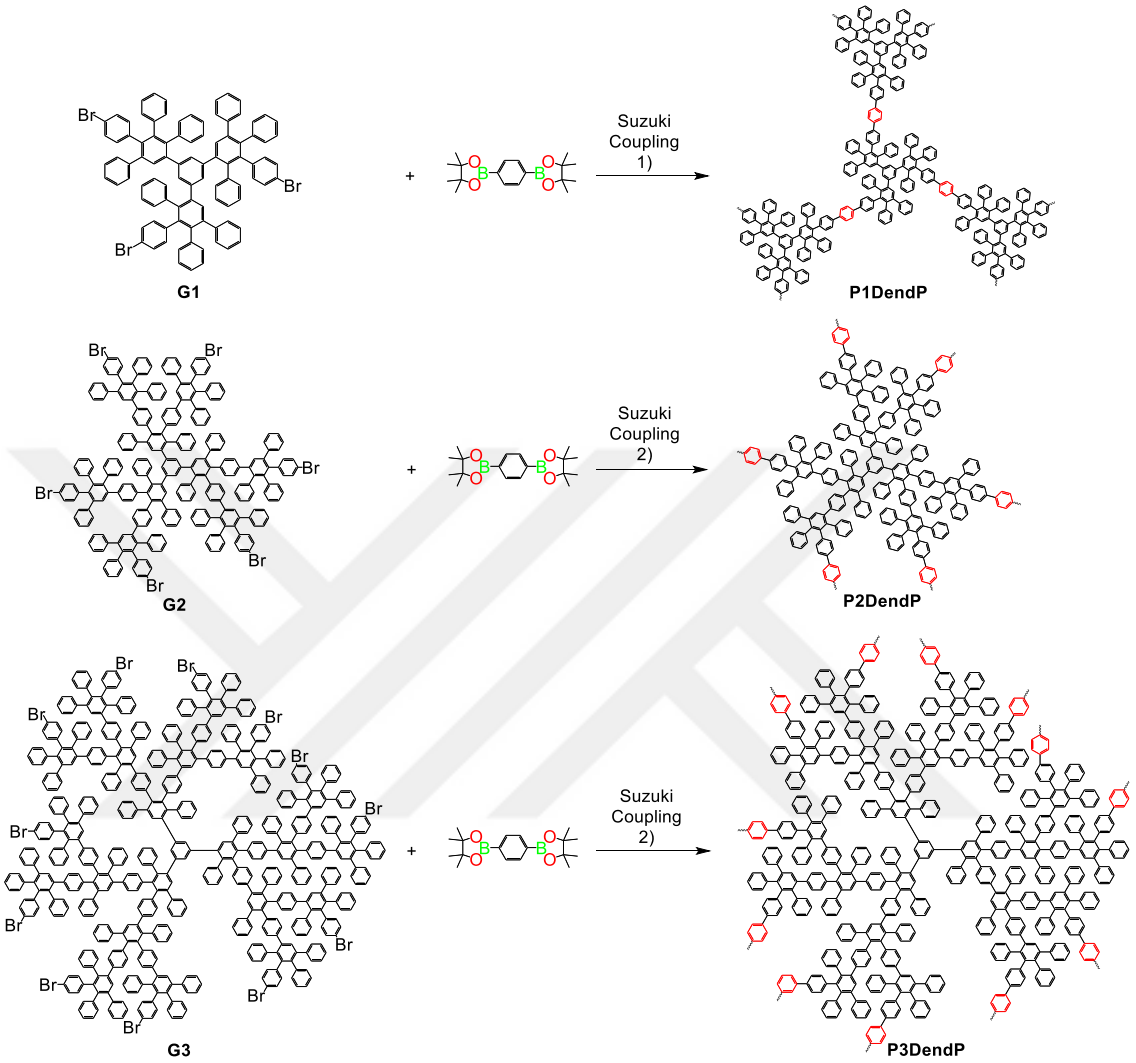

Figure 4.2. Synthesis of P1DendP, P2DendP, and P3DendP: Suzuki-Miyaura Coupling 1) $Pd(PPh_3)_4$, K_2CO_3, DMF, o-xylene, 150 ^oC; Suzuki-Miyaura Coupling 2) $Pd(PPh_3)_4$, K_2CO_3, DMF, 150 ^oC.

The Suzuki-Miyaura coupling reaction on three distinct PPD generations was used to synthesize P1DendP, P2DendP, and P3DendP, as demonstrated in Figure 4.2. The isolated yields for P1DendP, P2DendP, and P3DendP were 83, 79, and 79%, respectively. Some challenges were faced with the initial entry for P1DendP synthesis throughout the polymer synthesis optimizations since G1 was partially miscible in DMF. The isolated yield in the initial entry for G1 polymerization was poor, highlighting the necessity for

optimization using an appropriate solvent system, including DMF/o-xylene, which was illustrated in G1 polymerization. The result of this optimization gave rise to a good, desired percentage yield. The synthesis of P2DendP was performed without further optimization to provide effective polymerization since G2 dendrimer was soluble with numerous typical organic solvents, leading to an adequate isolated yield in the first trial. Lastly, the synthesis of P3DendP was carried out and isolated with a relatively high yield. Although three polymers (P1DendP, P2DendP, and P3DendP) showed high polymerization yield, they showed different porosity in terms of surface area and pore volume, which will be discussed in detail in the discussion part of this thesis (as shown in Figure 4.12 and Table 4.1). All produced compounds underwent additional characterization processes and were discussed in detail - G1a, G1ap, G2a, G2ap, G1, G2, G3, P1DendP, P2DendP, and P3DendP.

4.2. Porous Dendritic Polymers (PDendPs) Characterizations

Firstly, Fourier transform infrared (FT-IR) spectroscopy was used to verify the successful synthesis of the dendrimers and porous dendritic polymers (PDendPs) (Figure 4.3, 4.4, and 4.5). These spectra revealed the presence of polymeric and dendritic structures with a glimpse of the increases and decreases in some characteristic stretching bands of functionalities.

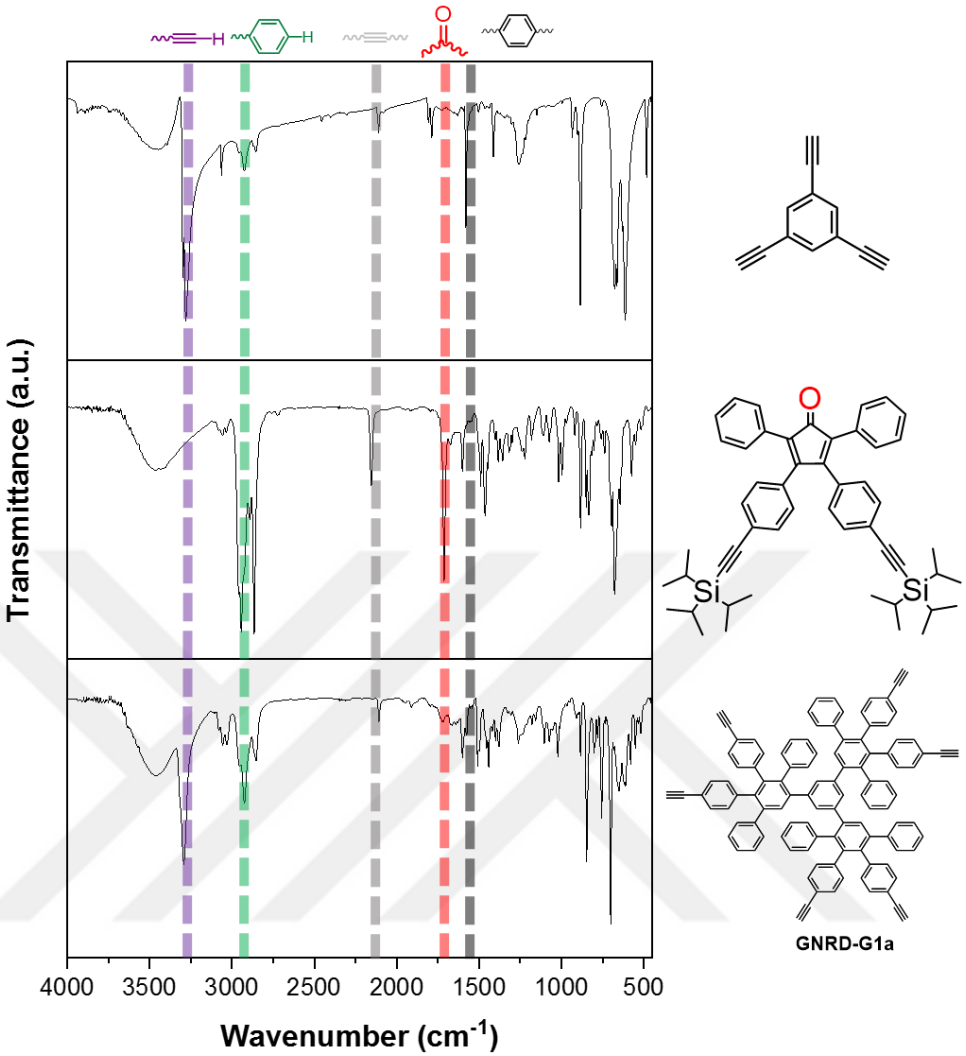

Figure 4.3. FT-IR spectra for the synthesized triethynylbenzene, CP-bis-sillyl and GNRD-G1a.

As seen in Figure 4.3, Fourier transform infrared spectroscopy initially confirms the formation of the dendritic macromolecular structure. The observed characteristic bands of both the C≡C and terminal alkyne (C≡C) C-H stretching bands in the regions of approximately 2100 cm^{-1} and 3200 cm^{-1}, respectively, verified the successful preparation of triethynylbenzene molecule. Similarly, the specific (C=O) stretching band of the bis-sillyl-cyclopentadienone molecule at around 1700 cm^{-1} clearly pointed out cyclopentadienone structure's presence. Besides the disappearance of the specific (C=O) stretching band of the bis-sillyl-cyclopentadienone molecule that appeared at around 1700 cm^{-1}, the presence of strong aromatic C-H stretching bands around 2800-2900 cm^{-1}

and aromatic C=C stretching bands around 1400-1600 cm^{-1} also suggested the successful synthesis of dendrimer GNRD-G1a. In addition, the observed peaks at around 2100 cm^{-1} and 3200 cm^{-1} can be attributed to the C≡C and the terminal alkyne (C≡C) C-H stretching bands, respectively, verifying the proposed chemical structure of the G1a dendrimer further.

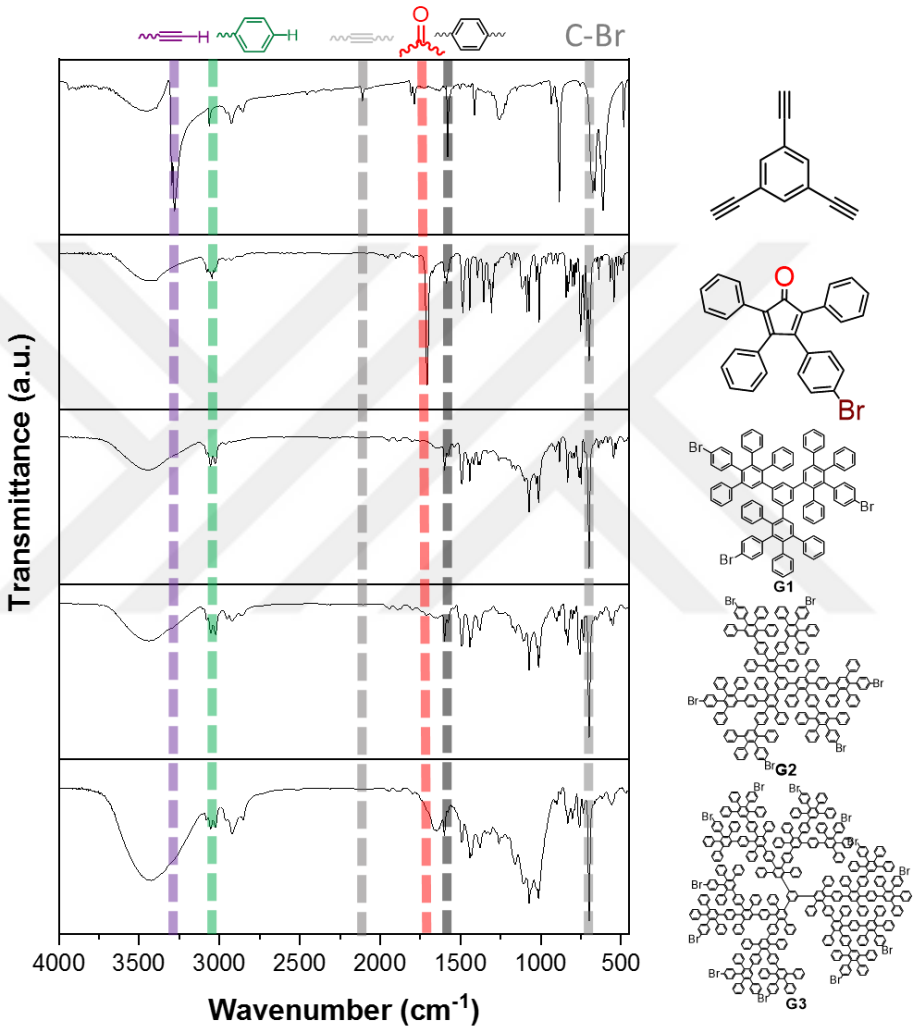

Figure 4.4. FT-IR spectra for the synthesized triethynylbenzene, CP-Br, G1, G2 and G3.

In a similar way, in Figure 4.4, the formation of dendrimers (G1, G2, and G3) to be used as monomers in the synthesis of dendritic polymers with peripheral bromines was also characterized using FT-IR spectroscopy. In the FT-IR spectra of G1, G2, and G3 dendrimers, aromatic C-H stretching bands around 3000 cm^{-1}, aromatic C=C stretching bands around 1400-1600 cm^{-1}, and a specific C-Br stretching band around 600 cm^{-1} were

readily demonstrated in the spectra.

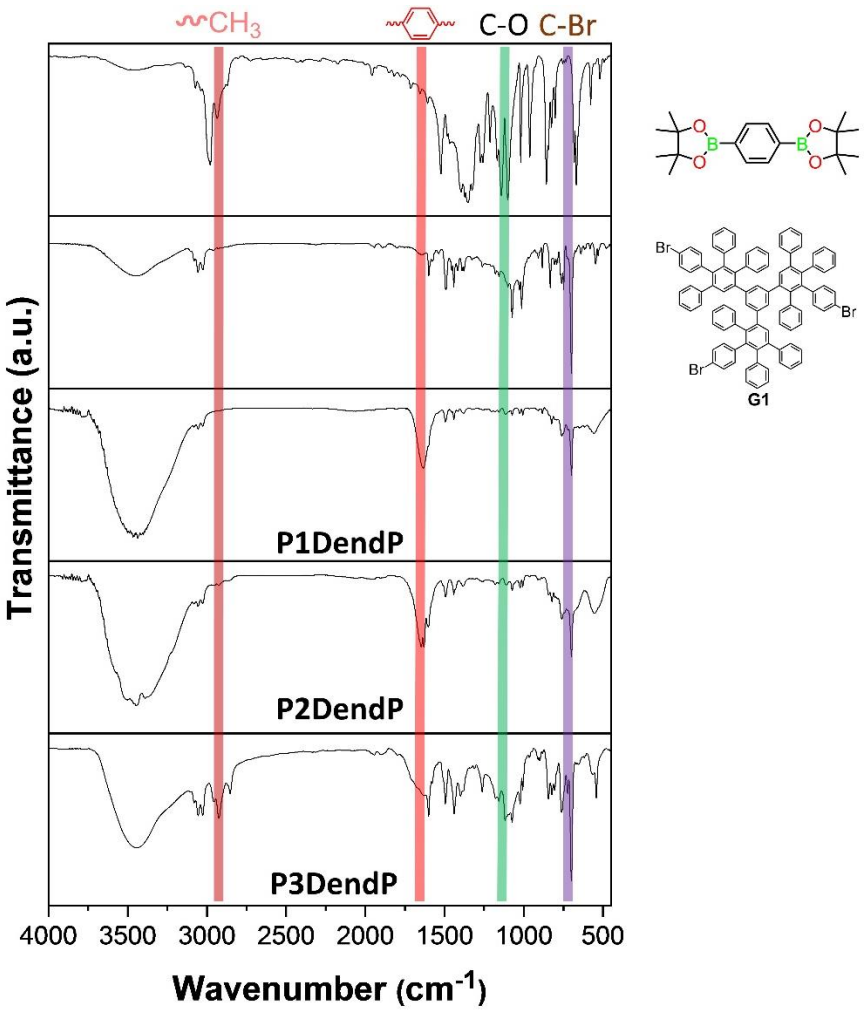

Figure 4.5. FT-IR spectra for the resulting phenylene bis-boronic ester, G1, P1DendP, P2DendP, and P3DendP.

The spectra of phenylene bis-boronic ester revealed the existence of methyl C-H stretching bands around 2900 cm^{-1}, aromatic C=C stretching bands in the 1300-1500 cm^{-1} region, and C-O stretching bands at 1000-1100 cm^{-1}. When the FT-IR spectra of PDendPs were compared to the spectra of G1, G2, and phenylene bis-boronic ester, a drastic decrease in the phenylene bis-boronic ester peaks in the 2900 cm^{-1} and 1000-1100 cm^{-1} bands, and the specific C-Br stretching peak at about 600 cm^{-1} band was observed (Figure 4.5). The increase in the aromatic C=C stretching bands around 1600 cm^{-1} also suggests the successful synthesis of PDendPs. While the FT-IR analysis of the PDendPs confirmed an effective polymerization via the Suzuki-Miyaura coupling reaction, the FT-

IR spectrum of the P3DendP polymer displayed a moderate reduction for the levels of the peaks in the 2900 cm^{-1} and 1000-1100 cm^{-1} regions of the phenylene bis-boronic ester and limited in C-Br stretching region at nearly 600 cm^{-1} compared to the observed alteration for P1DendP and P2DendP. The FT-IR spectrum suggested that not all the bromo atoms and phenylene bis-boronic ester cannot undergo a polymerization reaction due to the large generation of G3 dendrimer, leading to a large number of bromo atoms with steric hindrance. However, G3 dendrimers underwent polymerization with a ditopic boronic ester linker to afford the desired polymeric network.

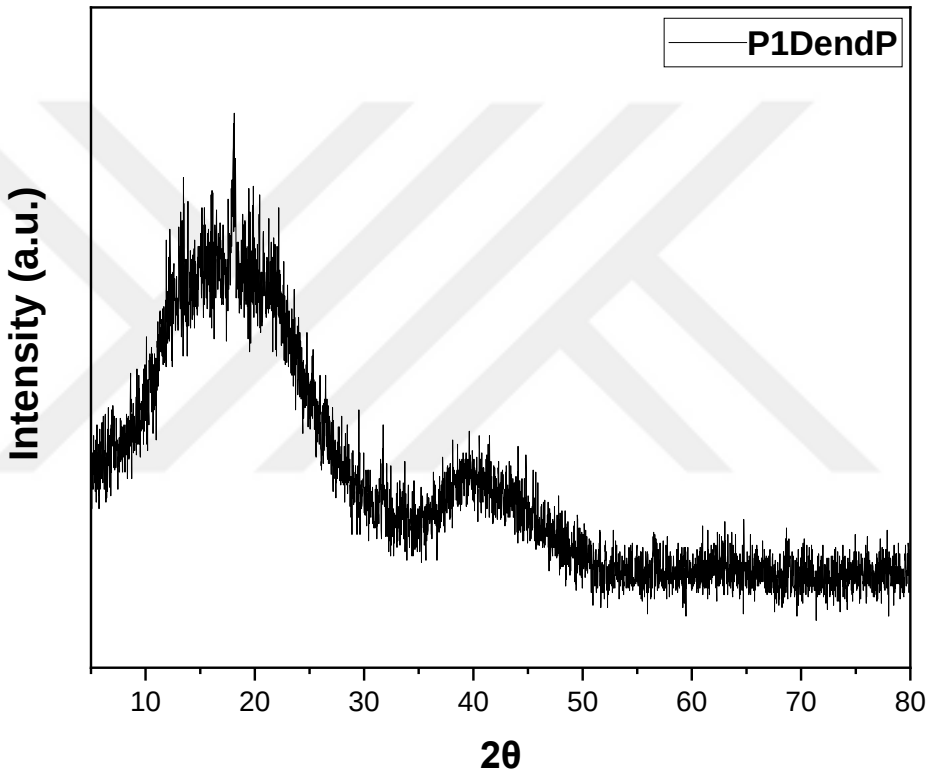

Figure 4.6. XRD spectrum of P1DendP.

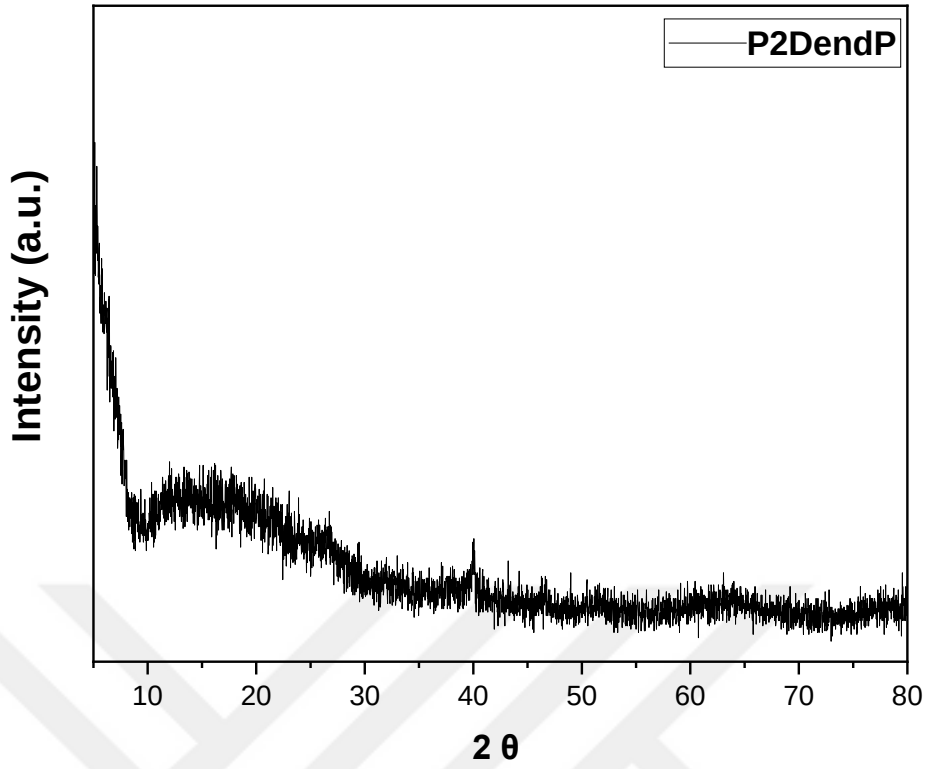

Figure 4.7. XRD spectrum of P2DendP.

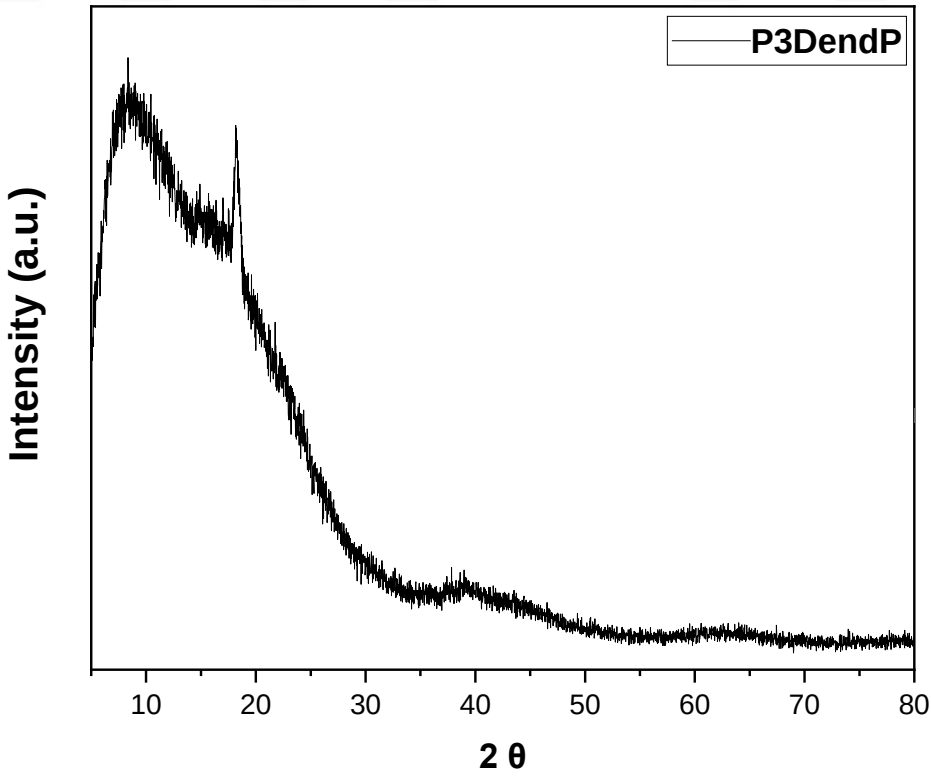

Figure 4.8. XRD spectrum of P3DendP.

The structural order of dendritic polymers was investigated using X-ray diffraction (XRD). Amorphous compounds are deficient in clearly defined crystallographic planes, resulting in a disordered distribution of atoms. This results in broad peaks in the collected XRD pattern rather than sharp, intense peaks in long-range order materials. The broad peaks result from short-range or regional compositional order in amorphous materials (lack of long-range order). As shown in Figure 4.6, Figure 4.7, and Figure 4.8, the XRD data collected for the polymers P1DendP, P2DendP, and P3DendP lack sharp and intense peaks and suggest their amorphous structure without a long-ranged pattern.

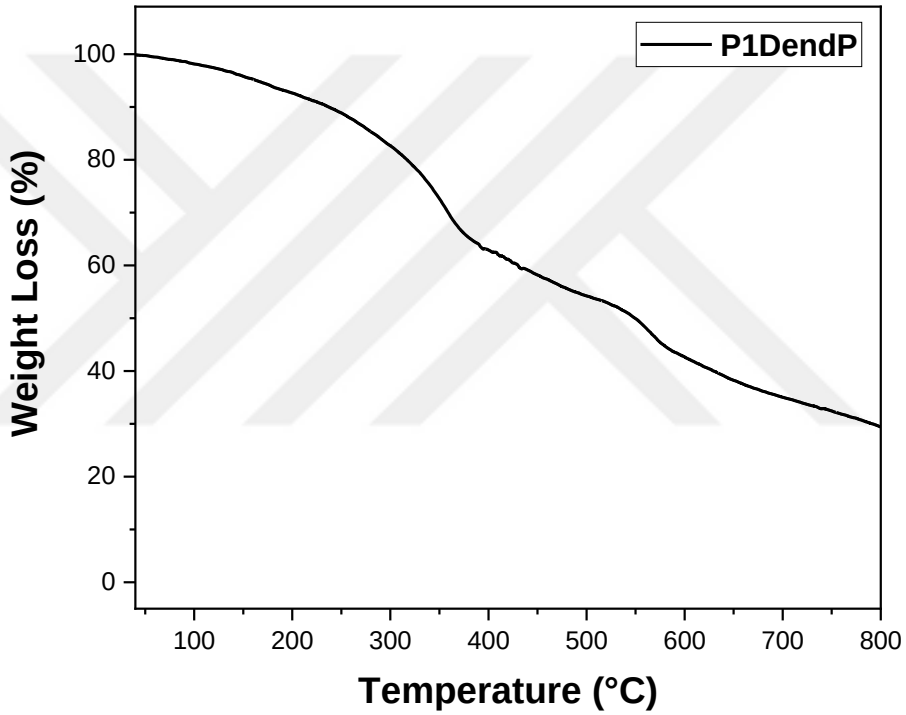

Figure 4.9. Thermogravimetric analysis (TGA) of P1DendP performed under a nitrogen atmosphere from 25 °C to 800 °C at a heating rate of 10 °C/min.

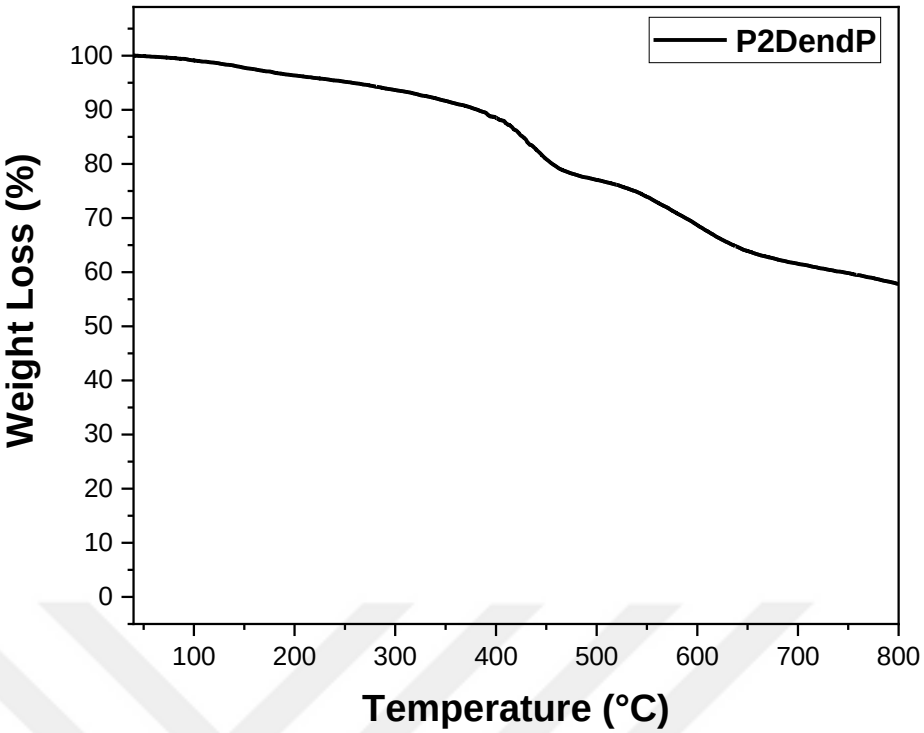

Figure 4.10. Thermogravimetric analysis (TGA) of P2DendP performed under a nitrogen atmosphere from 25 °C to 800 °C at a heating rate of 10 °C/min.

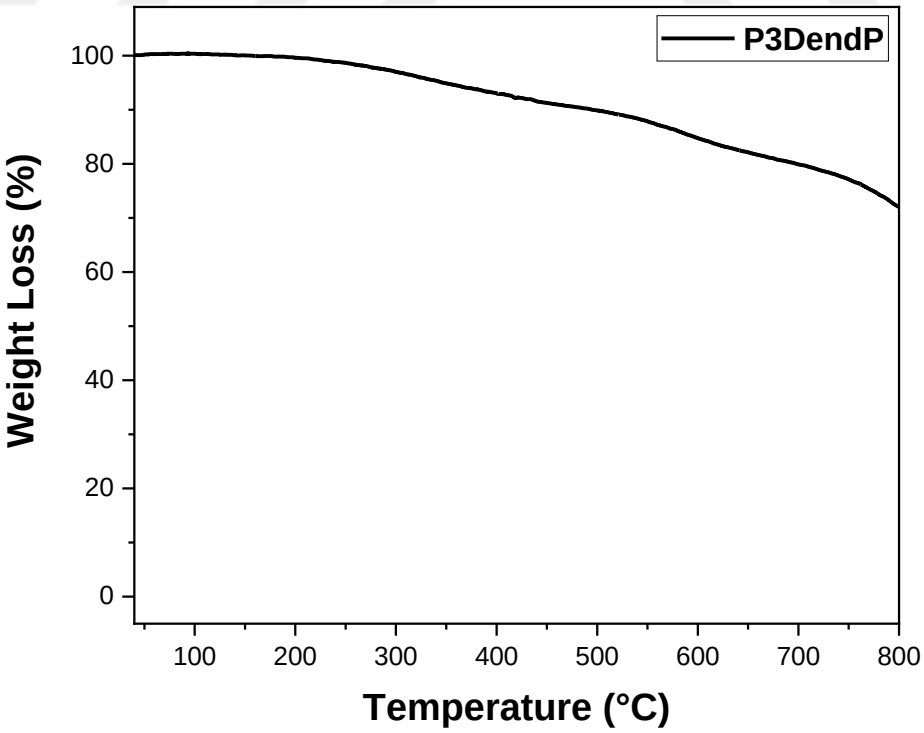

Figure 4.11. Thermogravimetric analysis (TGA) of P3DendP performed under a nitrogen atmosphere from 25 °C to 800 °C at a heating rate of 10 °C/min.

Thermogravimetric analysis (TGA) was used to assess the thermal stability of all manufactured dendritic polymers. As shown in Figure 4.9, a percentage-based decrease in weight of below 100 ^{o}C was observed from the TGA of P1DendP, stemming from the humidity trapped inside the pores of the polymers. Additionally, the P1DendP polymer showed good thermal stability at up to 250 °C. As observed in the P1DendP polymer, the TGA measurement of the P2DendP polymer revealed a moisture absorption phenomenon involving a percentage reduction in weight at around 100 ^{o}C. Furthermore, the P2DendP polymer has shown stability at even 300 °C (Figure 4.10). This condition demonstrated that P2DendP has a more thermally stable structure than P1DendP polymer due to its considerably larger branched backbone framework, which contains a thermally stable benzene-rich skeleton. Based on the TGA thermogram of P3DendP in Figure 4.11, the humidity uptake of P3DendP was limited compared to the amount of the P1DendP and P2DendP polymers. Additionally, P3DendP has demonstrated outstanding thermal stability up to 400 °C. The findings show that P3DendP has a more robust and thermally stable structure than P1DendP and P2DendP polymers due to the extremely branched skeleton inside the skeleton, which contains stiff ring structures made of benzene. It is important to note that the P3DendP showed greater char yield than P1DendP and P2DendP. Furthermore, because polymers can experience a cyclodehydrogenation process at elevated temperatures, resulting in the emission of H_2 gas, they may trigger decreases in weight at these locations. Then, as an outcome of the cyclodehydrogenation, they transform into molecules with greater thermal endurance. Similarly, it is evident that the P3DendP polymer with the most dendritic components possesses the capacity for a highly rapid level of cyclodehydrogenation reaction, and the production of broad nanographene nanostructures proves that it exhibits the best thermal durability and enhanced char yield throughout the process of transformation.[9]

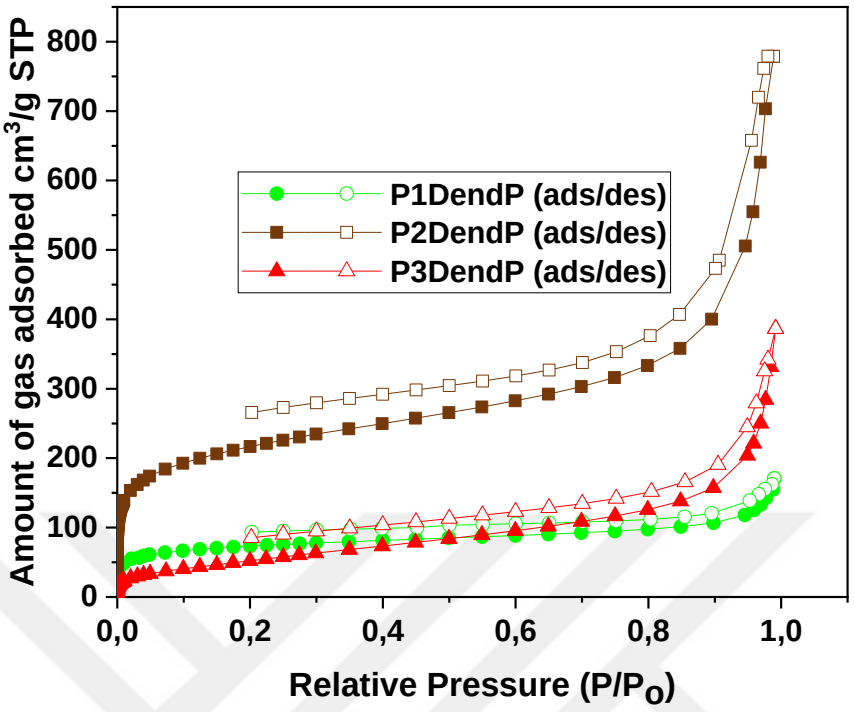

Figure 4.12. N_2 gas adsorption-desorption isotherms of P1DendP, P2DendP, P3DendP obtained at 77 K.

Table 4.1. Porosity analysis of P1DendP, P2DendP, P3DendP.

Polymers	BET[a] (m^2g^{-1})	S_{micro}[b] (m^2g^{-1})	S_{ext} (m^2g^{-1})	V_{total}[c] (cm^3g^{-1})	V_{micro}[d] (cm^3g^{-1})	V_{ext}[e] (cm^3g^{-1})
P1DendP	266	208	58	0.26	0.08	0.18
P2DendP	779	450	329	0.22	0.19	0.03
P3DendP	179	4	175	0.04	0.02	0.02

[a] BET surface area calculated using the relative pressure range (P/P_0) of 0.01–0.11. [b] Micropore surface area calculated using the t-plot method. [c] Total pore volume obtained at P/P_0=0.99. [d] Micropore volume calculated using the t-plot method. [e] $V_{external}=V_{total}-V_{micro}$.

Figure 4.12 shows that P2DendP outperforms the other two polymers in terms of gas adsorption properties. Furthermore, using the relative pressure (P/P_o) vs $1/[Q(P/P_o - 1)]$ graphs used in the Brunauer-Emmett-Teller theory, the S_{BET} surface area results for the synthesized polymers were easily calculated; P1DendP, P2DendP, and P3DendP were 266 $m^2 g^{-1}$, 779 $m^2 g^{-1}$, and 179 $m^2 g^{-1}$, respectively (Table 4.1). P3DendP exhibited lower porosity and surface area compared to other polymers. The primary reason for this occurrence is that more branching and a more significant number of phenylene rings result in the closure of pore openings. Furthermore, a microporosity study of the polymers revealed that the generated P1DendP and P2DendP polymers had an elevated micropore surface area and volume, as calculated using the t-plot technique. However, the P3DendP polymer has a 50% micropore volume while maintaining a modest micropore surface area.

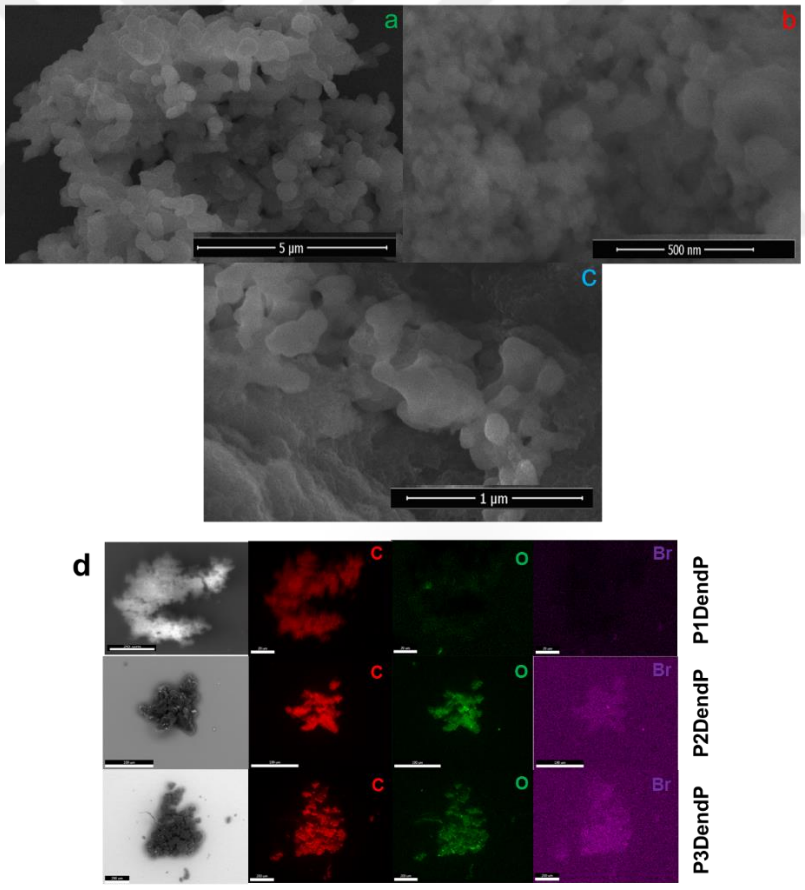

Figure 4.13. SEM images a) P1DendP b) P2DendP c) P3DendP d) SEM images and EDX elemental mapping of P1DendP, P2DendP and P3DendP for the elements of carbon (C), oxygen (O), bromine (Br).

The particle morphology of P1DendP (Figure 4.13.a), P2DendP (Figure 4.13.b), and P3DendP (Figure 4.13.c) was investigated utilizing scanning electron microscopy (SEM). Three porous dendritic polymers showed globular particle morphology. Energy dispersive X-ray spectroscopy (EDX) showed a homogenous distribution of carbon (C) across the polymers (Figure 4.13.d); furthermore, in the EDX investigation done for the potential elements oxygen (O), and bromine (Br), as well. The polymers-P1DendP, P2DendP, and P3DendP-were showed some residual bromine (Br) atoms that did not undergo polymerization reaction and oxygen (O) atoms mainly stemming from the humidity trapped inside the pores.

4.3.Gas Sensing Applications for PDendPs

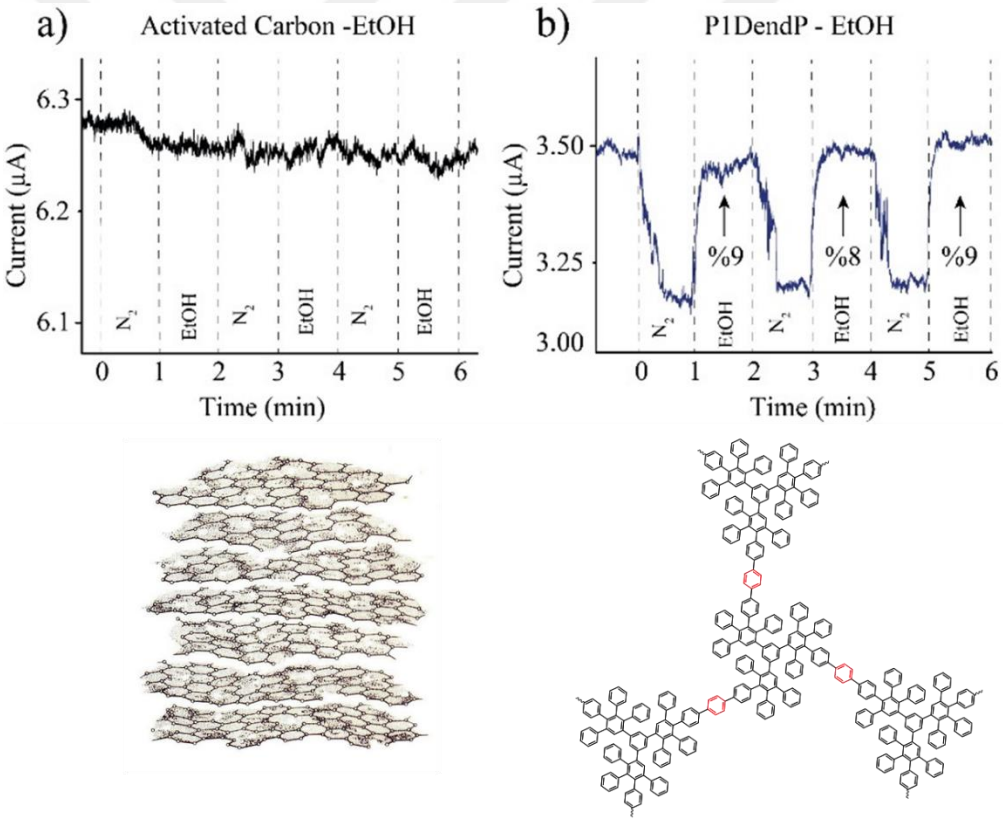

Figure 4.14. The sensor measurements for target gas of EtOH (a) activated carbon (%90 activated carbon and %10 PTFE), (b) P1DendP (%60 P1DendP, %30 activated carbon and %10 PTFE).

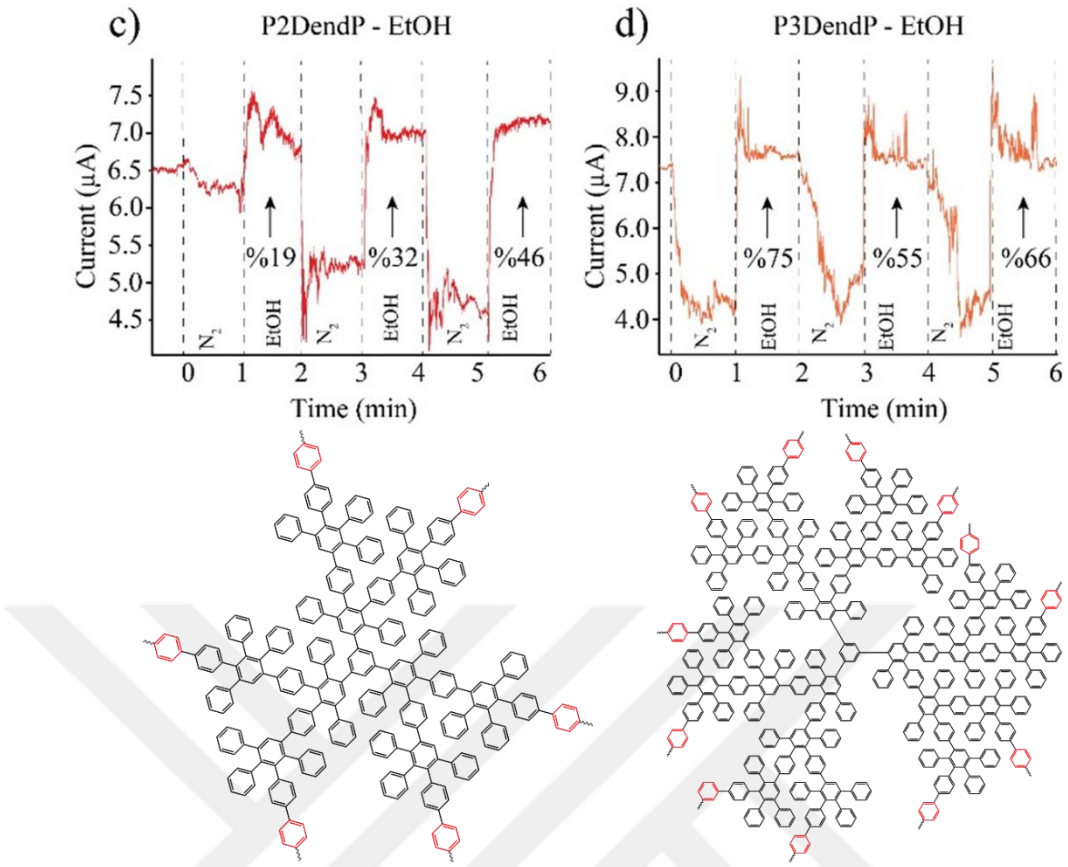

Figure 4.15. The sensor measurements for target gas of EtOH (c) P2DendP (%60 P2DendP, %30 activated carbon and %10 PTFE), (d) P3DendP (%60 P3DendP, %30 activated carbon and %10 PTFE).

A blend of PDendPs, polytetrafluoroethylene (PTFE), and activated carbon is used to test the sensing materials for sensor applications. While PTFE works as a binder, the activated carbon contributes to electrical conductivity. To test the effect of the presence of activated carbon, a control experiment was conducted using activated carbon as the only active material. The prepared activated carbon surface did not demonstrate any current change when N_2 and EtOH gases existed on the chemiresistor.

The activated carbon ratio and the binder (PTFE) were held constant at 30% and 10% for each gas sensing test of PDendPs. As seen in Figure 4.14 and Figure 4.15, the total amount of activated carbon did not alter; instead, the current increase variation demonstrated the polymers' sensitivity to ethanol vapor. The sizes are arranged by P3DendP>P2DendP>P1DendP in that order for three polymers, and a pattern was discovered in line with those sizes. As anticipated, P3DendP, having a greater number of branching, can come into contact with more ethanol molecules and cause the current to

grow further, thereby allowing the largest P3DendP polymer in this situation to increase in current. The outcomes for sensor tests are well correlated with these expectations. The primary cause of this pattern is the varying encapsulation capabilities and cavities of the three dendrimers, which are highly branched dendritic macromolecules. A dendrimer's encapsulation capability correlates precisely with the number of molecules it can interact. Therefore, a dendrimer's capacity is highest when it has the most branching units on the macromolecular structure. P3DendP>P2DendP>P1DendP is the quantity of dendrimer interaction with ethanol. The red benzene rings show the linkage sites in the schematized dendrimers.

The HPPM measurement is helpful for understanding whether materials have an n-type or p-type character. A negative voltage value means that the material has a p-type character, while a positive value means that the material has an n-type character. HPPM investigations have revealed the p-type nature of the sensing material, which was found to have a voltage value of -0.4mV for P1DendP. Finally, it was concluded that P1DendP has a p-type character.

In chemiresistor applications, the electrical charge transmission between the sensing material and the analyte gas is critical. This situation makes the conductivity type of device more crucial. Holes are the predominant charge carriers on p-type materials. More charge carriers are on the surface due to the p-type feature increasing due to a p-type device's contact with a p-dopant molecule. Once the sensor is measured, the current increases due to a boost of charge carriers over its surface.

According to computational studies, these three dendritic polymers were p-doped by ethanol. Thus, since ethanol gas was dropped upon the surface, it was observed that the current increased in ethanol gas sensing measurements utilizing P1DendP, P2DendP, and P3DendP as the sensing material. The literature places a great deal of importance on the ability of N_2 gas to remove contaminants from the surface. Prior to the ethanol adsorption, the surface was cleared of O_2 and other air adsorbates that had accumulated over it by one minute of exposure to nitrogen gas. Put another way, nitrogen gas removes molecules from the surface that contribute to p-type doping, like electron-accepting molecules oxygen and water, and the total amount of holes on the surface decreases, thereby substantially decreasing the p-type characteristic of the surface. As seen by our sensor observations in Figure 4.14, and Figure 4.15, this circumstance results in a decrease in current.

Schematic representation of dendritic polymer, one of its dendronic sites, and charge transfer between dendrimer and ethanol was demonstrated in Figure 4.16.a, Figure 4.16.b, and Figure 4.16.c, successively. The calculations indicated that each dendronic site donates 0.02 e^- to one p-dopant ethanol molecule, thereby significantly enhancing the p-type behavior of the surface in the sensing material of chemiresistor. The increased dendronic sites through generations cause elevated electron donation, holes, and percent response. Furthermore, the binding energy between polymer and ethanol was calculated as E_b = 347 meV, proving the weak Van der Waals interaction. In this manner, the calculation applied to PDendPs correlates well with the experimental findings, which reveal the increased current change or percent response with higher degrees of dendritic sites.

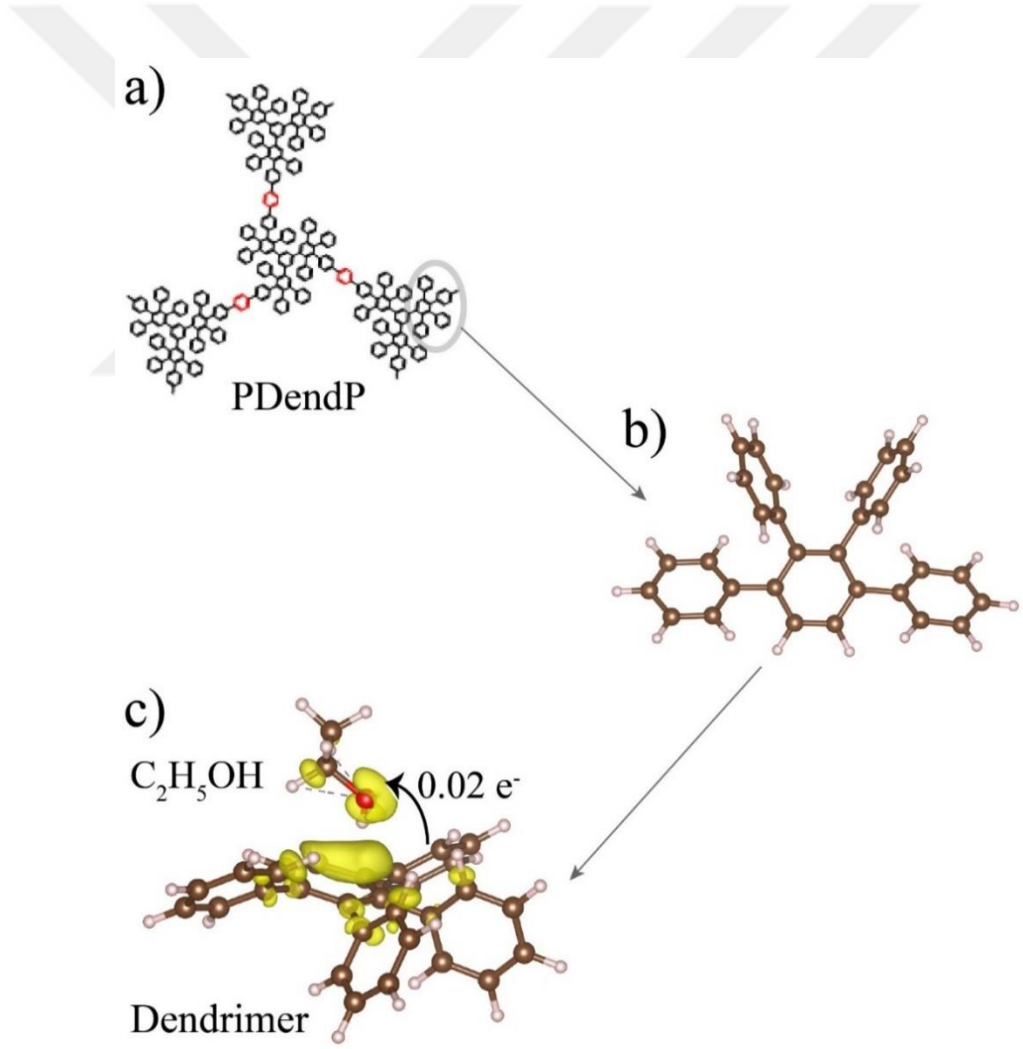

Figure 4.16. (a) Schematic illustration of PDendP, (b) computer illustration of its dendronic site, (c) charge transfer between dendrimer and ethanol molecule.

CHAPTER 5

CONCLUSION

The highly branched, rigid, porous dendritic polymers P1DendP, P2DendP, and P3DendP containing fully carbon atoms were presented as three novel materials for chemiresistor sensor applications. The Suzuki-Miyaura coupling reaction conditions were employed to synthesize P1DendP, P2DendP, and P3DendP with good yields of 83, 79, and 79%, respectively. Among the dendritic polymers, the thermal stability reaches up to 400 ^{o}C for P3DendP, and the largest S_{BET} surface area results is 779 m^2/g for P2DendP. Then, the XRD spectrum unambiguously demonstrated amorphous structures for all polymers and SEM images explicitly demonstrate globular-shaped structures along with EDX elemental mapping, highlighting a homogeneous dispersion of carbon atoms throughout the polymers.

Moreover, in gas-sensing applications, the outcomes regarding these porous dendritic polymers put forward highly branched P3DendP could be effectively employed for the detection of protic solvents such as ethanol. Then, theoretical calculations indicate that ethanol acts as a p-dopant for these three polymers. Consequently, during ethanol gas sensing measurements using P1DendP, P2DendP, and P3DendP as sensing materials, an increase in current is observed when ethanol gas is sent to the surface. Finally, this research paves the way not only to design carbon-based materials for sensing hazardous gases but also to develop a novel approach for the bottom-up solution synthesis of GNRs.

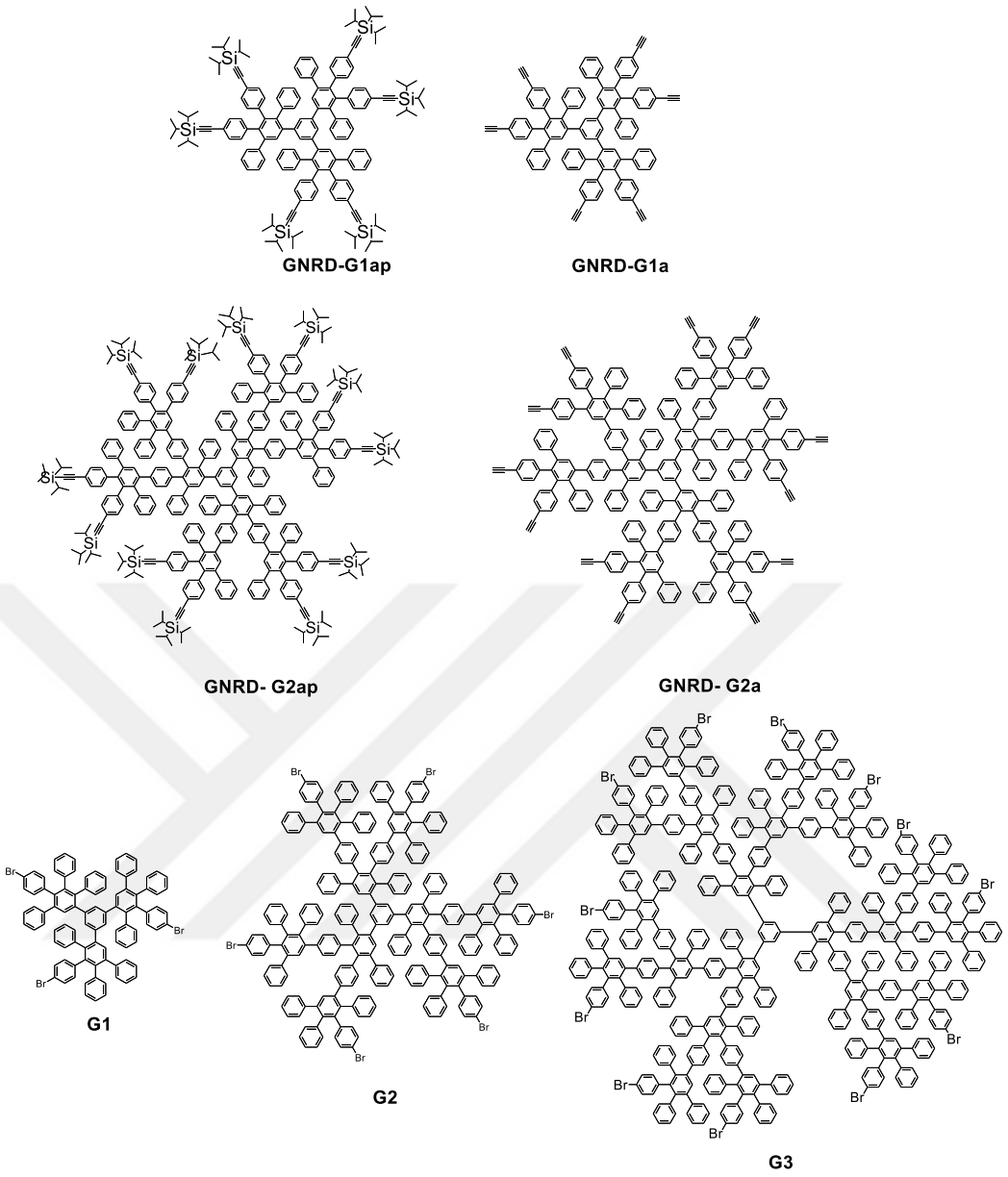

Figure 5.1. Summary of synthesized dendrimers.

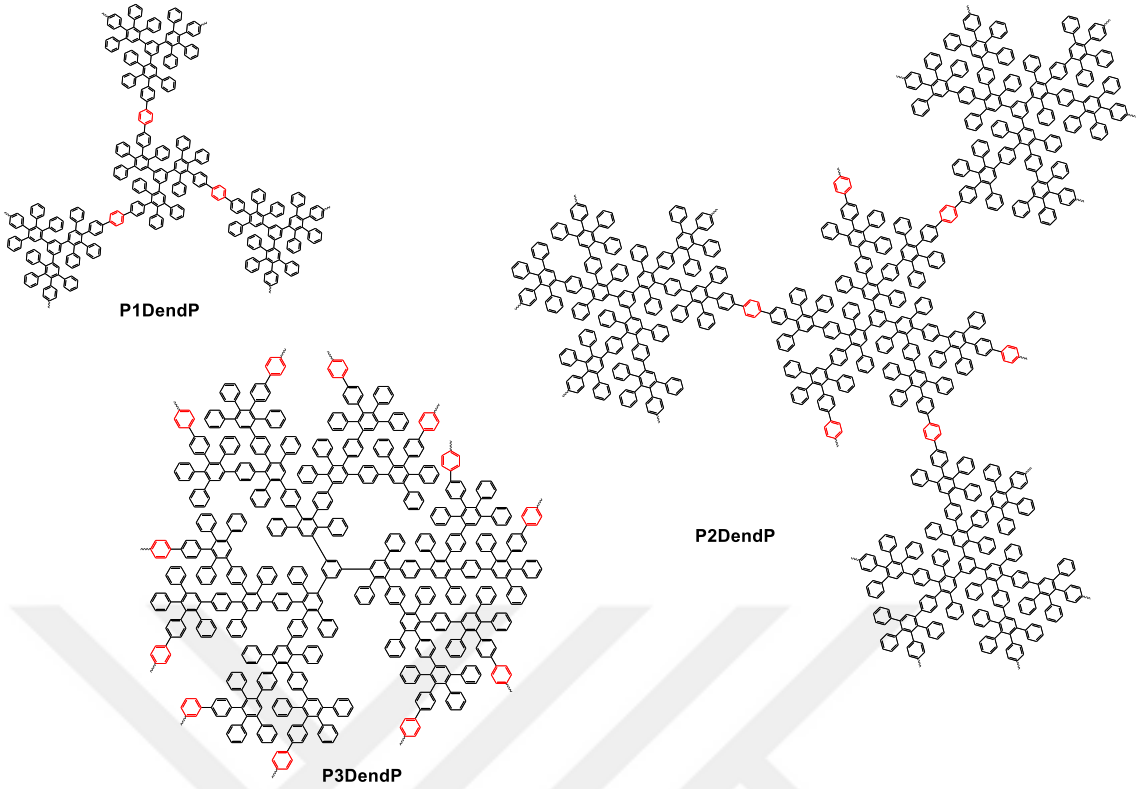

Figure 5.2. Summary of synthesized polymers.

REFERENCES

1. Feng, X.; Liang, Y.; Zhi, L.; Thomas, A.; Wu, D.; Lieberwirth, I.; Kolb, U.; Müllen, K., Synthesis of Microporous Carbon Nanofibers and Nanotubes from Conjugated Polymer Network and Evaluation in Electrochemical Capacitor. *Advanced Functional Materials* **2009**, *19* (13), 2125-2129. DOI: 10.1002/adfm.200900264

2. Hammer, B. A. G.; Müllen, K., Dimensional Evolution of Polyphenylenes: Expanding in All Directions. *Chemical Reviews* **2016**, *116* (4), 2103-2140. DOI: 10.1021/acs.chemrev.5b00515

3. Imai, M.; Arai, T., Synthesis and photochemical properties of polyphenylene dendrimers with photoreactive stilbene core. *Tetrahedron Letters* **2002**, *43* (30), 5265-5268. DOI: 10.1016/S0040-4039(02)01063-8

4. Shen, X.; Ho, D. M.; Pascal, R. A., Synthesis of Polyphenylene Dendrimers Related to "Cubic Graphite". *Journal of the American Chemical Society* **2004**, *126* (18), 5798-5805. DOI: 10.1021/ja030675c

5. Stangenberg, R.; Saeed, I.; Kuan, S. L.; Baumgarten, M.; Weil, T.; Klapper, M.; Müllen, K., Tuning Polarity of Polyphenylene Dendrimers by Patched Surface Amphiphilicity—Precise Control over Size, Shape, and Polarity. *Macromolecular Rapid Communications* **2014**, *35* (2), 152-160. DOI: 10.1002/marc.201300671

6. Stangenberg, R.; Türp, D.; Müllen, K., Shape persistent hybrid dendrimers from benzene and triazole via 'click chemistry'. *Tetrahedron* **2014**, *70* (19), 3178-3184. DOI: 10.1016/j.tet.2014.03.037

7. Türp, D.; Nguyen, T.-T.-T.; Baumgarten, M.; Müllen, K., Uniquely versatile: nano-site defined materials based on polyphenylene dendrimers. *New Journal of Chemistry* **2012**, *36* (2), 282-298. DOI: 10.1039/c1nj20449a

8. Wiesler, U. M.; Berresheim, A. J.; Morgenroth, F.; Lieser, G.; Müllen, K., Divergent Synthesis of Polyphenylene Dendrimers: The Role of Core and

Branching Reagents upon Size and Shape. *Macromolecules* **2001**, *34* (2), 187-199. DOI: 10.1021/ma991519m

9. Hammer, B. A. G.; Müllen, K., Expanding the limits of synthetic macromolecular chemistry through Polyphenylene Dendrimers. *Journal of Nanoparticle Research* **2018**, *20* (10), 262. DOI: 10.1007/s11051-018-4364-6

10. Hammer, B. A. G.; Moritz, R.; Stangenberg, R.; Baumgarten, M.; Müllen, K., The polar side of polyphenylene dendrimers. *Chemical Society Reviews* **2015**, *44* (12), 4072-4090. DOI: 10.1039/c4cs00245h

11. Müller, S.; Müllen, K., Expanding benzene to giant graphenes: towards molecular devices. *Philosophical Transactions of the Royal Society A: Mathematical, Physical and Engineering Sciences* **2007**, *365* (1855), 1453-1472. DOI: 10.1098/rsta.2007.2026

12. Binder, K.; Butt, H.-J.; Floudas, G.; Frey, H.; Hsu, H.-P.; Landfester, K.; Kolb, U.; Kühnle, A.; Maskos, M.; Müllen, K.; Paul, W.; Schmidt, M.; Spiess, H. W.; Virnau, P., Structure Formation of Polymeric Building Blocks: Complex Polymer Architectures. *Advances in Polymer Science* **2014**, *260*, 115-210. DOI: 10.1007/12_2013_230

13. Narita, A.; Wang, X.-Y.; Feng, X.; Müllen, K., New advances in nanographene chemistry. *Chemical Society Reviews* **2015**, *44* (18), 6616-6643. DOI: 10.1039/c5cs00183h

14. Watson, M. D.; Fechtenkötter, A.; Müllen, K., Big Is Beautiful−"Aromaticity" Revisited from the Viewpoint of Macromolecular and Supramolecular Benzene Chemistry. *Chemical Reviews* **2001**, *101* (5), 1267-1300. DOI: 10.1021/cr990322p

15. Bieri, M.; Nguyen, M.-T.; Gröning, O.; Cai, J.; Treier, M.; Aït-Mansour, K.; Ruffieux, P.; Pignedoli, C. A.; Passerone, D.; Kastler, M.; Müllen, K.; Fasel, R., Two-Dimensional Polymer Formation on Surfaces: Insight into the Roles of Precursor Mobility and Reactivity. *Journal of the American Chemical Society* **2010**, *132* (46), 16669-16676. DOI: 10.1021/ja107947z

16. Wind, M.; Saalwächter, K.; Wiesler, U. M.; Müllen, K.; Spiess, H. W., Solid-State NMR Investigations of Molecular Dynamics in Polyphenylene Dendrimers: Evidence of Dense-Shell Packing. *Macromolecules* **2002**, *35* (27), 10071-10086. DOI: 10.1021/ma021283d

17. Li, C.; Liu, M.; Pschirer, N. G.; Baumgarten, M.; Müllen, K., Polyphenylene-Based Materials for Organic Photovoltaics. *Chemical Reviews* **2010**, *110* (11), 6817-6855. DOI: 10.1021/cr100052z

18. Zhang, D.; Yao, H.; Zhou, D.; Dai, L.; Zhang, J.; Yuan, S., Synthesis, characteristics and adsorption properties of polyphenylene sulfide based strong acid ion exchange fiber. *Polymers for Advanced Technologies* **2014**, *25* (12), 1590-1595. DOI: 10.1002/pat.3407

19. Zhang, G.; Baumgarten, M.; Auer, M.; Trattnig, R.; List-Kratochvil, E. J. W.; Müllen, K., Core-and-Surface-Functionalized Polyphenylene Dendrimers for Solution-Processed, Pure-Blue Light-Emitting Diodes Through Surface-to-Core Energy Transfer. *Macromolecular Rapid Communications* **2014**, *35* (22), 1931-1936. DOI: 10.1002/marc.201400439

20. Morgenroth, F.; Kübel, C.; Müllen, K., Nanosized polyphenylene dendrimers based upon pentaphenylbenzene units. *Journal of Materials Chemistry* **1997**, *7* (7), 1207-1211. DOI: 10.1039/A700032D

21. Qin, T.; Ding, J.; Wang, L.; Baumgarten, M.; Zhou, G.; Müllen, K., A Divergent Synthesis of Very Large Polyphenylene Dendrimers with Iridium(III) Cores: Molecular Size Effect on the Performance of Phosphorescent Organic Light-Emitting Diodes. *Journal of the American Chemical Society* **2009**, *131* (40), 14329-14336. DOI: 10.1021/ja905118t

22. Wiesler, U.-M.; Müllen, K., Polyphenylene dendrimers via Diels–Alder reactions: the convergent approach. *Chemical Communications* **1999**, (22), 2293-2294. DOI: 10.1039/A907339F

23. Andreitchenko, E. V.; Bauer, R. E.; Kreutz, C.; Baumgarten, M.; Bargon, J.; Müllen, K., Size and Shape Variation of Polyphenylene Dendrimers through the

Heterogeneous Hydrogenation of Embedded Triple Bonds. *Macromolecules* **2008**, *41* (3), 548-558. DOI: 10.1021/ma701996j

24. Nguyen, T.-T.-T.; Baumgarten, M.; Rouhanipour, A.; Räder, H. J.; Lieberwirth, I.; Müllen, K., Extending the Limits of Precision Polymer Synthesis: Giant Polyphenylene Dendrimers in the Megadalton Mass Range Approaching Structural Perfection. *Journal of the American Chemical Society* **2013**, *135* (11), 4183-4186. DOI: 10.1021/ja311430r

25. Nguyen, T.-T.-T.; Türp, D.; Wagner, M.; Müllen, K., Photoswitchable Conductivity in a Rigidly Dendronized Salt. *Angewandte Chemie International Edition* **2013**, *52* (2), 669-673. DOI: 10.1002/ange.201206010

26. Wu, J.; Gherghel, L.; Watson, M. D.; Li, J.; Wang, Z.; Simpson, C. D.; Kolb, U.; Müllen, K., From Branched Polyphenylenes to Graphite Ribbons. *Macromolecules* **2003**, *36* (19), 7082-7089. DOI: 10.1021/ma0257752

27. Bieri, M.; Treier, M.; Cai, J.; Aït-Mansour, K.; Ruffieux, P.; Gröning, O.; Gröning, P.; Kastler, M.; Rieger, R.; Feng, X.; Müllen, K.; Fasel, R., Porous graphenes: two-dimensional polymer synthesis with atomic precision. *Chemical Communications* **2009**, (45), 6919-6921. DOI: 10.1039/b915190g

28. Simpson, C. D.; Mattersteig, G.; Martin, K.; Gherghel, L.; Bauer, R. E.; Räder, H. J.; Müllen, K., Nanosized Molecular Propellers by Cyclodehydrogenation of Polyphenylene Dendrimers. *Journal of the American Chemical Society* **2004**, *126* (10), 3139-3147. DOI: 10.1021/ja036732j

29. Narita, A.; Feng, X.; Hernandez, Y.; Jensen, S. A.; Bonn, M.; Yang, H.; Verzhbitskiy, I. A.; Casiraghi, C.; Hansen, M. R.; Koch, A. H. R.; Fytas, G.; Ivasenko, O.; Li, B.; Mali, K. S.; Balandina, T.; Mahesh, S.; De Feyter, S.; Müllen, K., Synthesis of structurally well-defined and liquid-phase-processable graphene nanoribbons. *Nature Chemistry* **2014**, *6* (2), 126-132. DOI: 10.1038/NCHEM.1819

30. Maus, M.; Mitra, S.; Lor, M.; Hofkens, J.; Weil, T.; Herrmann, A.; Müllen, K.; De Schryver, F. C., Intramolecular Energy Hopping in Polyphenylene

Dendrimers with an Increasing Number of Peryleneimide Chromophores. *The Journal of Physical Chemistry A* **2001**, *105* (16), 3961-3966. DOI: 10.1021/jp003643+

31. Weil, T.; Reuther, E.; Müllen, K., Shape-Persistent, Fluorescent Polyphenylene Dyads and a Triad for Efficient Vectorial Transduction of Excitation Energy. *Angewandte Chemie International Edition* **2002**, *114* (11), 1980-1984. DOI: 10.1002/1521-3757(20020603)114:11<1980::AID-ANGE1980>3.0.CO;2-Z

32. Hammer, B. A. G.; Wu, Y.; Fischer, S.; Liu, W.; Weil, T.; Müllen, K., Controlling Cellular Uptake and Toxicity of Polyphenylene Dendrimers by Chemical Functionalization. *ChemBioChem* **2017**, *18* (10), 960-964. DOI: 10.1002/cbic.201700079

33. Stangenberg, R.; Wu, Y.; Hedrich, J.; Kurzbach, D.; Wehner, D.; Weidinger, G.; Kuan, S. L.; Jansen, M. I.; Jelezko, F.; Luhmann, H. J.; Hinderberger, D.; Weil, T.; Müllen, K., A Polyphenylene Dendrimer Drug Transporter with Precisely Positioned Amphiphilic Surface Patches. *Advanced Healthcare Materials* **2015**, *4* (3), 377-384. DOI: 10.1002/adhm.201400291

34. Wagner, J.; Li, L.; Simon, J.; Krutzke, L.; Landfester, K.; Mailänder, V.; Müllen, K.; Ng, D. Y. W.; Wu, Y.; Weil, T., Amphiphilic Polyphenylene Dendron Conjugates for Surface Remodeling of Adenovirus 5. *Angewandte Chemie International Edition* **2020**, *59* (14), 5712-5720. DOI: 10.1002/ange.201913708

35. Xiang, S.; Wagner, J.; Lückerath, T.; Müllen, K.; Ng, D. Y. W.; Hedrich, J.; Weil, T., Reversing Aβ Fibrillation and Inhibiting Aβ Primary Neuronal Cell Toxicity Using Amphiphilic Polyphenylene Dendrons. *Advanced Healthcare Materials* **2022**, *11* (2), 2101854. DOI: 10.1002/adhm.202101854

36. Serenko, O. A.; Kalinin, M. V.; Kuchkina, N. V.; Serkova, E. S.; Strashnov, P. V.; Shifrina, Z. B., Surface Properties of Low-Generation Polyphenylene Dendrimers. *Polymer Science, Series A* **2018**, *60* (3), 260-265. DOI: 10.1134/S0965545X18030094

37. Serenko, O.; Strashnov, P.; Kapustin, G.; Kalinin, M.; Kuchkina, N.; Serkova, E.; Shifrina, Z.; Muzafarov, A., Adsorption properties of pyridylphenylene dendrimers. *RSC Advances* **2017**, *7* (13), 7870-7875. DOI: 10.1039/c6ra27064f

38. Bennett, T. D.; Coudert, F.-X.; James, S. L.; Cooper, A. I., The changing state of porous materials. *Nature Materials* **2021**, *20* (9), 1179-1187. DOI: 10.1038/s41563-021-00957-w

39. Davis, M. E., Ordered porous materials for emerging applications. *Nature* **2002**, *417* (6891), 813-821. DOI: 10.1038/nature00785

40. Mostefai, R.; Kadri, M. M.; Senoussi, E.-A.; Hacini, M.; Awadh, Pore Structure Characterization of Shale Reservoir Using Nitrogen Adsorption-Desorption. *Iraqi Geological Journal* **2023**, *56* (1D), 1-13. DOI: 10.46717/igj.56.1D.1ms-2023-4-10

41. Mohamed, M. G.; El-Mahdy, A. F. M.; Kotp, M. G.; Kuo, S.-W., Advances in porous organic polymers: syntheses, structures, and diverse applications. *Materials Advances* **2022**, *3* (2), 707-733. DOI: 10.1039/d1ma00771h

42. Lee, J.-S. M.; Cooper, A. I., Advances in Conjugated Microporous Polymers. *Chemical Reviews* **2020**, *120* (4), 2171-2214. DOI: 10.1021/acs.chemrev.9b00399

43. Fioravanti, A.; Carotta, M. C. Year 2020: A Snapshot of the Last Progress in Flexible Printed Gas Sensors. *Applied Sciences* **2020**, *10*(5), 1741-1762. DOI: 10.3390/app10051741

44. Zhang, J.; Liu, L.; Yang, Y.; Huang, Q.; Li, D.; Zeng, D., A review on two-dimensional materials for chemiresistive- and FET-type gas sensors. *Physical Chemistry Chemical Physics* **2021**, *23* (29), 15420-15439. DOI: 10.1039/d1cp01890f

45. Hermawan, A.; Septiani, N. L. W.; Taufik, A.; Yuliarto, B.; Suyatman; Yin, S., Advanced Strategies to Improve Performances of Molybdenum-Based Gas Sensors. *Nano-Micro Letters* **2021**, *13* (1), 207. DOI: 10.1007/s40820-021-00724-1

46. Sharma, N.; Pandey, V.; Gupta, A.; Tan, S. T.; Tripathy, S.; Kumar, M., Recent progress on group III nitride nanostructure-based gas sensors. *Journal of Materials Chemistry C* **2022**, *10* (34), 12157-12190. DOI: 10.1039/d2tc02103j

47. He, W.; Duan, J.; Liu, H.; Qian, C.; Zhu, M.; Zhang, W.; Liao, Y., Conjugated microporous polymers for advanced chemical sensing applications. *Progress in Polymer Science* **2024**, *148*, 101770. DOI: 10.1016/j.progpolymsci.2023.101770

48. McGarrity, M.; Zhao, F. Graphene-Based Chemiresistor Sensors for Drinking Water Quality Monitoring. *Sensors* **2023**, *23*, 9828. DOI: 10.3390/s23249828

49. Majhi, S. M.; Navale, S. T.; Mirzaei, A.; Kim, H. W.; Kim, S. S., Strategies to boost chemiresistive sensing performance of In_2O_3-based gas sensors: an overview. *Inorganic Chemistry Frontiers* **2023**, *10* (12), 3428-3467. DOI: 10.1039/d3qi00099k

50. Mirzaei, A.; Kim, J.-H.; Kim, H. W.; Kim, S. S., Resistive-based gas sensors for detection of benzene, toluene and xylene (BTX) gases: a review. *Journal of Materials Chemistry C* **2018**, *6* (16), 4342-4370. DOI: 10.1039/c8tc00245b

51. Zhu, L.-Y.; Ou, L.-X.; Mao, L.-W.; Wu, X.-Y.; Liu, Y.-P.; Lu, H.-L., Advances in Noble Metal-Decorated Metal Oxide Nanomaterials for Chemiresistive Gas Sensors: Overview. *Nano-Micro Letters* **2023**, *15* (1), 89. DOI: 10.1007/s40820-023-01047-z

52. Barandun, G.; Gonzalez-Macia, L.; Lee, H. S.; Dincer, C.; Güder, F., Challenges and Opportunities for Printed Electrical Gas Sensors. *ACS Sensors* **2022**, *7* (10), 2804-2822. DOI: 10.1021/acssensors.2c01086

53. Ansari, H. R.; Mirzaei, A.; Shokrollahi, H.; Kumar, R.; Kim, J.-Y.; Kim, H. W.; Kumar, M.; Kim, S. S., Flexible/wearable resistive gas sensors based on 2D materials. *Journal of Materials Chemistry C* **2023**, *11* (20), 6528-6549. DOI: 10.1039/d3tc00806a

54. Bhati, V. S.; Kumar, M.; Banerjee, R., Gas sensing performance of 2D nanomaterials/metal oxide nanocomposites: a review. *Journal of Materials Chemistry C* **2021**, *9* (28), 8776-8808. DOI: 10.1039/d1tc01857d

55. Pavel, I.-A.; Lakard, S.; Lakard, B. Flexible Sensors Based on Conductive Polymers. *Chemosensors* **2022**, *10*, 97. DOI: 10.3390/chemosensors10030097

56. Kumar, A.; Kumar, A.; Kwoka, M.; Gang, M.; Kumar, M., IoT-enabled surface-active Pd-anchored metal oxide chemiresistor for H_2S gas detection. *Sensors and Actuators B: Chemical* **2024**, *402*, 135065. DOI: 10.1016/j.snb.2023.135065

57. Vorokhta, M.; Khalakhan, I.; Vondráček, M.; Tomeček, D.; Vorokhta, M.; Marešová, E.; Nováková, J.; Vlček, J.; Fitl, P.; Novotný, M.; Hozák, P.; Lančok, J.; Vrňata, M.; Matolínová, I.; Matolín, V., Investigation of gas sensing mechanism of SnO_2 based chemiresistor using near ambient pressure XPS. *Surface Science* **2018**, *677*, 284-290. DOI: 10.1016/j.susc.2018.08.003

58. Roy, N.; Sinha, R.; Nemade, H. B.; Mandal, T. K., Synthesis of MoS_2-CuO nanocomposite for room temperature acetone sensing application. *Journal of Alloys and Compounds* **2022**, *910*, 164891. DOI: 10.1016/j.jallcom.2022.164891

59. Ozkendir Inanc, D.; Ng, Z. K.; Baskurt, M.; Keles, B.; Vardar, G.; Sahin, H.; Tsang, S. H.; Palaniappan, A.; Yildiz, U. H.; Teo, E. H. T., A multi-layered graphene based gas sensor platform for discrimination of volatile organic compounds via differential intercalation. *Journal of Materials Chemistry C* **2023**, *11* (14), 4703-4710. DOI: 10.1039/d3tc00313b

60. Choi, J.; Park, E. J.; Park, D. W.; Shim, S. E., MWCNT–OH adsorbed electrospun nylon 6,6 nanofibers chemiresistor and their application in low molecular weight alcohol vapours sensing. *Synthetic Metals* **2010**, *160* (23), 2664-2669. DOI: 10.1016/j.synthmet.2010.10.022

61. Dos Reis, M. A. L.; Thomazi, F.; Del Nero, J.; Roman, L. S. Development of a Chemiresistor Sensor Based on Polymers-Dye Blend for Detection of Ethanol Vapor. *Sensors* **2010**, *10*, 2812-2820. DOI: 10.3390/s100402812

62. Kumar, M.; Sharma, S.; Pal, R.; Vidhani, B.; Supreet, A novel gas sensor based on activated charcoal and polyaniline composites for selective sensing of methanol vapors. *Sensors and Actuators A: Physical* **2023**, *353*, 114210. DOI: 10.1016/j.sna.2023.114210

63. Vossmeyer, T.; Guse, B.; Besnard, I.; Bauer, R. E.; Müllen, K.; Yasuda, A., Gold Nanoparticle/Polyphenylene Dendrimer Composite Films: Preparation and Vapor-Sensing Properties. *Advanced Materials* **2002**, *14* (3), 238-242. DOI: 10.1002/1521-4095(20020205)14:3<238::AID-ADMA238>3.0.CO;2-%23

64. Kamal, M. S.; Razzak, S. A.; Hossain, M. M., Catalytic oxidation of volatile organic compounds (VOCs) – A review. *Atmospheric Environment* **2016**, *140*, 117-134. DOI: 10.1016/j.atmosenv.2016.05.031

65. Rana, S. V.; Malik, A., Hydrogen Breath Tests in Gastrointestinal Diseases. *Indian Journal of Clinical Biochemistry* **2014**, *29* (4), 398-405. DOI: 10.1007/s12291-014-0426-4

66. Hakimi, M.; Salehi, A.; Boroumand, F. A.; Mosleh, N., Fabrication of a Room Temperature Ammonia Gas Sensor Based on Polyaniline With N-Doped Graphene Quantum Dots. *IEEE Sensors Journal* **2018**, *18* (6), 2245-2252. DOI: 10.1109/JSEN.2018.2797118

67. Dessler, A. E.; Sherwood, S. C. J. S., A matter of humidity. *Science* **2009**, *323* (5917), 1020-1021. DOI: 10.1126/science.1171264

68. Chou, C. S.; Wu, Y. C.; Lin, C. H., High performance oxygen sensor utilizing ultraviolet irradiation assisted ZnO nanorods under low operation temperature. *The 8th Annual IEEE International Conference on Nano/Micro Engineered and Molecular Systems* **2013**, *7-10 April 2013*, 72-75. DOI: 10.1109/NEMS.2013.6559685

69. Colindres, S. C.; Aguir, K.; Cervantes Sodi, F.; Vargas, L. V.; Salazar, J. A. M.; Febles, V. G. Ozone Sensing Based on Palladium Decorated Carbon Nanotubes. *Sensors* **2014**, *14*, 6806-6818. DOI: 10.3390/s140406806

70. Rasyid, M. U. H. A.; Nadhori, I. U.; Alnovinda, Y. T. In CO and CO_2 pollution monitoring based on wireless sensor network. *2015 IEEE International Conference on Aerospace Electronics and Remote Sensing Technology (ICARES)* **2015**, *3-5 Dec. 2015*, 1-5. DOI: 10.1109/ICARES.2015.7429818

71. Kumar, A.; Samanta, S.; Singh, A.; Roy, M.; Singh, S.; Basu, S.; Chehimi, M. M.; Roy, K.; Ramgir, N.; Navaneethan, M.; Hayakawa, Y.; Debnath, A. K.;

Aswal, D. K.; Gupta, S. K., Fast Response and High Sensitivity of ZnO Nanowires—Cobalt Phthalocyanine Heterojunction Based H_2S Sensor. *ACS Applied Materials & Interfaces* **2015**, *7* (32), 17713-17724. DOI: 10.1021/acsami.5b03652

72. Khan, R. R.; Siddiqui, M. J. A., Review on effects of particulates: sulfur dioxide and nitrogen dioxide on human health. *International Research Journal of Environment Sciences* **2014**, *3* (4), 70-73. CORPUS ID: 131359901

73. Gatty, H. K.; Leijonmarck, S.; Antelius, M.; Stemme, G.; Roxhed, N., An amperometric nitric oxide sensor with fast response and ppb-level concentration detection relevant to asthma monitoring. *Sensors and Actuators B: Chemical* **2015**, *209*, 639-644. DOI: 10.1016/j.snb.2014.11.147

74. Shu, J. H.; Wikle, H. C.; Chin, B. A., Passive chemiresistor sensor based on iron (II) phthalocyanine thin films for monitoring of nitrogen dioxide. *Sensors and Actuators B: Chemical* **2010**, *148* (2), 498-503. DOI: 10.1016/j.snb.2010.05.017

75. Das, S.; Pal, S.; Mitra, M., Significance of Exhaled Breath Test in Clinical Diagnosis: A Special Focus on the Detection of Diabetes Mellitus. *Journal of Medical and Biological Engineering* **2016**, *36* (5), 605-624. DOI 10.1007/s40846-016-0164-6

76. Arena, A.; Donato, N.; Saitta, G.; Bonavita, A.; Rizzo, G.; Neri, G., Flexible ethanol sensors on glossy paper substrates operating at room temperature. *Sensors and Actuators B: Chemical* **2010**, *145* (1), 488-494. DOI: 10.1016/j.snb.2009.12.053

77. Güntner, A. T.; Koren, V.; Chikkadi, K.; Righettoni, M.; Pratsinis, S. E., E-Nose Sensing of Low-ppb Formaldehyde in Gas Mixtures at High Relative Humidity for Breath Screening of Lung Cancer? *ACS Sensors* **2016**, *1* (5), 528-535. DOI: 10.1021/acssensors.6b00008

78. Van Dang, T.; Duc Hoa, N.; Van Duy, N.; Van Hieu, N., Chlorine Gas Sensing Performance of On-Chip Grown ZnO, WO_3, and SnO_2 Nanowire Sensors. *ACS Applied Materials & Interfaces* **2016**, *8* (7), 4828-4837. DOI: 10.1021/acsami.5b08638

79. Turgut, P.; Arif Gurel, M.; Kadir Pekgokgoz, R., LPG explosion damage of a reinforced concrete building: A case study in Sanliurfa, Turkey. *Engineering Failure Analysis* **2013**, *32*, 220-235. DOI: 10.1016/j.engfailanal.2013.04.004

80. Di Credico, B.; Fabrizi de Biani, F.; Gonsalvi, L.; Guerri, A.; Ienco, A.; Laschi, F.; Peruzzini, M.; Reginato, G.; Rossin, A.; Zanello, P., Cyclopentadienyl Ruthenium(II) Complexes with Bridging Alkynylphosphine Ligands: Synthesis and Electrochemical Studies. *Chemistry – A European Journal* **2009**, *15* (44), 11985-11998. DOI: 10.1002/chem.200901642

81. Morgenroth, F.; Reuther, E.; Müllen, K., Polyphenylene Dendrimers: From Three-Dimensional to Two-Dimensional Structures. *Angewandte Chemie International Edition in English* **1997**, *36* (6), 631-634. DOI: 10.1002/anie.199706311

82. Morgenroth, F.; Müllen, K., Dendritic and hyperbranched polyphenylenes via a simple Diels-Alder route. *Tetrahedron* **1997**, *53* (45), 15349-15366. DOI: 10.1016/S0040-4020(97)00967-8

83. Wiesler, U. M.; Berresheim, A. J.; Morgenroth, F.; Lieser, G.; Müllen, K., Divergent Synthesis of Polyphenylene Dendrimers: The Role of Core and Branching Reagents upon Size and Shape. *Macromolecules* **2001**, *34* (2), 187-199. DOI: 10.1021/ma991519m

84. Mazaheri, A.; Lee, M.; van der Zant, H. S. J.; Frisenda, R.; Castellanos-Gomez, A., MoS_2-on-paper optoelectronics: drawing photodetectors with van der Waals semiconductors beyond graphite. *Nanoscale* **2020**, *12* (37), 19068-19074. DOI: 10.1039/d0nr02268c

85. Nouri, B.; Castellanos-Gomez, A.; Ghasemi, F., Paper-based flexible supercapacitors with drawn van der Waals materials. *Journal of Alloys and Compounds* **2023**, *959*, 170554. DOI: 10.1016/j.jallcom.2023.170554

86. Sakhuja, N.; Kumar, R.; Katare, P.; Bhat, N., Structure-Driven, Flexible, Multilayered, Paper-Based Pressure Sensor for Human–Machine Interfacing. *ACS Sustainable Chemistry & Engineering* **2022**, *10* (30), 9697-9706. DOI: 10.1021/acssuschemeng.1c08491

87. Qin, Z.; Song, X.; Wang, J.; Li, X.; Wu, C.; Wang, X.; Yin, X.; Zeng, D., Development of flexible paper substrate sensor based on 2D WS_2 with S defects for room-temperature NH_3 gas sensing. *Applied Surface Science* **2022**, *573*, 151535. DOI: 10.1016/j.apsusc.2021.151535

88. Perdew, J. P.; Burke, K.; Ernzerhof, M., Generalized Gradient Approximation Made Simple. *Physical Review Letters* **1996**, *77* (18), 3865-3868. DOI: 10.1103/PhysRevLett.77.3865

89. Perdew, J. P.; Burke, K.; Ernzerhof, M., Perdew, Burke, and Ernzerhof Reply. *Physical Review Letters* **1998**, *80* (4), 891-891. DOI: 10.1103/PhysRevLett.80.891

90. Blöchl, P. E., Projector augmented-wave method. *Physical Review B* **1994**, *50* (24), 17953-17979. DOI: 10.1103/PhysRevB.50.17953

APPENDIX A

^{1}H-NMR SPECTRA OF COMPOUNDS

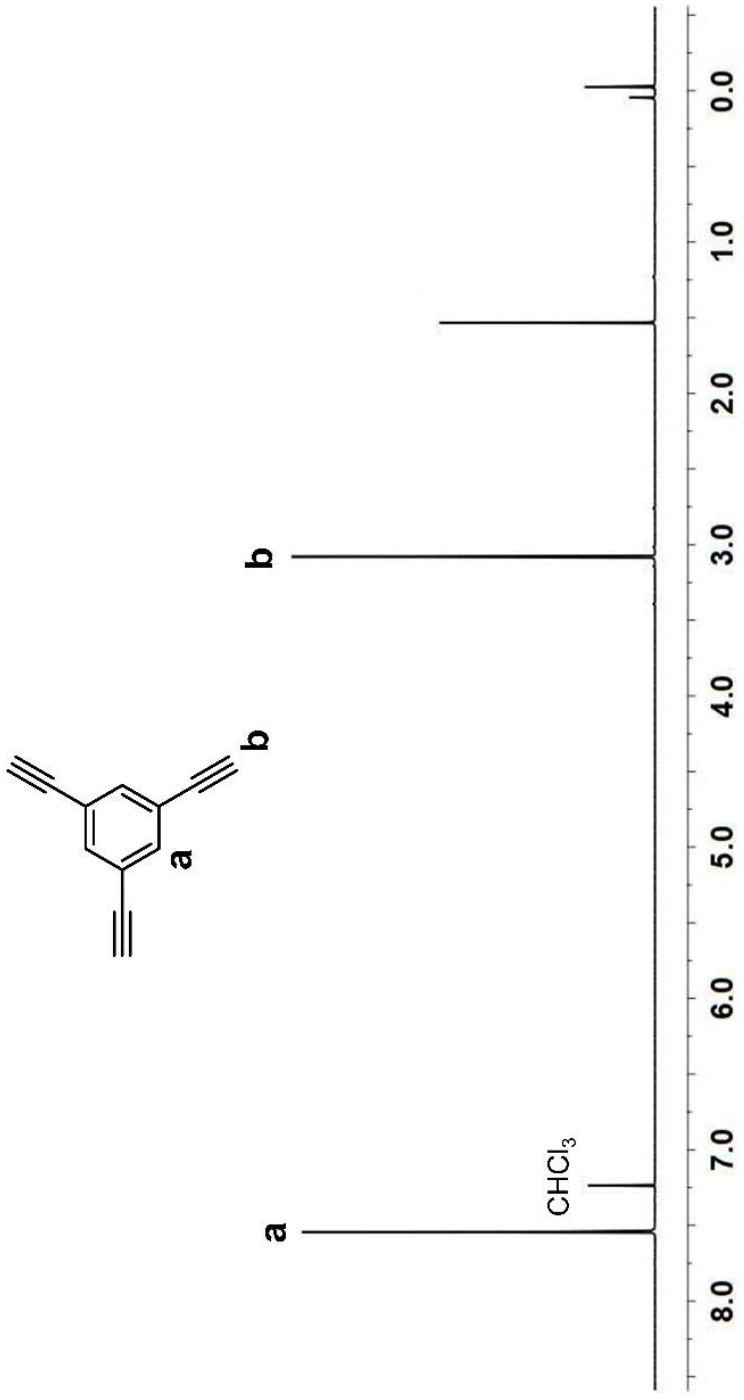

Figure A.1. ^{1}H NMR spectrum of 1,3,5-triethynylbenzene in $CDCl_3$ at R.T.

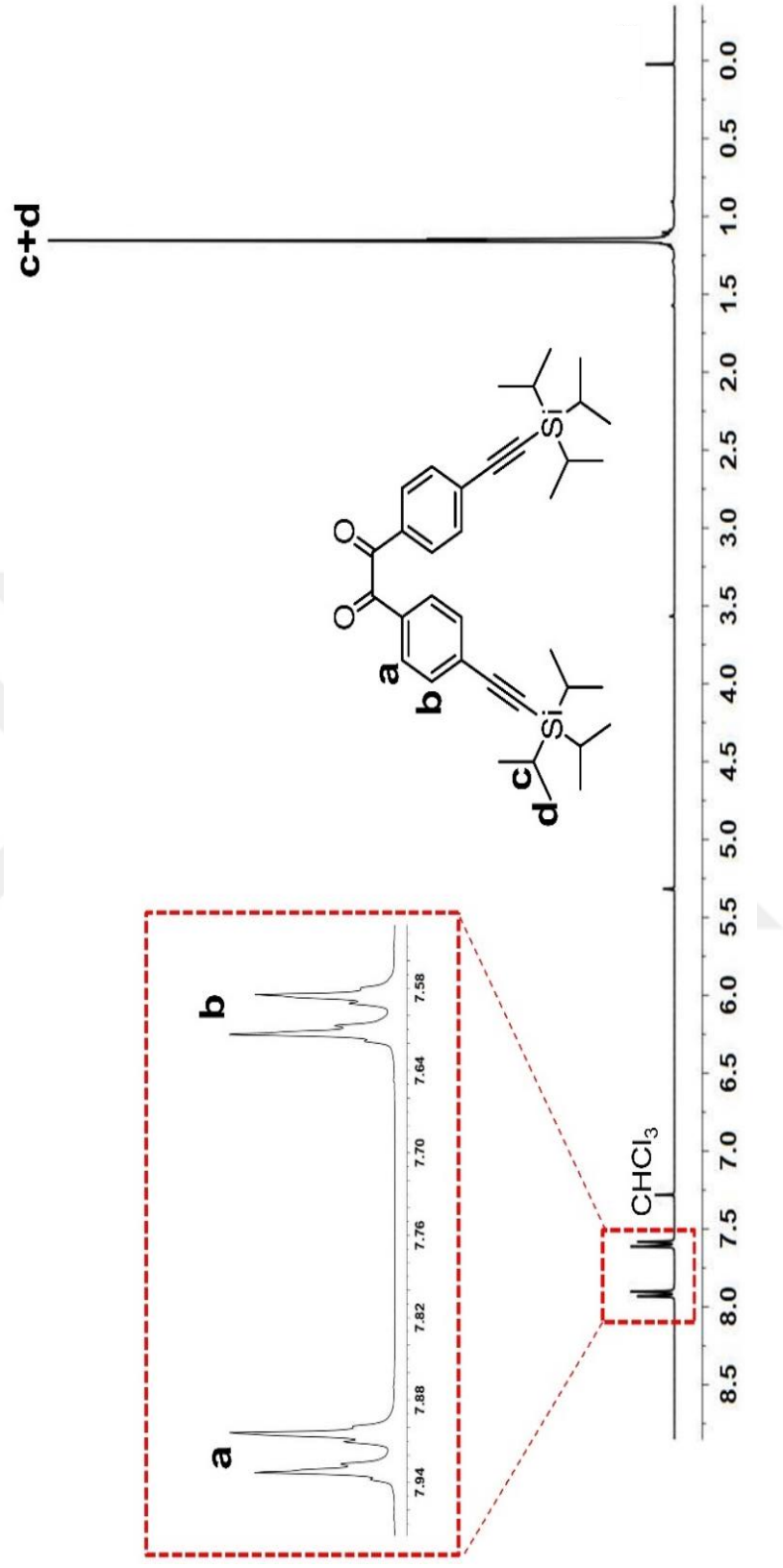

Figure A.2. ^{1}H NMR spectrum of 4,4'-bis(tri isopropyl silylethynyl) benzil in $CDCl_3$ at R.T.

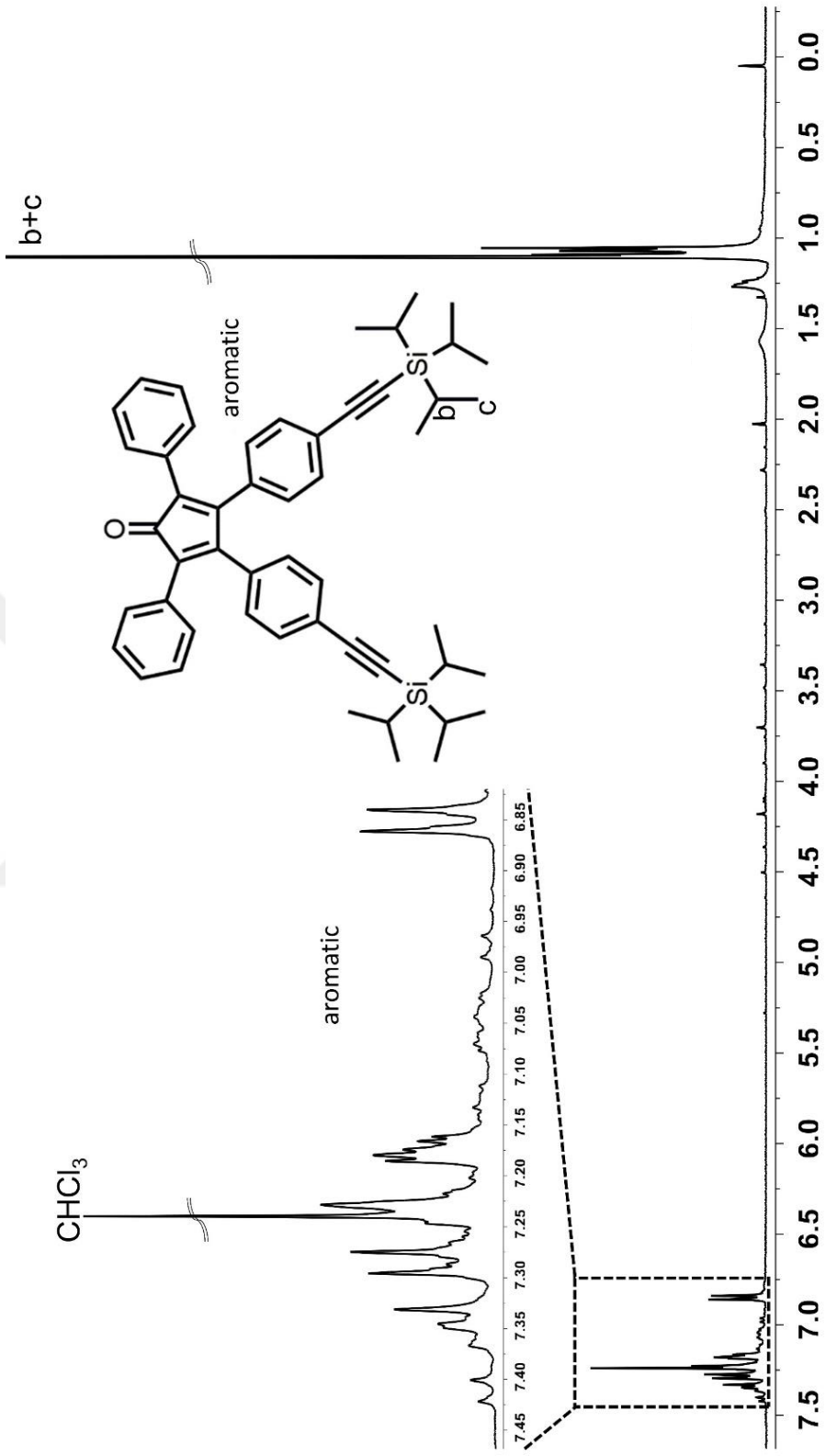

Figure A.3. ^{1}H NMR spectrum of 2,5-diphenyl-3,4-bis(4-((triisopropylsilyl) ethynyl)phenyl)cyclopenta-2,4-dien-1-one in $CDCl_3$ at R.T.

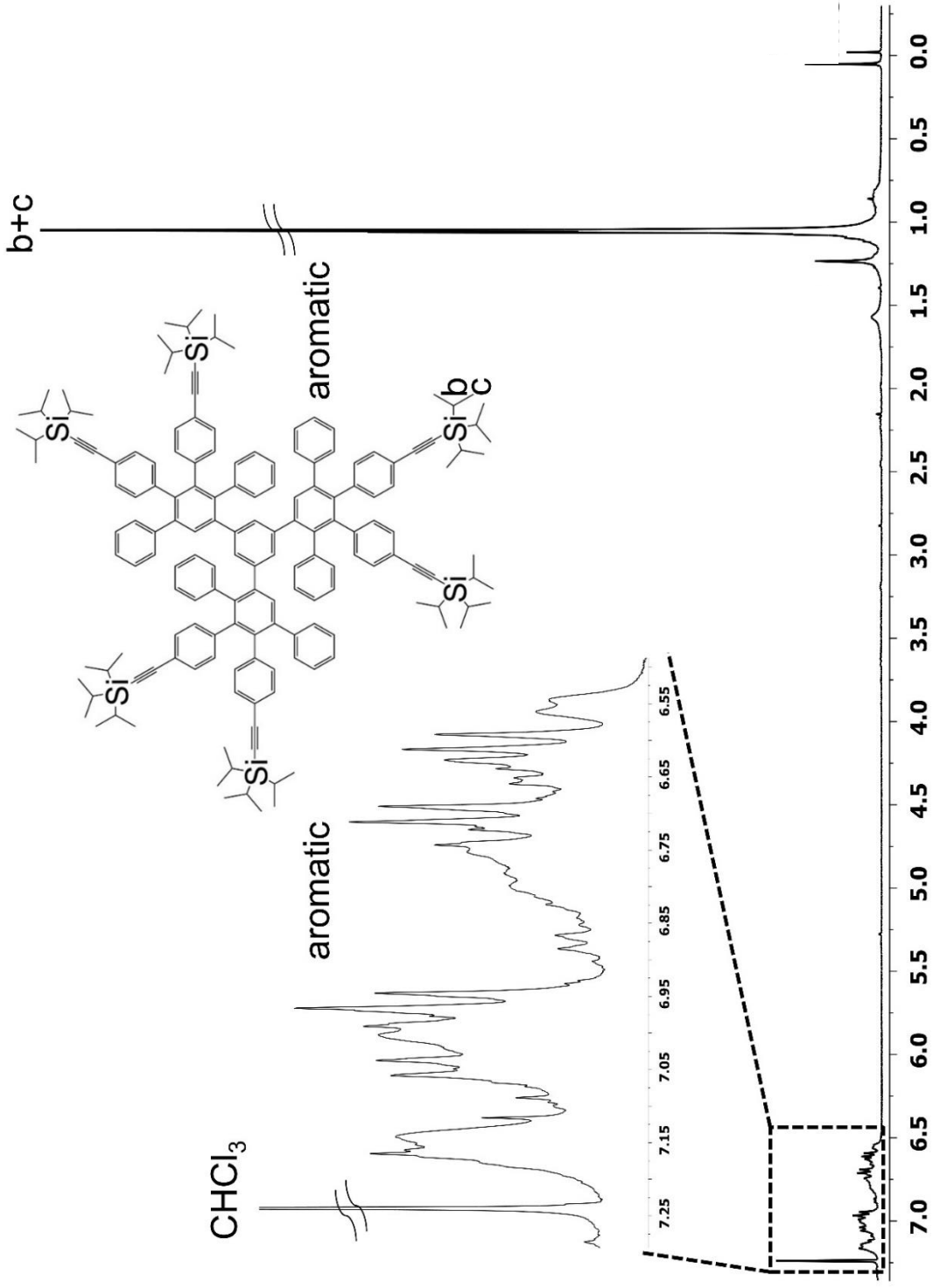

Figure A.4. ^{1}H NMR spectrum of GNRD-G1ap in $CDCl_3$ at R.T.

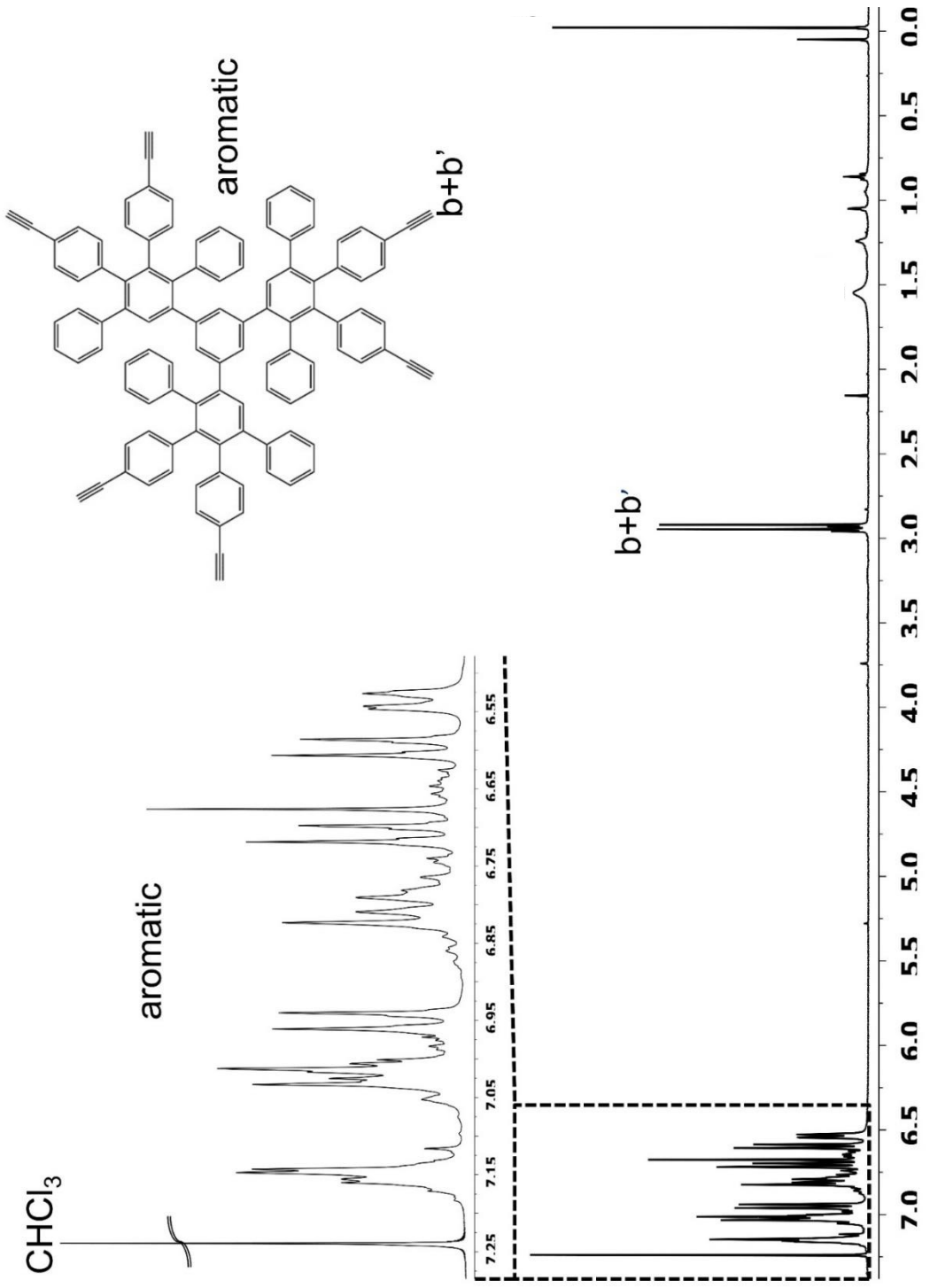

Figure A.5. ^{1}H NMR spectrum of GNRD-G1a in $CDCl_3$ at R.T.

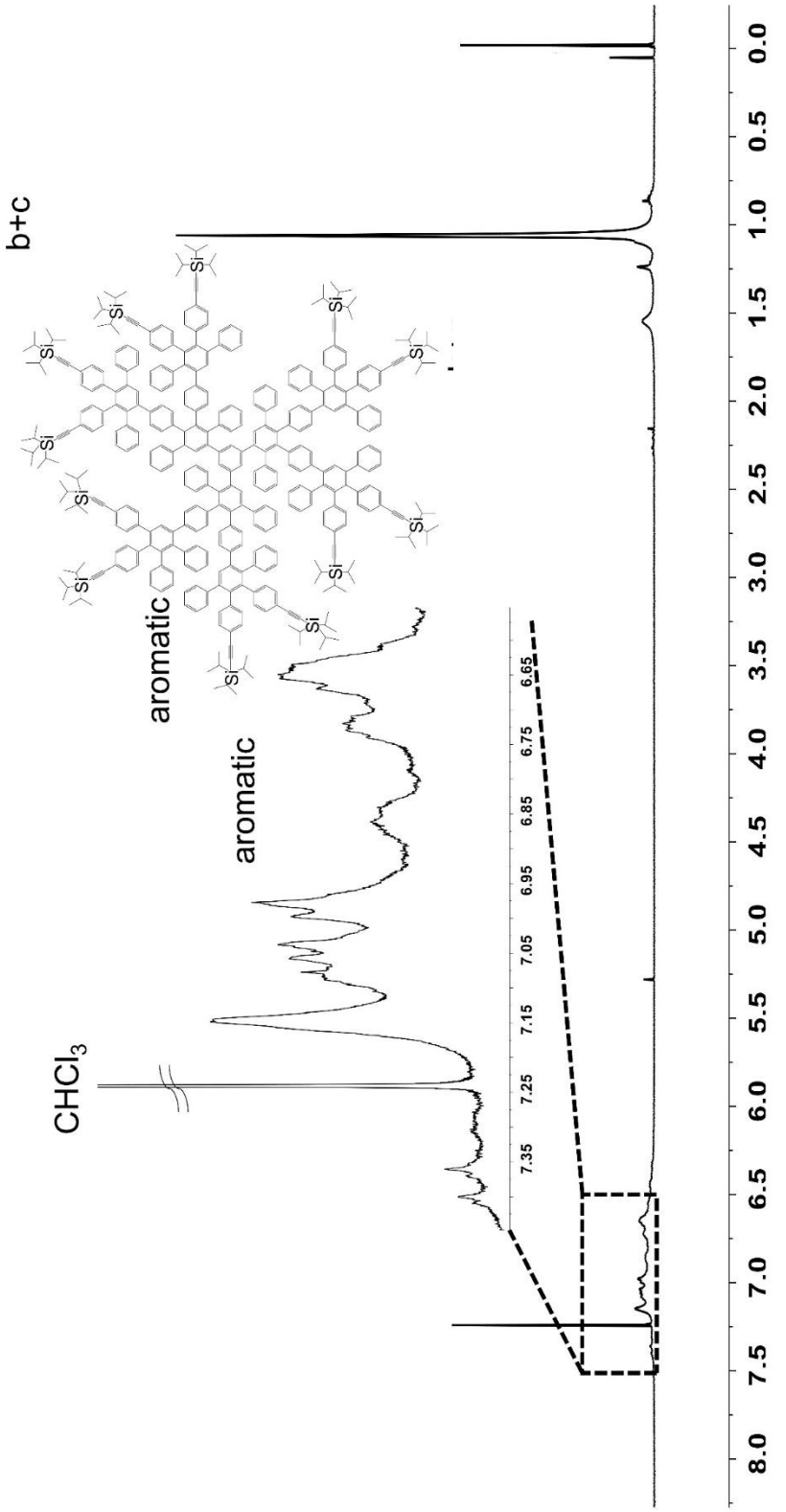

Figure A.6. ^{1}H NMR spectrum of GNRD-G2ap in $CDCl_3$ at R.T.

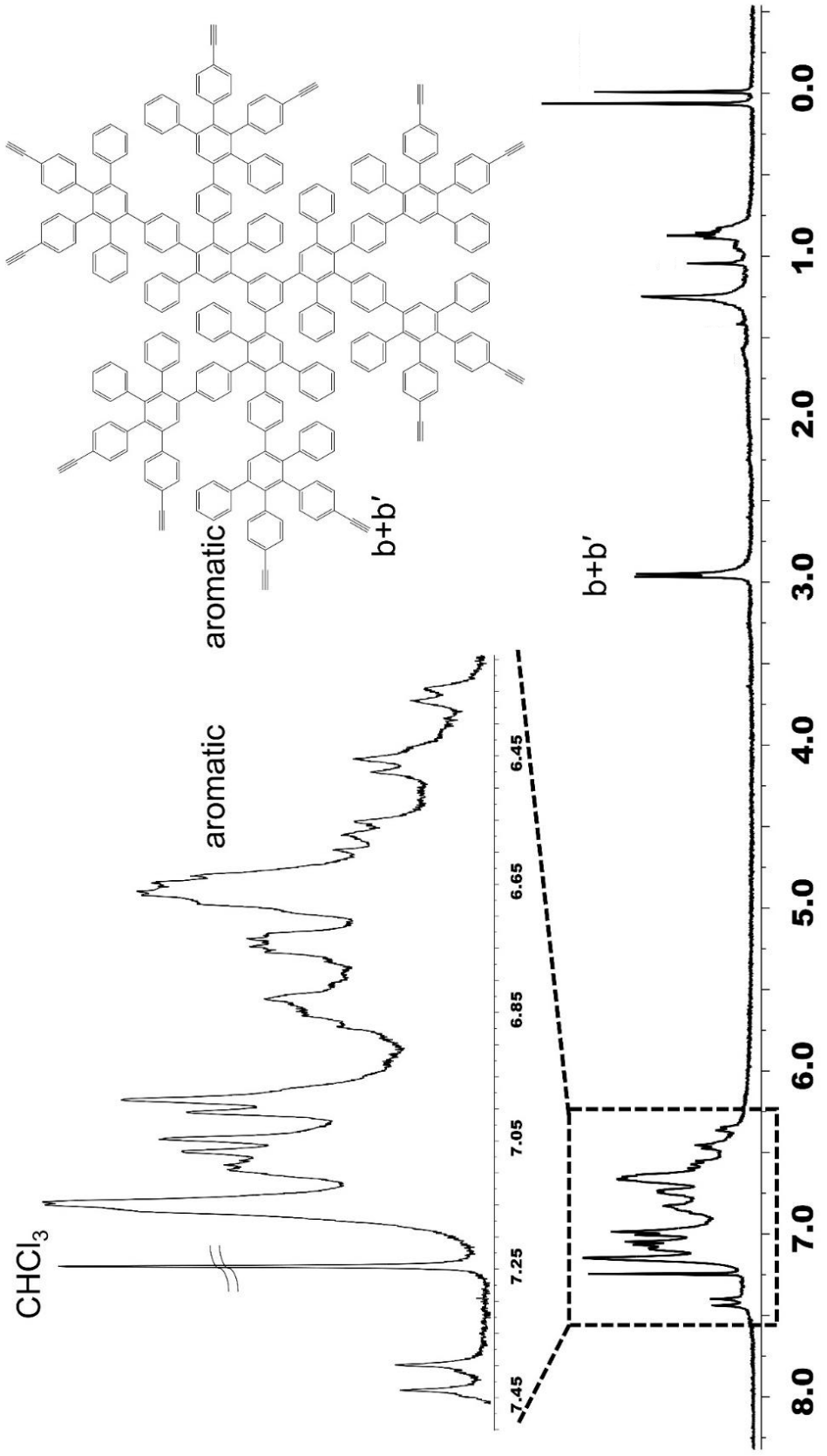

Figure A.7. ^{1}H NMR spectrum of GNRD-G2a in $CDCl_3$ at R.T.

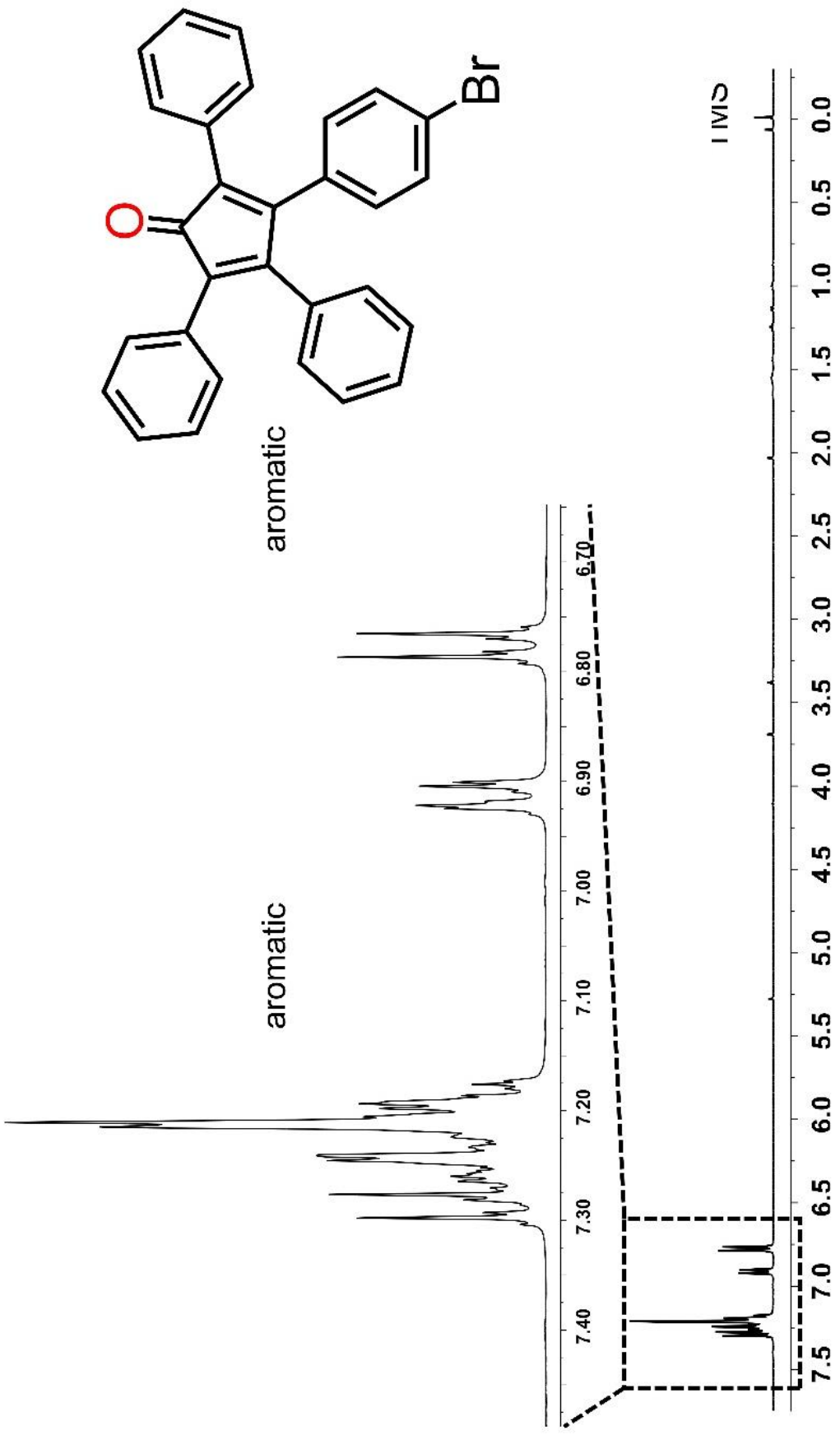

Figure A.8. ^{1}H NMR spectrum of CP-Br in $CDCl_3$ at R.T.

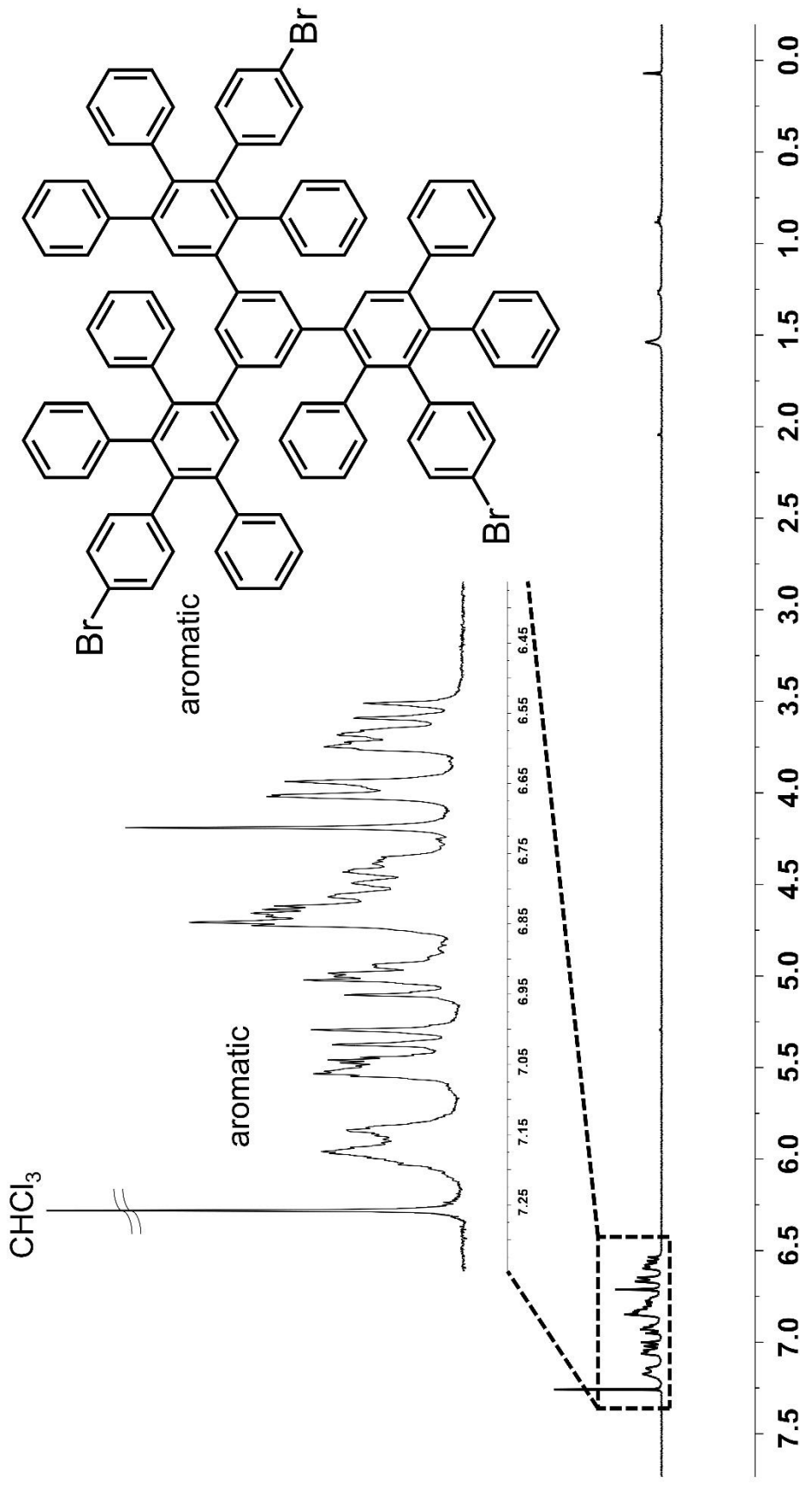

Figure A.9. ^{1}H NMR spectrum of G1 in $CDCl_3$ at R.T.

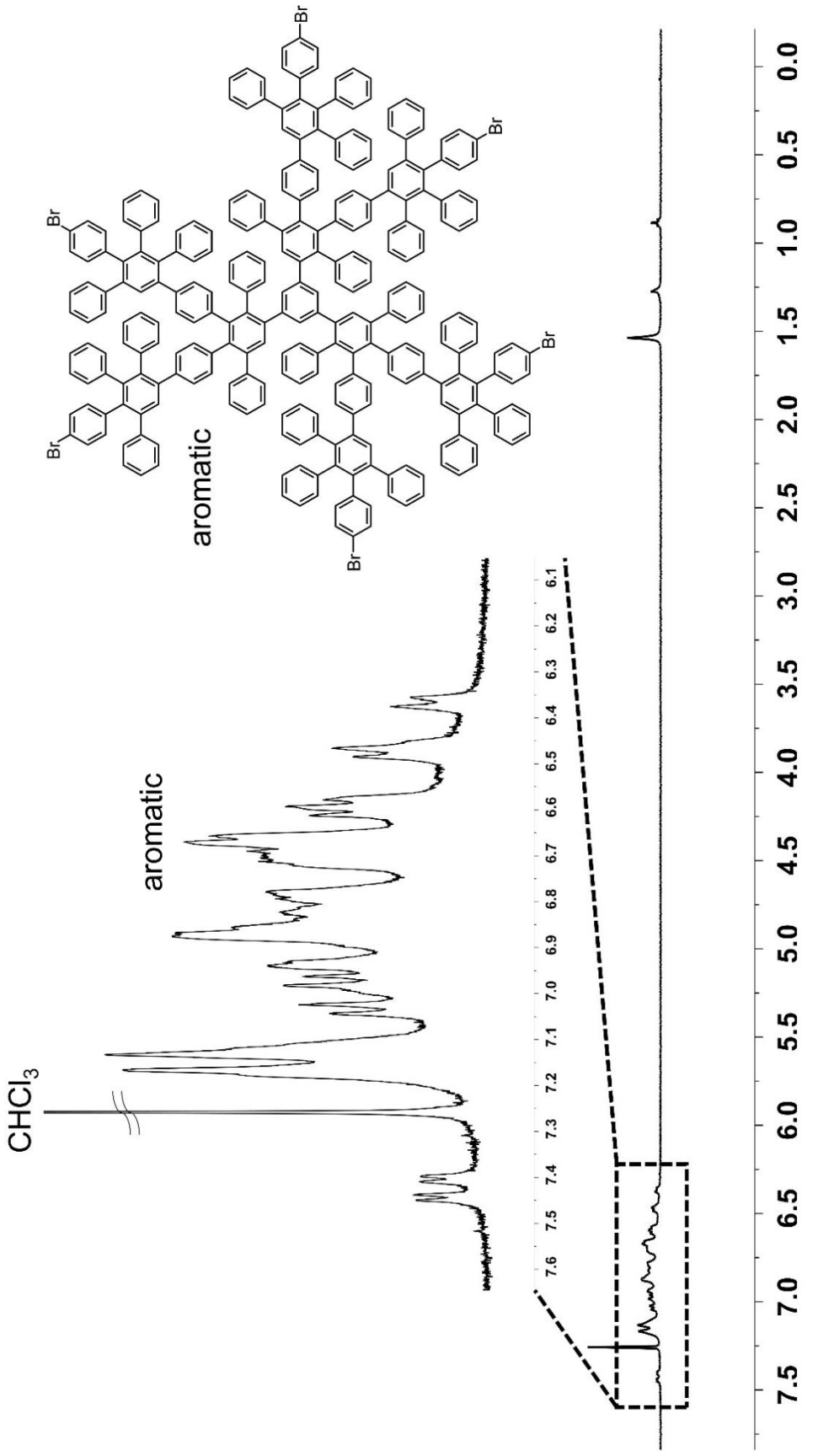

Figure A.10. ^{1}H NMR spectrum of G2 in $CDCl_3$ at R.T.

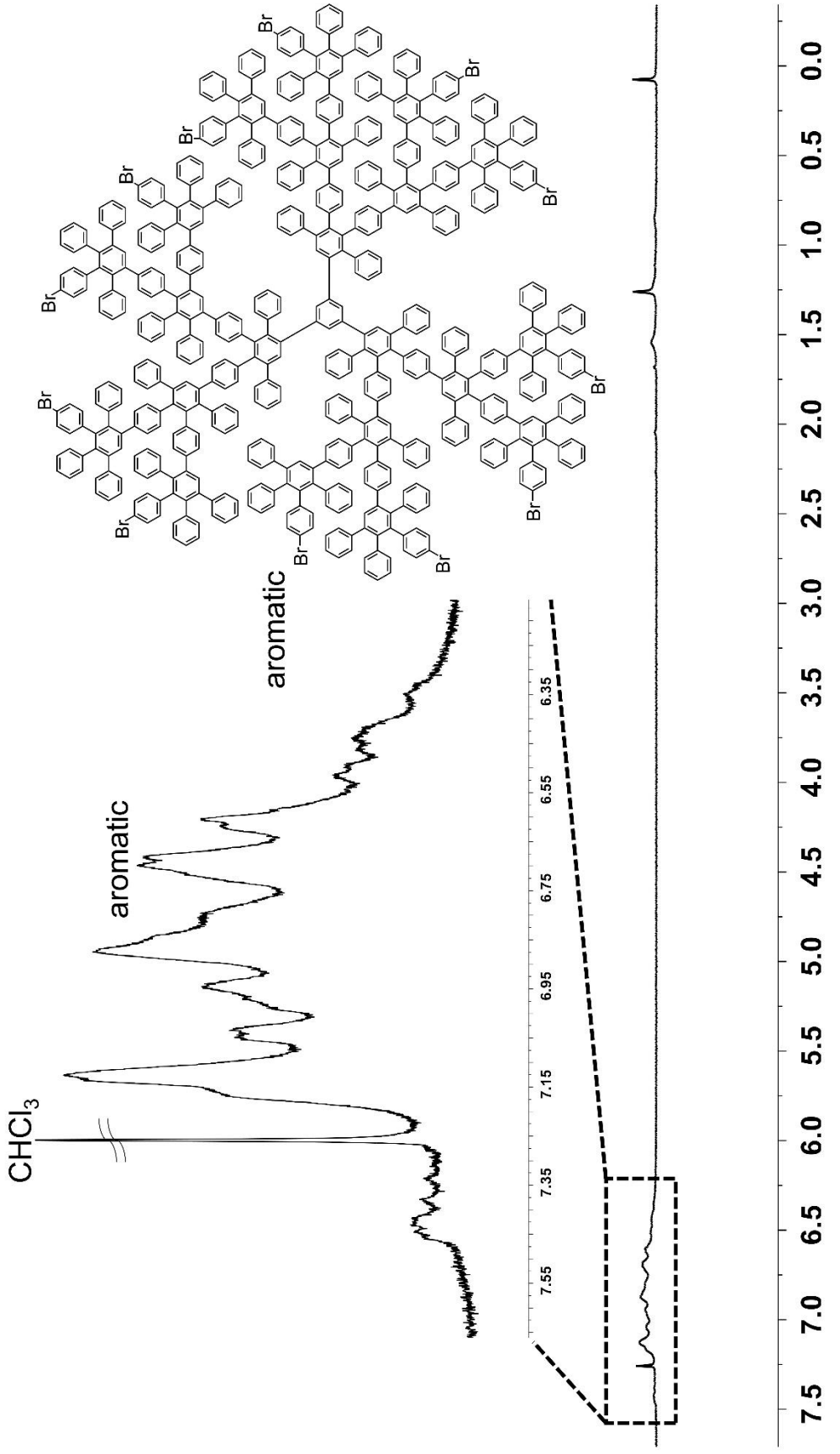

Figure A.11. ^{1}H NMR spectrum of G3 in $CDCl_3$ at R.T.

APPENDIX B

IR SPECTRA OF COMPOUNDS

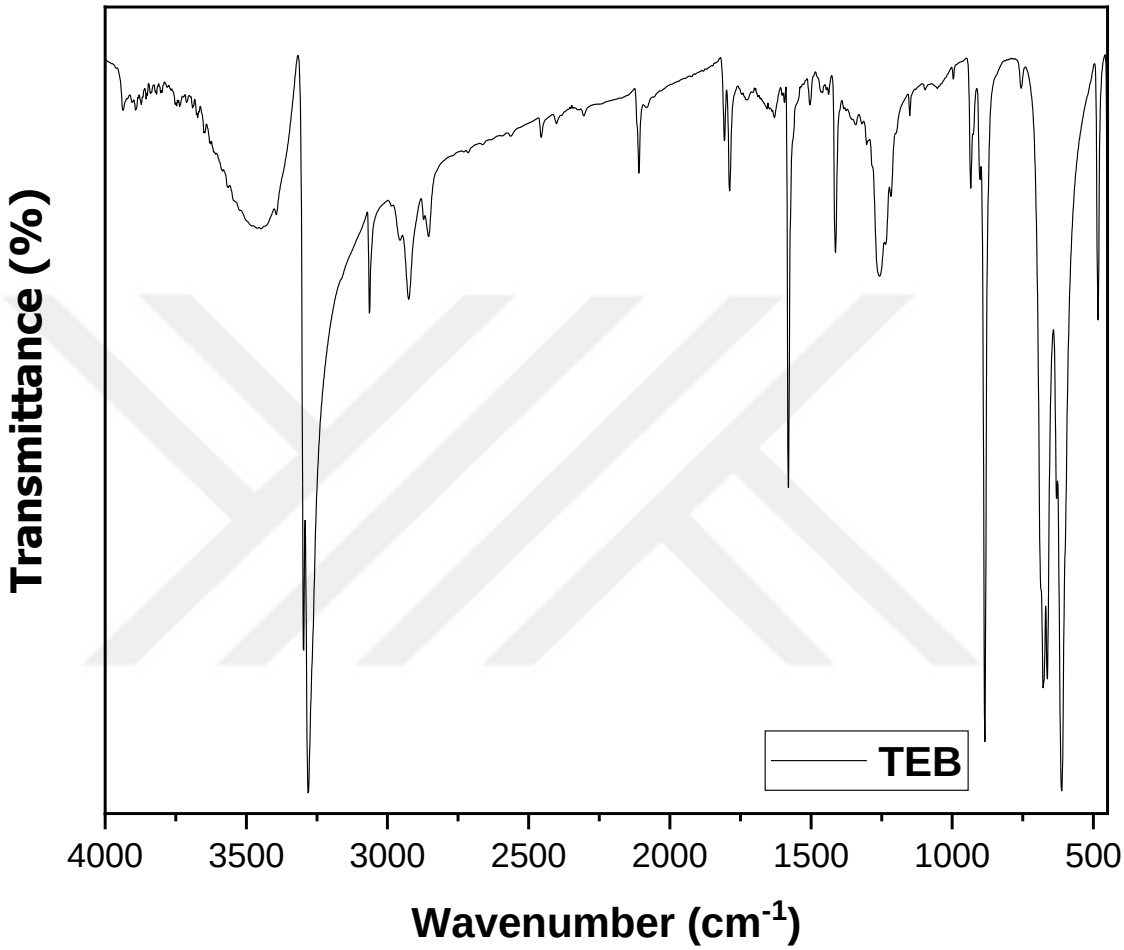

Figure B.1. IR spectrum of 1,3,5-triethynylbenzene.

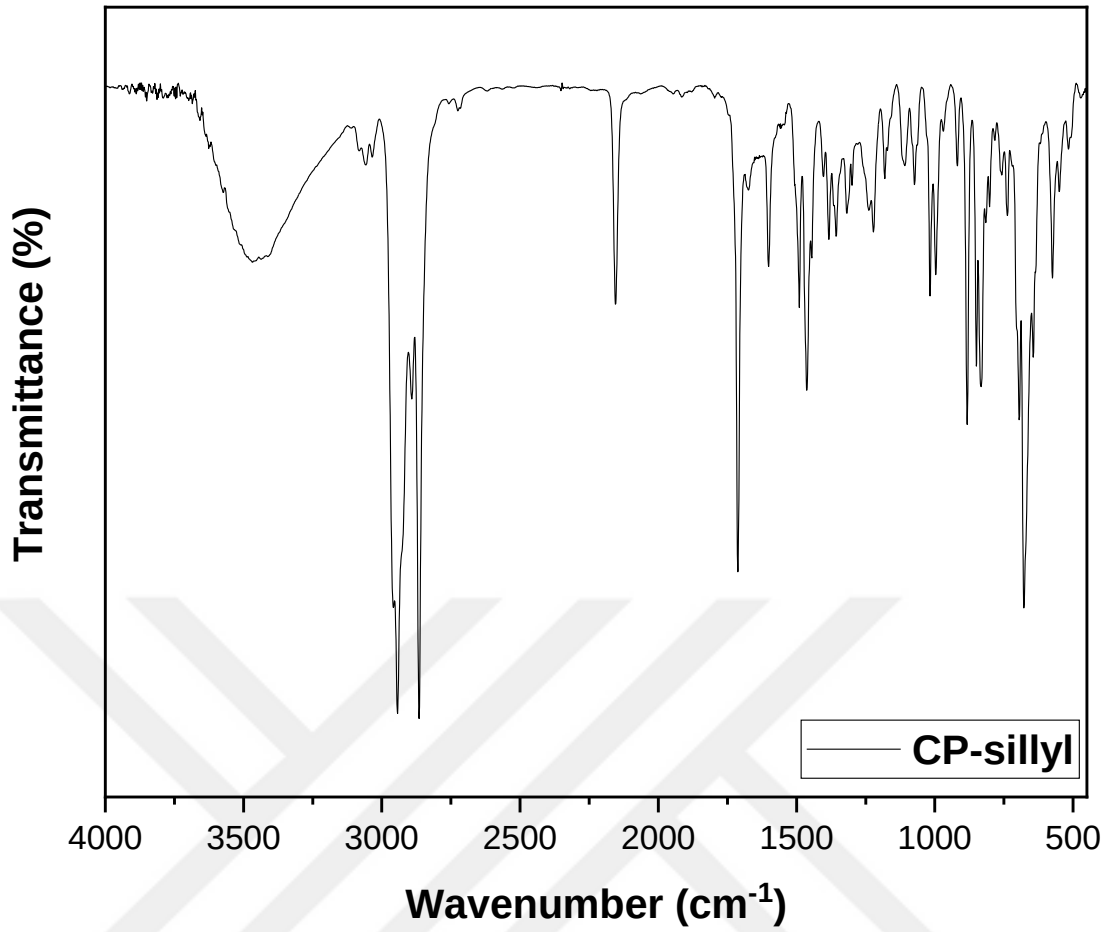

Figure B.2. IR spectrum of 2,5-diphenyl-3,4-bis(4-((triisopropylsilyl) ethynyl)phenyl)cyclopenta-2,4-dien-1-one.

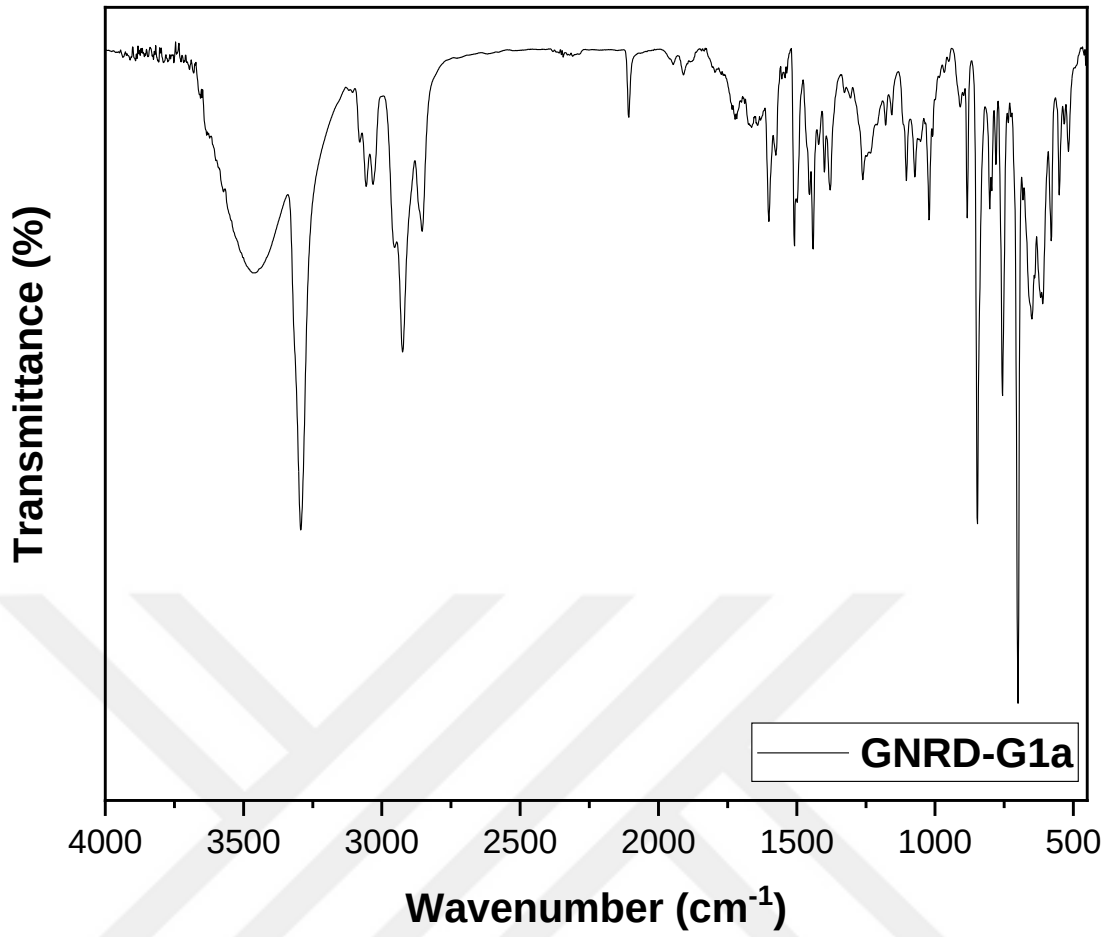

Figure B.3. IR spectrum of GNRD-G1a.

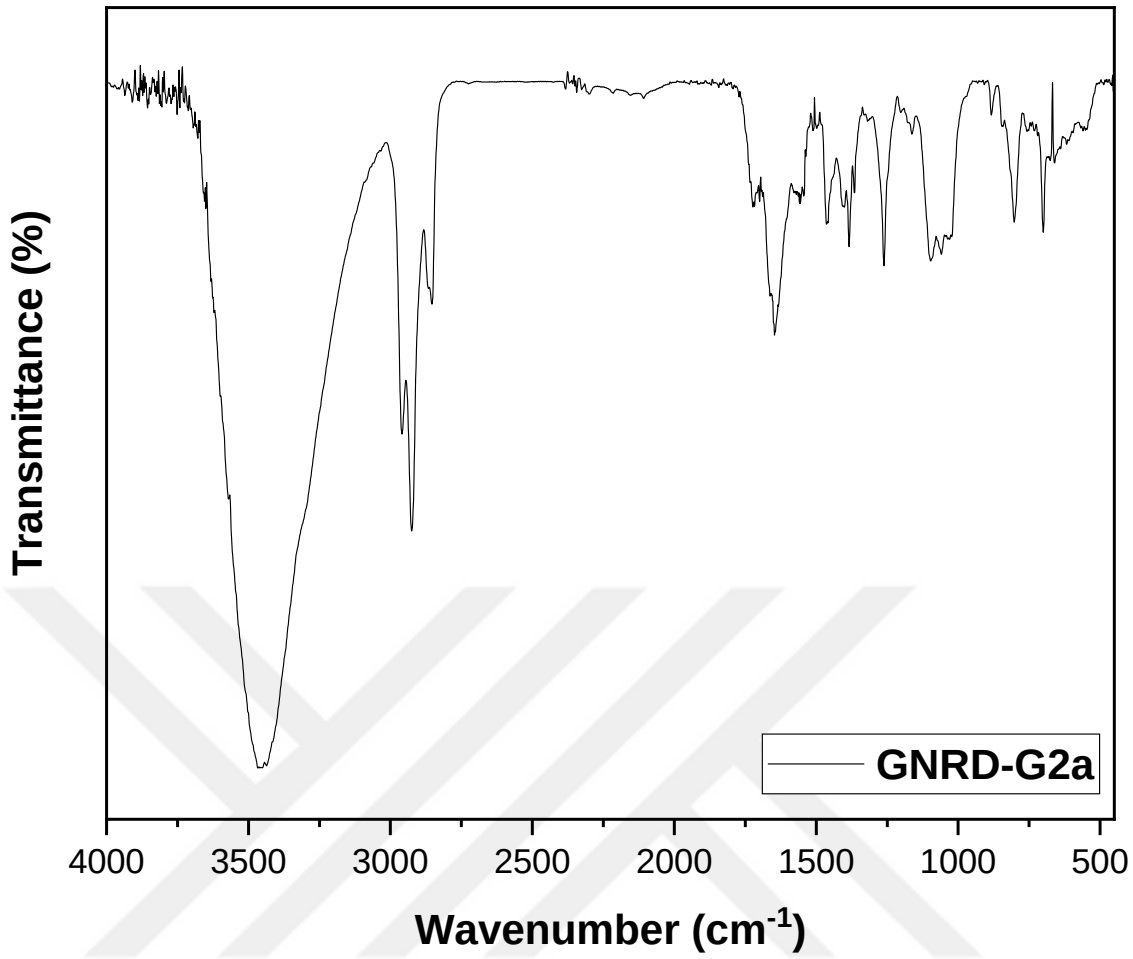

Figure B.4. IR spectrum of GNRD-G2a.

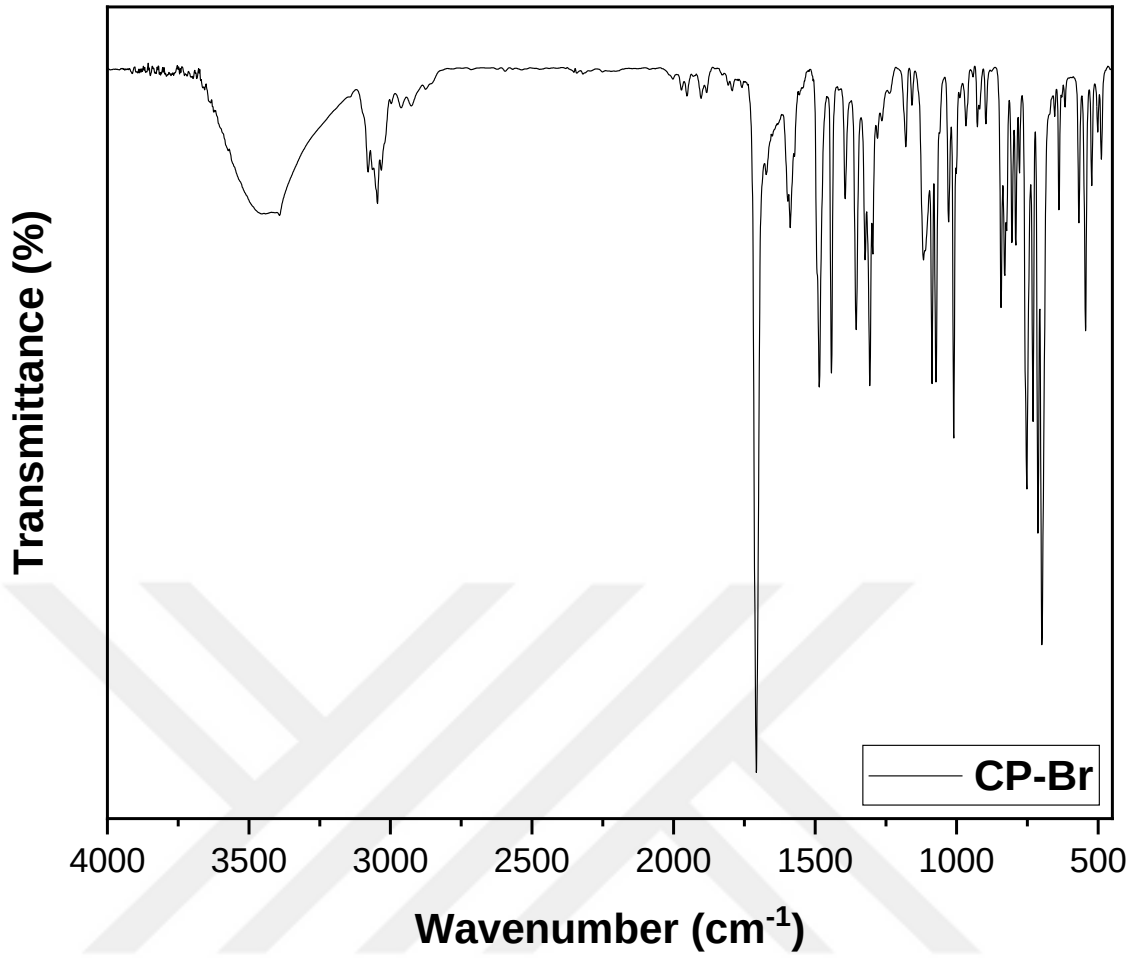

Figure B.5. IR spectrum of CP-Br.

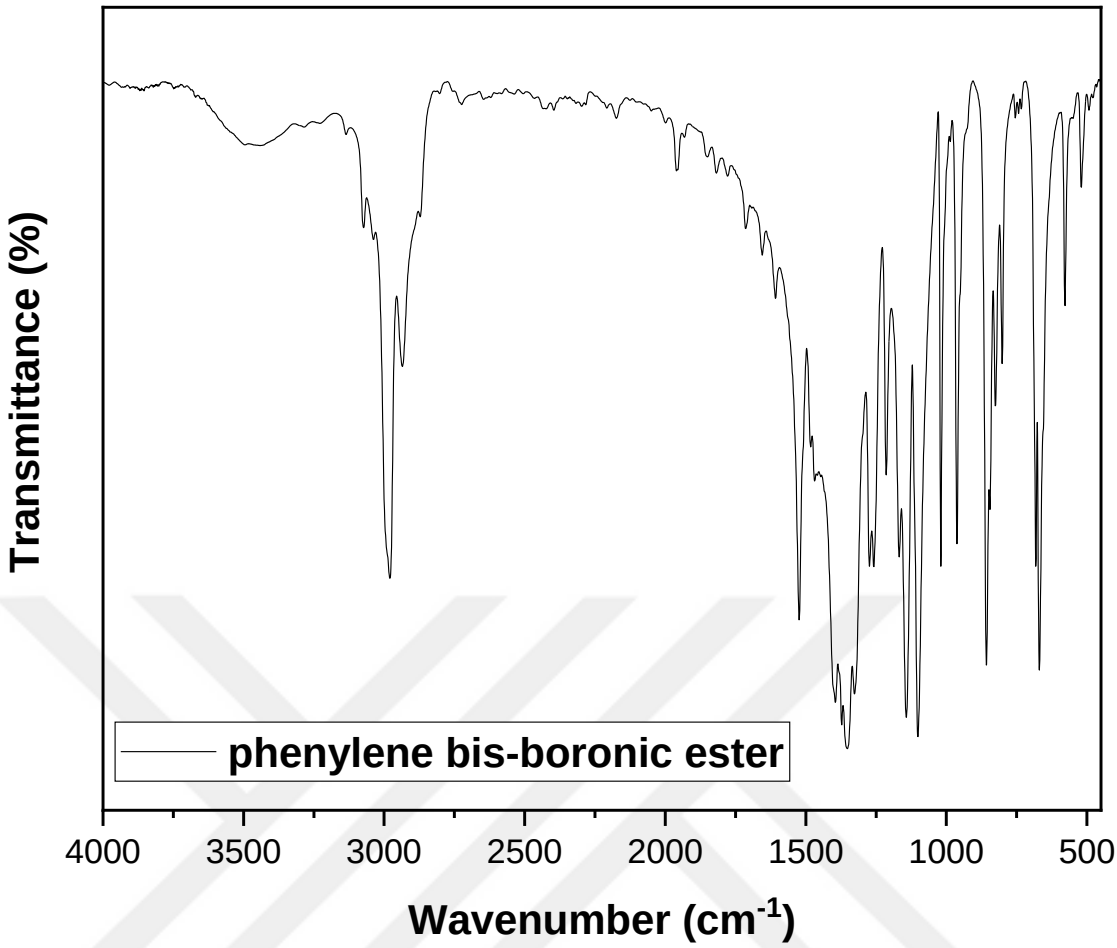

Figure B.6. IR spectrum of phenylene bis-boronic ester.

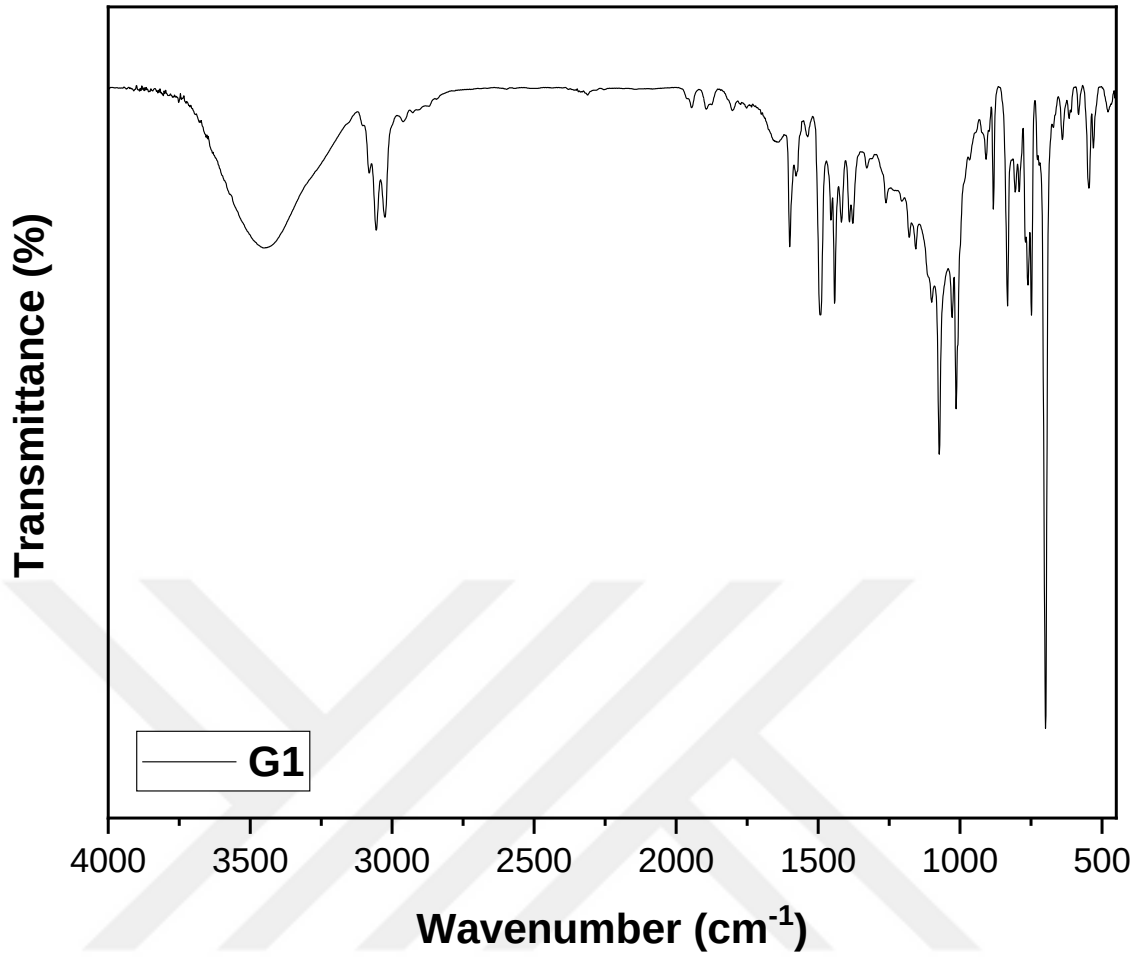

Figure B.7. IR spectrum of G1.

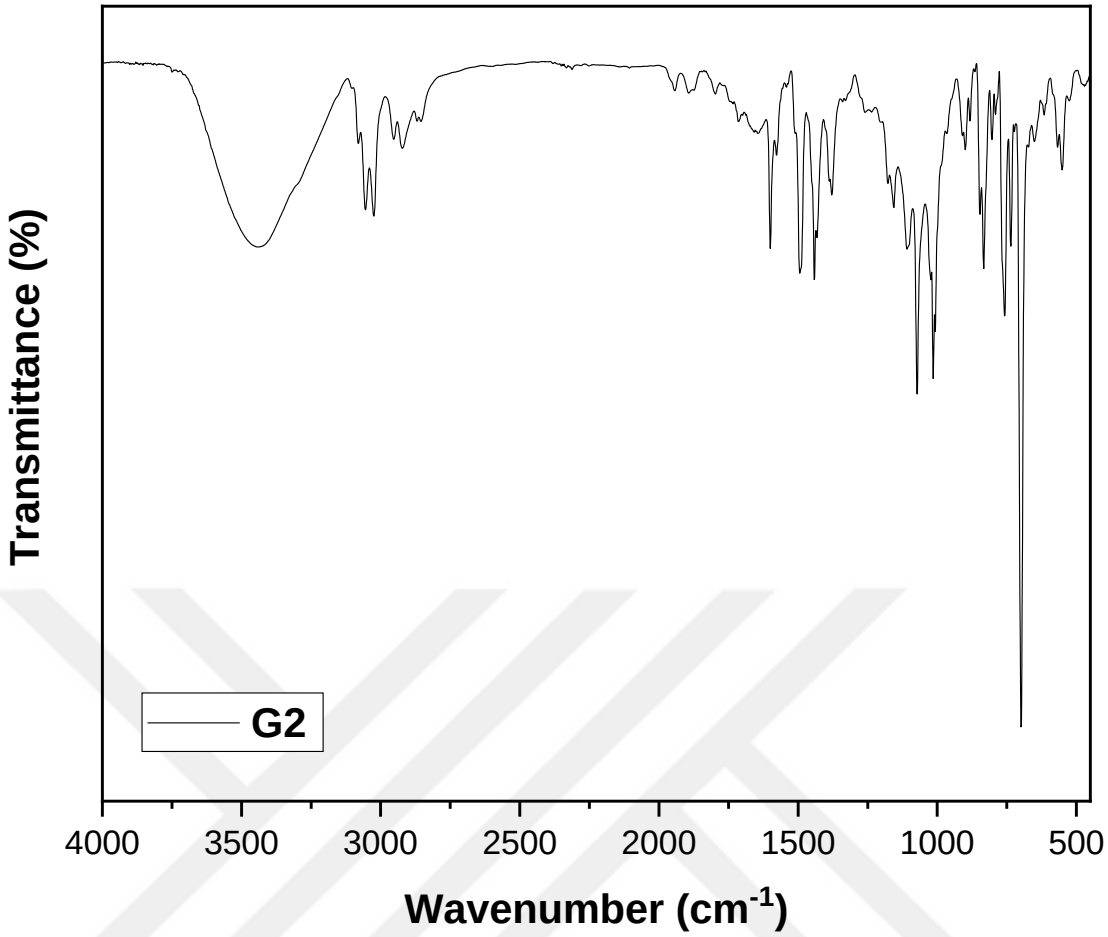

Figure B.8. IR spectrum of G2.

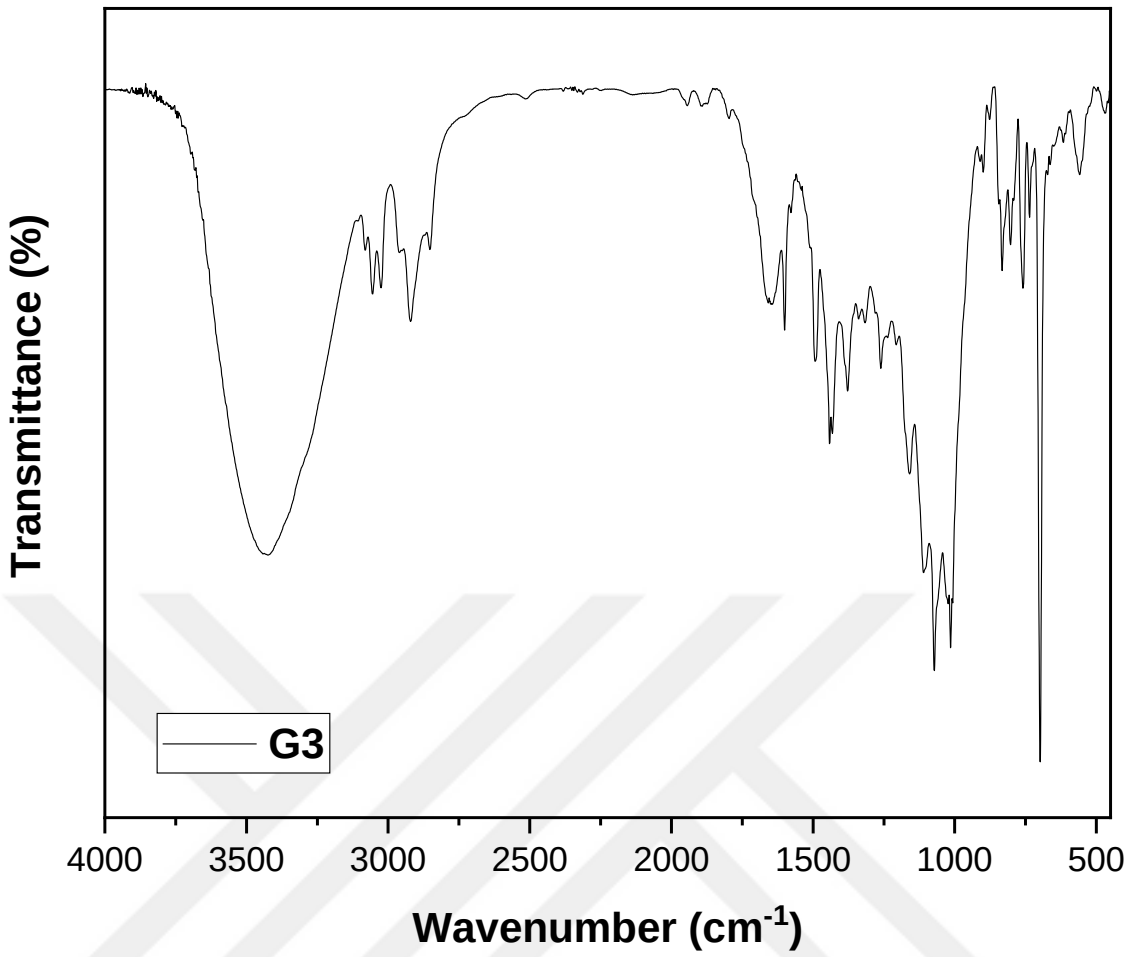

Figure B.9. IR spectrum of G3.

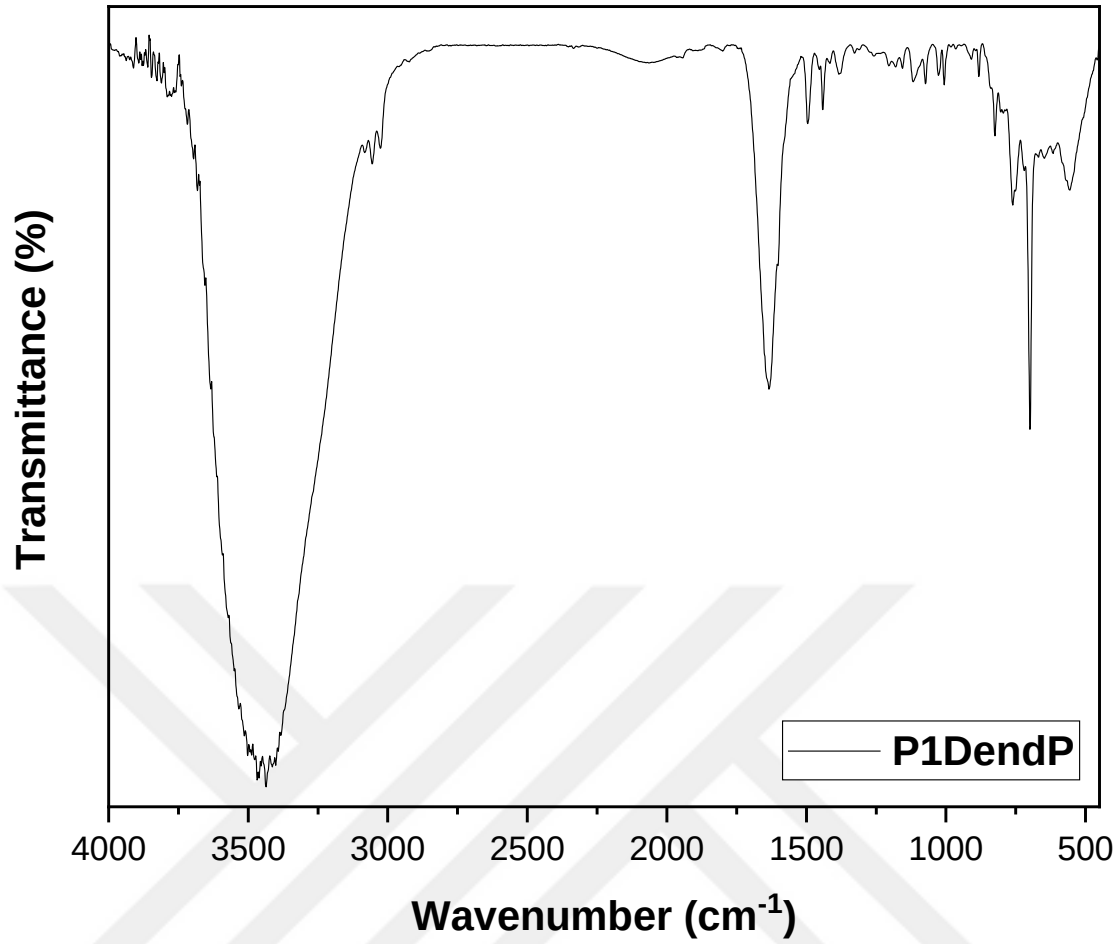

Figure B.10. IR spectrum of P1DendP.

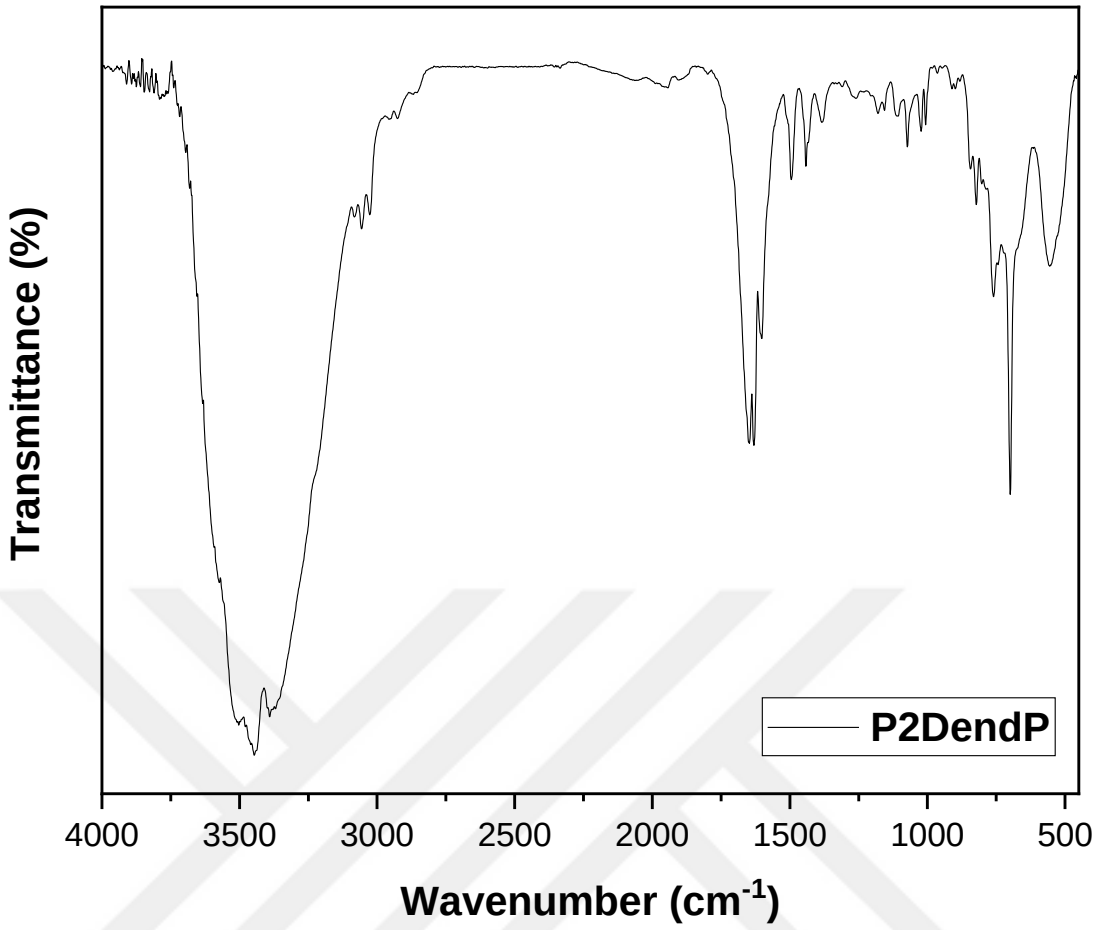

Figure B.11. IR spectrum of P2DendP.

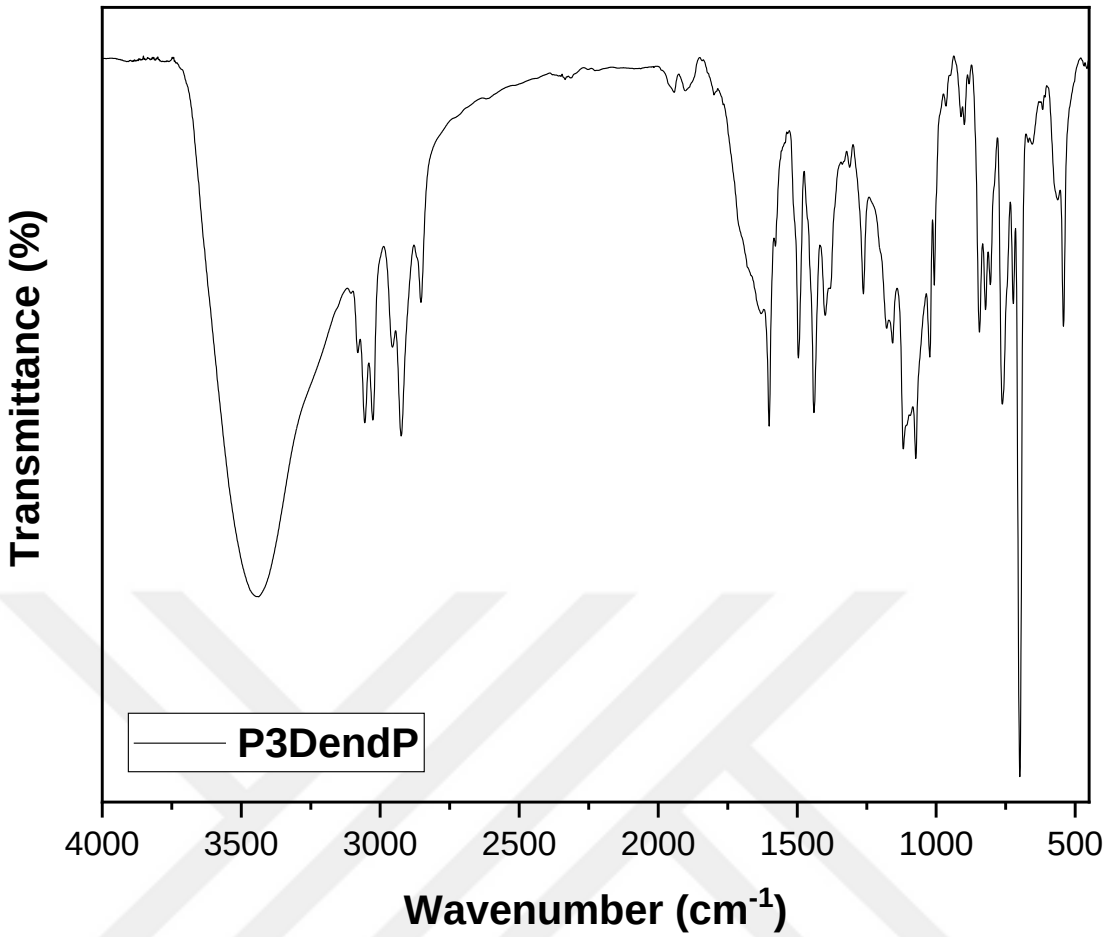

Figure B.12. IR spectrum of P3DendP.

VITA

EDUCATION

Degree Institution Year of Graduation

PhD İzmir Institute of Technology 2024

MSc İzmir Institute of Technology 2016

BSc İzmir Institute of Technology 2014

WORK EXPERIENCE

2015 – Selanik Sarma, Chemist

2013 – Bak Ambalaj, Trainee

FOREIGN LANGUAGE

English (Advanced)

PUBLICATIONS

1) A new fluorescent 'turn on' probe for rapid detection of biothiols. doi:10.1080/10610278.2021.1893321.

2) A rare γ-pyranopyrazole skeleton: design, one-pot synthesis and computational study. doi:10.1039/C6OB01099G.

3) Access to benzo-fused g-pyranopyrazole skeleton via intramolecular Ullmann-type C-O coupling. (submitted)

4) Synthesis of porous dendritic polymers for gas sensing applications. (to be submitted)